INVESTIGATION OF THE ATMOSPHERIC OZONE FORMATION POTENTIAL OF TOLUENE DIISOCYANATE

Final Report to
The Society for the Plastics Industry, Inc.

by
William P. L. Carter, Dongmin Luo, and Irina L. Malkina

December 2, 1997

College of Engineering
Center for Environmental Research and Technology
University of California
Riverside, California 92521

97-AP-RT4E-001-FR

ABSTRACT

Environmental chamber experiments and computer model calculations were conducted to assess the atmospheric ozone formation potentials of 2,4- and 2,6-toluene diisocyanate. The experiments consisted of determining the effects of adding the TDI isomer on ozone formation, NO oxidation, and integrated OH radical levels in three different simulated photochemical smog systems in ~5000-liter, blacklight-irradiated Teflon environmental chambers. TDI was found to inhibit radical levels and ozone formation rates and yields in all experiments. This is apparently due to the presence of both radical sinks and NO_x sinks in TDI's overall atmospheric reactions. Although the mechanism for TDI's atmospheric reactions is unknown, the results of the experiments could be fit by simple parameterized models assuming 70% radical inhibition, no NO to NO_x conversions, and formation of significant yields of products, such as cresols or nitrophenols, whose subsequent reactions cause NO_x removal. The NO_x sinks are clearly more important than any NO_x source which might result from the oxidation of the NCO groups. The lack of apparent NO to NO_2 conversions in TDI's overall mechanism suggests that TDI will not cause significant ozone formation even under conditions which are not sensitive to its radical and NO_x inhibition effects. An 18-hour irradiation indicated that the ozone inhibition effects of TDI continue over at least a two day time period. Both 2,4-TDI and 2,6-TDI were simulated with essentially the same mechanism, indicating no major isomeric differences affecting TDI's reactivity.

The TDI photooxidation models which fit the chamber data were used to estimate TDI's impacts on ozone formation in one-day EKMA model scenarios representing various ozone pollution episodes throughout the United States. TDI was predicted to have a negative effect on ozone formation in all those episodes. Similar results were obtained in a limited number of calculations using multi-day scenarios. It is concluded that emissions of TDI are unlikely to have a positive effect on ozone formation under any atmospheric conditions, and thus it should not be considered to be an ozone precursor.

ACKNOWLEDGEMENTS

The authors acknowledge Mr. Mark Spense of Dow Chemical Company for helpful discussions regarding TDI analysis and Dow Chemical Company for analyzing TDI samples from our chamber to verify our analyses. We also acknowledge Mr. Dennis Fitz for assistance in administering this program and in implementing the TDI analysis method, and Mr. Prem Avani and Charles Do for assistance in carrying out the experiments. Although this work was funded by the Society for the Plastics Industry, the opinions and conclusions expressed in this report are entirely those of the primary author, Dr. William P. L. Carter. Mention of trade names or commercial products do not constitute endorsement or recommendation for use.

TABLE OF CONTENTS

LIST OF TABLES

LIST OF FIGURES

INTRODUCTION

Ozone in photochemical smog is formed from the gas-phase reactions of volatile organic compounds (VOCs) and oxides of nitrogen (NO_x) in sunlight. Although Los Angeles has one of the worst ozone problems in the United States, other areas of the country also have episodes where ozone exceeds the federal air quality standard. Ozone control strategies in the past have focused primarily on VOC controls, though the importance of NO_x control has become recognized in recent years. VOC and NO_x controls have differing effects on ozone formation. NO_x is required for ozone formation, and if the levels of NO_x are low compared to the levels of reactive VOCs, then changing VOC emissions will have relatively little effect on ozone. Since NO_x is removed from the atmosphere more rapidly than VOCs, ozone in areas far downwind from the primary sources tend to be more NO_x limited, and thus less responsive to VOC controls. VOC controls tend to reduce the rate that O_3 is formed when NO_x is present, so VOC controls are the most beneficial in reducing O_3 in the urban source areas, where NO_x is relatively plentiful, and where O_3 yields are determined primarily by how rapidly it is being formed. Because of this, any comprehensive ozone control strategy should involve reduction of emissions of both NO_x and VOCs.

Many different types of VOCs are emitted into the atmosphere, each reacting at different rates and having different mechanisms for their reactions. Because of this, they can differ significantly in their effects on ozone formation, or their "reactivities". Some compounds, such as CFCs, do not react in the lower atmosphere at all, and thus make no contribution to ground-level ozone formation. Others, such as methane, react and contribute to ozone formation, but react so slowly that their practical effect on ozone formation in urban atmospheres is negligible. Obviously, it does not make sense to regulate such compounds as ozone precursors. In recognition of this, the EPA has exempted certain compounds from such regulations on the basis of having "negligible" effects on ozone formation. Although the EPA has no formal policy on what constitutes "negligible" reactivity, in practice it has used the ozone formation potential of ethane as the standard in this regard. This is because ethane is the most reactive of the compounds that the EPA has exempted to date. Therefore, the ozone formation potential of a compound relative to ethane is of particular interest when assessing whether it might be a likely candidate for exemption from regulation as an ozone precursor.

Toluene diisocyanate (TDI) is used in a number of manufacturing processes, and the appropriateness of regulating it as an ozone precursor is of interest to its users and suppliers. Commercial TDI generally is composed of two isomers, 2,4- and 2,6-TDI. Although these compounds have relatively low volatility, they have sufficiently high vapor pressures that they can be emitted into the gas phase as a result of their normal use, where they may undergo reactions which may contribute to ozone formation.

There is relatively limited information concerning the atmospheric reactions of TDI isomers and related compounds. A qualitative study of the fate of TDI in air was carried out by Batelle (Holdren et al, 1985), which is summarized by Duff (1984) and Gilbert (1987). The results indicated that TDI indeed undergoes gas-phase reaction in photochemical smog systems, though no information was obtained on the products formed or its effect on ozone formation. Becker et al (1988) obtained data indicating that TDI reacts in the atmosphere with hydroxyl (OH) radicals at approximately the same rate as does toluene, indicating that if TDI would have significant ozone reactivity if the rate of reaction were the only relevant factor. Although toluene and other aromatics are relatively reactive towards ozone formation (e.g., Carter and Atkinson, 1989; Carter, 1994a), other compounds, such as benzaldehyde (Carter et al, 1982; Carter, 1994a) and volatile silicone compounds (Carter et al, 1992) react in such a way that they actually inhibit ozone formation. Indeed, volatile silicone compounds have been exempted from regulation as ozone precursors on this basis, even though they react in the atmosphere more rapidly than does ethane.

To obtain data needed to evaluate the appropriateness of regulating TDI isomers as ozone precursors, the Society of the Plastics Industry contracted the College of Engineering Center for Environmental Research and Technology (CE-CERT) to carry out the environmental chamber experiments to measure the ozone impacts of these compounds under various simulated atmospheric conditions, to develop and evaluate models for their effects on ozone and other observations which are consistent with these data, and then to use these models to calculate their ozone impacts under a variety of atmospheric conditions. The results of this study are documented in this report.

METHODS

Overall Experimental Approach

Most of the environmental chamber experiments for this program consisted of measurements of "incremental reactivities" of TDI isomers under various conditions. These involve two types of irradiations of model photochemical smog mixtures. The first is a "base case" experiment where a mixture of reactive organic gases (ROGs) representing those present in polluted atmospheres (the "base ROG surrogate") is irradiated in the presence of oxides of nitrogen (NO_x) in air. The second is the "test" experiment which consists of repeating the base case irradiation except that the VOC whose reactivity is being assessed is added. The differences between the results of these experiments provide a measure of the atmospheric impact of the test compound, and the difference relative to the amount added is a measure of its reactivity. These data can then be used to test the ability of various chemical mechanisms or models for TDI's atmospheric reactions to predict the reactivities of TDI under various conditions in the atmosphere.

To provide data to test predictions of reactivities of TDI under varying atmospheric conditions, three types of base case experiments were carried out:

1. Mini-Surrogate Experiments. This base case employed a simplified ROG surrogate and relatively high NO_x levels and low ROG/NO_x ratios. Low ROG/NO_x ratios represent "maximum incremental reactivity" (MIR) conditions, which are most sensitive to VOC effects. Low ROG/NO_x experiments are useful because they provide a sensitive test for the model, and also because it is most important that the model correctly predict a VOC's reactivity under conditions where the atmosphere is most sensitive to the VOCs. The ROG mini-surrogate mixture employed consisted of ethene, n-hexane, and m-xylene. This same surrogate was employed in our previous studies (Carter et al, 1993a,b; 1995a,b.), and was found to provide a more sensitive test of aspects of the mechanism concerning radical initiation and termination effects than the more complex surrogates which more closely represent atmospheric conditions (Carter et al, 1995b). This high sensitivity to these important mechanistic effects makes the mini-surrogate experiments highly useful for mechanism evaluation.

2. Full Surrogate Experiments. This base case employed a more complex ROG surrogate under somewhat higher, though still relatively low, ROG/NO_x conditions. While less sensitive to radical initiation and termination effects in the mechanisms of the VOCs studied, they provide a means to test other aspects of the mechanisms, such as numbers of NO to NO_2 conversions, etc. Furthermore, experiments with a more representative ROG surrogate are needed to evaluate the mechanism under conditions that more closely resembling the atmosphere. The ROG surrogate employed was the same as

the 8-component "lumped molecule" surrogate as employed in previous studies (e.g., Carter et al. 1995b), and consists of n-butane, n-octane, ethene, propene, trans-2-butene, toluene, m-xylene, and formaldehyde. Calculations have indicated that use of this 8-component mixture will give essentially the same results in incremental reactivity experiments as actual ambient mixtures (Carter et al. 1995b).

3. Full Surrogate, low NO_x Experiments. This base case employing the same 8-component lumped molecule surrogate as the full surrogate experiments described above, except that lower NO_x levels (higher ROG/NO_x ratios) were employed to represent NO_x-limited conditions. Such experiments are necessary to assess the ability of the model to properly simulate reactivities under conditions where NO_x is low. The initial ROG and NO_x reactant concentrations were comparable to those employed in our previous studies (Carter et al. 1995b).

An appropriate set of control and characterization experiments necessary for assuring data quality and characterizing the conditions of the runs for mechanism evaluation were also carried out. These are discussed where relevant in the Modeling Methods or Results sections.

Environmental Chamber

The environmental chamber system employed in this study was the CE-CERT "Dividable Teflon Chamber" (DTC) with a blacklight light source. This consists of two ~5000-liter 2-mil heat-sealed FEP Teflon reaction bags located adjacent to each other and fitted inside an 8' x 8' x 8' framework, and which uses two diametrically opposed banks of 32 Sylvania 40-W BL black lights as the light source. The lighting system in the DTC was found to provide so much intensity that only half the lights were used for irradiation. The air conditioner for the chamber room was turned on before and during the experiments. Four air blowers which are located in the bottom of the chamber were used to help cool the chamber as well as mix the contents of the chamber. The CE-CERT DTC is very similar to the SAPRC DTC which is described in detail elsewhere (Carter et al, 1995b,c).

The DTC is designed to allow simultaneous irradiations of experiments with and without added test reactants under the same reaction conditions. Since the chamber is actually two adjacent FEP Teflon reaction bags, two mixtures can be simultaneously irradiated using the same light source and with the same temperature control system. These two reaction bags are referred to as the two "sides" of the chamber (Side A and Side B) in the subsequent discussion. The sides are interconnected with two ports, each with a box fan, which rapidly exchange their contents to assure that base case reactants have equal concentrations in both sides. In addition, a fan is located in each of the reaction bags to rapidly mix the reactants within each chamber. The ports connecting the two reactors can then be closed to allow separate injections on each side, and separate monitoring of each side.

Experimental Procedures

The reaction bags were flushed with dry air produced by an AADCO air purification system for 14 hours (6 PM - 8 AM) on the nights before experiments. The continuous monitors were connected prior to reactant injection and the data system began logging data from the continuous monitoring systems. The reactants were injected as described below (see also Carter et al, 1993a,, 1995c). The common reactants were injected in both sides simultaneously using a three-way (one inlet and two outlets connected to side A and B respectively) bulb of 2 liters in the injection line and were well mixed before the chamber was divided. The contents of each side were blown into the other using two box fans located between them. Mixing fans were used to mix the reactants in the chamber during the injection period, but these were turned off prior to the irradiation. The sides were then separated by closing the ports which connected them, after turning all the fans off to allow their pressures to equalize. After that, reactants for specific sides (the test compound in the case of reactivity experiments) were injected and mixed. The irradiation began by turning on the lights and proceeded for 6 hours, except for one run (DTC462) where the lights were kept on for two days (~18 hours). After the run, the contents of the chamber were emptied by allowing the bag to collapse, and then was flushed with purified air. The contents of the reactors were vented into a fume hood.

The procedures for injecting the various types of reactants were as follows. The NO and NO_2 were prepared for injection using a high vacuum rack. Known pressure of NO, measured with MKS Baratron capacitance manometers, were expanded into Pyrex bulbs with known volumes, which were then filled with nitrogen (for NO) or oxygen (for NO2). The contents of the bulbs were then flushed into the chamber with AADCO air. The other gas reactants were prepared for injection either using a high vacuum rack or a gas-tight syringes whose amounts were calculated. The gas reactants in a gas-tight syringe was usually diluted to 100-ml with nitrogen in a syringe. The volatile liquid reactants were injected, using a micro syringe, into a 1-liter Pyrex bulb equipped with stopcocks on each end and a port for the injection of the liquid. The port was then closed and one end of the bulb was attached to the injection port of the chamber and the other to a dry air source. The stopcocks were then opened, and the contents of the bulb were flushed into the chamber with a combination of dry air and heat gun for approximately 5 minutes. Formaldehyde was prepared in a vacuum rack system by heating paraformaldehyde in an evacuated bulb until the pressure corresponded to the desired amount of formaldehyde. The bulb was then closed and detached from the vacuum system and its contents were flushed into the chamber with dry air through the injection port.

Since the TDI isomers have high boiling points (~129-133˚C at 18 mm Hg), they may condense in cold spots if the usual liquid injection procedure is used. Therefore, a heated injection system was employed for these compounds. This involved placing the desired quantity of the TDI (typical 150 µl) in a "T"-shaped glass tube (with one port for liquid injection, and the other two for the gas inlet and output) which was surrounded with heat tape. After the sample was introduced into the tube, it was then

heated to around 200˚C and its contents were flushed into chamber with purified dry air at 2 liters/minute for about 15 minutes.

Analytical Methods

Reactants other than TDI

Ozone and nitrogen oxides (NO_x) were continuously monitored using commercially available continuous analyzers with Teflon sample lines inserted directly into the chambers. The sampling lines from each side of the chamber were connected to solenoids which switched from side to side every 10 minutes, so the instruments alternately collected data from each side. Ozone was monitored using a Dasibi 1003AH UV photometric ozone analyzer and NO and total oxides of nitrogen (the latter also responding to HNO_3 and organic nitrates) were monitored using a Teco Model 14B chemiluminescent NO/NO_x monitor. The output of these instruments, along with that from the temperature sensors and the formaldehyde instrument, were attached to a computer data acquisition system, which recorded the data at 10 minutes intervals for ozone, NO and temperature (and at 15 minutes for formaldehyde), using 30 second averaging times. This yielded a sampling interval of 20 minutes for taking data from each side.

The Teco instrument and Dasibi CO analyzer were calibrated with a certified NO and CO source and CSI gas-phase dilution system. This was done prior to chamber experiment for each run. The NO_2 converter efficiency check was carried out in regular intervals. The Dasibi ozone analyzer was calibrated against a transfer standard ozone analyzer approximately once every three months and it was checked with a CSI ozone generator (set to 400 ppb) prior to each experiment to assure that the instrument worked properly. The details were discussed elsewhere (Carter et al, 1995c)

Organic reactants other than formaldehyde and TDI were measured by gas chromatography with FID and ECD detections as described elsewhere (Carter et al. 1993a; 1995c). GC samples were taken for analysis at intervals from 20 minutes to 30 minutes either using 100 ml gas-tight glass syringes or by collecting the 100 ml sample from the chamber onto Tenax-GC solid adsorbent cartridge. These samples were taken from ports directly connected to the chamber after injection and before irradiation and at regular intervals after irradiation. The sampling method employed for injecting the sample onto the GC column depended on the volatility or "stickiness" of the compound. For analysis of the more volatile species, the contents of the syringe were flushed through a 2 ml or 3 ml stainless steel or 1/8’ Teflon tube loop and subsequently injected onto the column by turning a gas sample valve. The only low volatility species monitored during this program was TDI, which could not be monitored by GC methods.

The calibrations for the GC analyses for most compounds were carried out by sampling from chambers or vessels of known volume into which known amounts of the reactants were injected, as described previously (Carter et al, 1995c).

TDI analysis by HPLC

TDI concentrations in our experiments were determined by two using a total carbon analyzer (as described in the following section) and by using an HPLC method. The latter was based on the OSHA 42 analysis method, with some modifications as indicated below. This method involves passing air from the chamber through coated filters to collect the TDI, then extracting the filter into a liquid solution and analyzing it by HPLC. Since the OSHA method was designated for analysis of TDI at much lower ambient concentrations than employed in our chamber (~0.3 to 2 ppm), the sampling air volume was reduced from the recommended 15 liters to 5 liters, with the sampling rate being 1 liter/min.

The sampling system employed a three-piece polystyrene cassette that contained a glass fiber filter coated with 0.1 mg of 1-(2-pyridyl) piperazine (1-2PP) and a backup pad. The coated filters were prepared by applying 0.5 ml of a solution of 0.2 mg/ml 1-2PP in methylene chloride to each glass fiber filter. The wet filters were allowed to air dry before placing them in a jar, which is evacuated to remove residual methylene chloride. The coated filters were stored in refrigerator prior to their use. The inlet and outlet of the cassette were covered except when being used for sampling.

The sampling procedure was as follows. A sampling pump was connected to a dry gas flowmeter to control the flow to within 5% of the desired flow rate of 1 liter/min. The inlet cover was removed from the three-piece cassette and saved for installation after sampling. The cassette was then attached in the sampling line of chamber and sampled at a flow rate of 1 liter/min. The total air volume sampled was 5 liters except for DTC453, one liter was sampled because it employed a higher TDI concentration (4 ppm). After sampling for the appropriate time, the sampling device was removed and the small plug and inlet cover were reinstalled. A blank sample taken prior to TDI injection into the chamber; usually two samples were taken after TDI injection prior to the beginning of the irradiation, and approximately hourly samples were taken after the run began. Samples were taken during the first and last ~6 hours of the ~18-hour two-day run DTC462.

The samples were prepared for HPLC analysis by opening the polystyrene cassette and placing the glass fiber filter into a 4-ml vial so that the filter was flat against the inside surface of the vial, not folded or crumpled. Two milliliters of 90/10 (v/v) acetonitrile/dimethyl sulfoxide (ACN/DMSO) solution were added in the vial, which was then shaken to remove large air bubbles from between the filter and the glass. At least one hour elapsed until the solution was transferred into a 2-ml vial for HPLC analysis.

A Shimadzu HPLC system was used to analyze the extracted filter samples. It consists of a system controller (SCL-10A), pumps (LC-10AS), an auto injector (SIL-10A), a column oven (CTO-10A) and a UV-VIS detector (SPD). The column was 25-cm x 4.7 mm i.d. stainless steel packed with 1 µm Alltech C8. The mobile phase was 0.01 M ammonium acetate in 37.5/62.5 ACN/water (v/v) adjusted to PH 6.2 with acetic acid and the flow rate was set at 1 ml/min. Two wavelengths (254 and 313 nm) were

used to detect the TDI derivatives. A isothermal temperature program (30°C) was used and the run time was 20 minutes. The sample injection amount was 5µl. The 2,4- and 2,6-TDI peaks had retention time 11.3 and 14.8, respectively, on this system.

The possibility of sample breakthrough was tested by placing two filters in series when sampling from the chamber. Large sample breakthrough indicated that the use of the 15 liter sample sizes as recommended in the OSHA method was found to cause near-saturation of the filters when analyzing in the concentration range in our experiments. Unfortunately, this sampling volume was used in the initial TDI dark decay tests, and resulted in the HPLC data from those tests being rejected. However, there was no measurable TDI on the second filter when the ≤5 liter samples were taken. Five liter samples were employed for all the experimental runs after DTC447.

Two calibration standards were used for the HPLC TDI analysis. The first was prepared as follows. A solution containing the desired amount (~3 g in this study) of 2,4-TDI in 25 ml of methylene chloride was slowly added to a stirred solution of 7.25 g of 1-2PP in 100 ml of methylene chloride. The solution was then heated to 35°C for 10 minutes. The volume of methylene chloride was reduced to about 10 ml with a stream of dry nitrogen. The product was precipitated with hexane (precipitation started without adding hexane), filtered, redissolved in a minimal volume of methylene chloride and reprecipitated. The precipitate was filtered and washed with hexane. A standard solution was prepared by dissolving the diisocyanate into DMSO (dimethyl sulfoxide). To express the derivative as free diisocyanate, the amount of 2,4- and 2,6-TDI urea weighted is multiplied by the ratio of the molecular weights of TDI to urea. The calculated volume were diluted to 100 ml with acetonitrile, which were subsequently diluted to the working range with acetonitrile. The second calibration standard consisted of a solution containing 1,000 µg/mL 2,4-bis(4-(2-Pyridyl)1-piper-azinylcarbamyl) toluene in DMSO, which was purchased from Supelco company. Several desired amounts of standard 2,4-TDI derivative were diluted to 1 ml with acetonitrile, individually.

Figure 1 shows the calibration curves obtained for 2,4- and 2,6-TDI. The calibration curve for 2,4-TDI was not linear over the full range for which it was calibrated, with a somewhat lower response factor being obtained in the higher concentration range. The solid lines on Figure 1 show the calibration curves used to derive the concentrations for the various concentration ranges for 2,4-TDI. The 2,6-TDI analysis and calibration involved a lower dynamic range, and a single factor was used for all data for the two runs where this was the reactant.

TDI analysis by the THC Method

To supplement and provide a check on the HPLC method, data was obtained concerning the initial TDI concentration in the chamber runs, and concerning the wall loss rate of THC in the chamber in the absence of other reactants, using a total hydrocarbon (THC) analyzer. In the experimental runs,

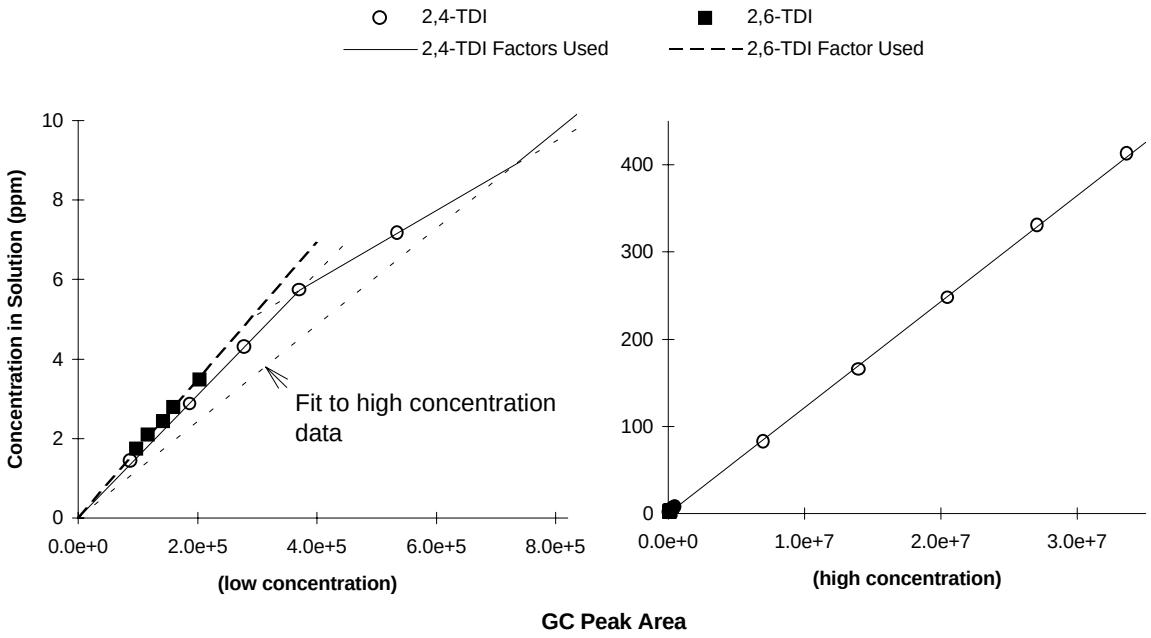

Figure 1. Plots of TDI Calibration Data.

Figure 1. Plots of TDI HPLC calibration data.

the THC concentration was determined using the THC analyzer both prior to and after the TDI injection, with the difference being used to derive the amount of TDI injected.

An Eagle model EM-7000 completely heated, high temperature THC analyzer was employed for this purpose. It utilizes the Flame Ionization Detection (FID) principle to perform its function. The FID is based on measuring the current produced by ions through an electrostatic field which is caused by combustion and polarization. A signal directly proportional to the hydrocarbon number is generated by the ionization of the sampling gas. This signal is then amplified and used to used to drive a digital panel meter on the font panel of the instrument. The panel meter, digitally displays the hydrocarbon concentration in ppm. Four measuring ranges are available and range 2, whose output is 0-10 Volts corresponding to 0-100 ppm, was used in this study. The output signal was connected to our Keithley data acquisition system which logs data every 10 minutes with 30 seconds averaging time. The analyzer was zeroed with nitrogen.

The analyzer was calibrated using ~10 ppm methane. The applicability of the methane-derived calibration factor to aromatic hydrocarbons was checked by analyzing known concentrations of toluene, and the ppmC response by the analyzer agreed with the amount of toluene injected to within 5%. However, the FID response to the isocyanate group is uncertain, but was assumed to be small. Therefore, the TDI concentration in ppm was estimated by multiplying the ppmC reading (as derived using the methane calibration) times 7, the number of carbons in TDI except for those in the isocyanate groups.

This is uncertain and may be somewhat underestimating the actual gas-phase concentrations of TDI. This is discussed further in the Results section.

Characterization Methods

Three thermocouples were used to monitor the temperature of the reaction chambers, two of which were located in the sampling line of continuous analyzers drawing sample from each side, and the third being located in the chamber between the reaction gabs. The temperature in these experiments was typically in the 21-25 C range.

The light intensity in the DTC chamber was monitored by periodic NO_2 actinometry experiments utilizing the quartz tube method of Zafonte et al (1977), with the data analysis method modified as discussed by Carter et al. (1995c). The results of these experiments were tracked over time in this chamber since it was first constructed in early 1994, and were fit by a curve where the NO_2 photolysis rate decayed relatively rapidly from its initial values of ~0.31 min^{-1} when the chamber and lights were new, then declining only slowly during the time up to around the time of actinometry run DTC429, and then somewhat more rapidly during the period of these experiments. A set of curves through the full set of actinometry results predicted NO_2 photolysis rates in the range of 0.172 - 0.157 min^{-1} during the time of these experiments.

The spectrum of the blacklight light source was measured using a LiCor LI-1200 spectra radiometer, and found to be essentially the same as the general blacklight spectrum recommended by Carter et al (1995c) for use in modeling blacklight chamber experiments.

The dilution of the DTC chamber due to sampling is expected to be small because the flexible reaction bags can collapse as samples are withdrawn for analysis. However, some dilution occurs with the aging of reaction bags because of small leaks. Information concerning dilution in an experiment can be obtained from relative rates of decay of added VOCs which react with OH radicals with differing rate constants (Carter et al., 1993a; 1995c). Most experiments had a more reactive compounds such as m-xylene and n-octane present either as a reactant or added in trace amounts to monitor OH radical levels. Trace amounts (~0.1 ppm) of n-butane were also added to experiments if needed to provide a less reactive compound for monitoring dilution. In addition, specific dilution check experiments such as CO irradiations were carried out. Based on these results, the dilution rates were found to average ~1% per hour on both sides during the period of these experiments.

Various characterization runs were carried out to measure the chamber radical source, background effects, and to test side equivalency. The results of these experiments are described in the Results and in the Environmental Chamber Modeling Methods sections.

Reactivity Data Analysis Methods

The results of the environmental chamber experiments are analyzed to yield two measures of reactivity for the TDI isomer. The first is the effect of TDI on the change in the quantity $[O_3]$-[NO], or $([O_3]_t$-$[NO]_t)$-$([O_3]_0$-$[NO]_0)$, which is abbreviated as $d(O_3$-NO) in the subsequent discussion. As discussed elsewhere (e.g., Johnson, 1983; Carter and Atkinson, 1987; Carter and Lurmann, 1990, 1991, Carter et al, 1993a, 1995a), this gives a direct measure of the amount of conversion of NO to NO_2 by peroxy radicals formed in the photooxidation reactions, which is the process that is directly responsible for ozone formation in the atmosphere. (Johnson calls it "smog produced" or "SP".) The incremental reactivity of the compound relative to this quantity, which is calculated for each hour of the experiment, is given by

$$IR[d(O_3\text{-NO})]_t^{VOC} = \frac{d(O_3\text{-NO})_t^{test} - d(O_3\text{-NO})_t^{base}}{[VOC]_0} \qquad (I)$$

where $d(O_3\text{-NO})_t^{test}$ is the $d(O_3$-NO) measured at time t from the experiment where the test compound was added, $d(O_3\text{-NO})_t^{base}$ is the corresponding value from the corresponding base case run, and $[VOC]_0$ is the amount of test compound added. The units used are ppm for O_3 and NO, and ppmC for $[VOC]_0$, so the incremental reactivity units are moles of O_3 formed and NO oxidized per mole VOC sample added. An estimated uncertainty for IR[$d(O_3$-NO)] is derived based on assuming an ~3% uncertainty or imprecision in the measured $d(O_3$-NO) values. This is consistent with the results of the side equivalency tests, where equivalent base case mixtures are irradiated on each side of the chamber.

Note that reactivity relative to $d(O_3$-NO) is essentially the same as reactivity relative to O_3 in experiments where O_3 levels are high, because under such conditions $[NO]_t^{base} \approx [NO]_t^{test} \approx 0$, so a change $d(O_3$-NO) caused by the test compound is due to the change in O_3 alone. However, $d(O_3$-NO) reactivity has the advantage that it provides a useful measure of the effect of the compound on processes responsible for O_3 formation even in experiments where O_3 formation is suppressed by relatively high NO levels.

The second measure of reactivity is the effect of the test compound on integrated hydroxyl (OH) radical concentrations in the experiment, which is abbreviated as "IntOH" in the subsequent discussion. This is an important factor affecting reactivity because radical levels affect how rapidly all VOCs present, including the ROG surrogate components, react to form ozone. If a compound is present in the experiment which reacts primarily with OH radicals, then the IntOH at time t can be estimated from

$$IntOH_t = \int_0^t [OH]_\tau \, d\tau = \frac{\ln\left(\frac{[tracer]_0}{[tracer]_t}\right) - D\,t}{kOH^{tracer}}, \qquad (II)$$

where $[tracer]_0$ and $[tracer]_t$ are the initial and time=t concentrations of the tracer compound, kOH^{tracer} is its OH rate constant, and D is the dilution rate in the experiments. The latter was found to be small and was neglected in our analysis. The concentration of tracer at each hourly interval was determined by

linear interpolation of the experimentally measured values. M-xylene was used as the OH tracer in these experiments because it is a base case component present in all incremental reactivity experiments, its OH rate constant is known (the value used was 2.36×10^{-11} cm^3 $molec^{-1}$ s^{-1} [Atkinson, 1989]), and it reacts sufficiently rapidly that its consumption rate can be measured with reasonable precision.

The effect of TDI on OH radicals can thus be measured by its IntOH incremental reactivity, which is defined as

$$IR[IntOH]_t = \frac{IntOH_t^{test} - IntOH_t^{base}}{[VOC]_0} \qquad \text{(III)}$$

where $IntOH_t^{test}$ and $IntOH_t^{base}$ are the IntOH values measured at time t in the added compound and the base case experiment, respectively. The results are reported in units of 10^6 min per ppm. The uncertainties in IntOH and IR[IntOH] are estimated based on assuming an ~2% imprecision in the measurements of the m-xylene concentrations. This is consistent with the observed precision of results of replicate analyses of this compound.

Chemical Mechanisms Used in the Model Simulations

General Atmospheric Photooxidation Mechanism

Ozone formation in photochemical smog is due to the gas-phase reactions of oxides of nitrogen (NO_x) and various reactive organic gases (ROGs) in sunlight. Various reaction schemes have been developed to represent these processes (e.g., Gery et al., 1988; Carter, 1990; Stockwell et al., 1990), but the one used in this work was an updated version of the detailed SAPRC mechanism (Carter, 1990, 1995; Carter et al., 1993b, 1997a). This is detailed in the sense that it explicitly represents a large number of different types of organic compounds, but it uses a condensed representation for most of their reactive products. The major characteristics of this mechanism are described by Carter (1990). The reactions of inorganics, CO, formaldehyde, acetaldehyde, peroxyacetyl nitrate, propionaldehyde, peroxypropionyl nitrate, glyoxal and its PAN analog, methyl glyoxal, and several other product compounds are represented explicitly. The reactions of unknown photoreactive products formed in the reactions of aromatic hydrocarbons are represented by model species whose yields and photolysis rate are adjusted based on fits of model simulations to environmental chamber experiments. A "chemical operator" approach is used to represent peroxy radical reactions. Generalized reactions with variable rate constants and product yields are used to represent the primary emitted alkane, alkene, aromatic, and other VOCs (with rate constants and product yields appropriate for the individual compounds being represented in each simulation). Most of the higher molecular weight oxygenated product species are represented using the "surrogate species" approach, where simpler molecules such as propionaldehyde or 2-butanone are used to represent the reactions of higher molecular weight analogues that are assumed to react similarly.

The mechanism of Carter (1990) was updated several times prior to this work. A number of changes were made to account for new kinetic and mechanistic information for certain classes of compounds as described by Carter et. al. (1993b) and Carter (1995). Further modifications to the uncertain portions of the mechanisms for the aromatic hydrocarbons were made to satisfactorily simulate results of experiments carried out using differing light sources (Carter et al. 1997a). The latest version of the general mechanism is discussed by Carter et al. (1997a). A complete listing of this mechanism is given in Appendix A to this report.

Models for TDI Reactions

There is relatively limited information concerning the atmospheric reactions of TDI and related compounds. A qualitative study of the fate of TDI in air was carried out by Batelle (Holdren et al, 1983), which is summarized by Duff (1984) and Gilbert (1987). They observed that TDI undergoes a relatively rapid wall loss in humidified air in large Teflon chambers, with dark decay rates ranging from ~15-30%/hour in a 17,300-liter Teflon chamber. The decay rate increases when TDI is photolyzed in the presence of an ROG - NO_x "urban mix", and increases further when a compound which is apparently a radical initiator, but is approximately the same as the dark decay rate when photolyzed in the presence of a radical inhibitor. The latter result indicates that TDI probably does not undergo significant decomposition via direct photolysis, though it does react with radicals formed in photochemical smog. The dark decay is attributed to absorption on the walls, and was found to be independent of humidity in the 7-70% range. No evidence for the formation of toluenediamine (TDA) was observed in either the irradiation or the dark decay experiments.

The enhanced rate of decay of TDI when irradiated in the presence of an urban mixture is probably due to its reaction with OH radicals. This is expected since reaction with OH radicals is the major atmospheric fate for most aromatics. Becker et al. (1988) measured the OH radical rate constant for TDI to be $(7.4\pm0.2) \times 10^{-12}$ cm^3 $molec^{-1}$ s^{-1}, which is only slightly larger than that of toluene. No information is available concerning other atmospheric reactions of TDI except, as noted above, the Batelle data indicated that photodecomposition is probably not significant. It is likely that reaction with OH radicals is the major atmospheric fate of TDI, though the possibility of some reaction with O_3 or NO_3 radicals has not been ruled out. No information is available concerning the products formed in the OH reaction, except that TDA formation is apparently not significant.

If the mechanism for TDI were similar to that of aromatic hydrocarbons such as toluene, then it would have significant radical initiating characteristics, since these compounds form products which are highly photoreactive (Atkinson, 1990; Carter, 1990, and references therein). This causes them to have high O_3 reactivities under relatively high NO_x conditions, such as those used to derive the MIR scale (Carter, 1994a). However, the interactions of the -NCO with the intermediates formed in the OH reactions are unknown, and the overall mechanism may well be significantly different that of toluene. Aromatic

hydrocarbons tend to have low or even negative reactivities very low NO_x conditions, due to formation of products such as phenols and benzaldehyde which cause significant NO_x sinks when they react (Atkinson, 1990; Carter, 1990, and references therein). If the TDI isomers formed high yields of products such as these, then they may significantly inhibit O_3 formation under lower NO_x conditions. Furthermore, there is a possibility that the TDI isomers may be radical inhibitors, which would give them low or negative O_3 reactivity under high NO_x or MIR conditions. This may result from a possible formation of α-peroxy isocyanate species following OH addition ortho or para to an -NCO group and addition of O_2 to the radical position next to the -NCO, with the α-peroxy isocyanate subsequently decomposing to a carbonyl + NO + CO. This can be shown schematically as,

$$OH + C^{CC}_{CC}CNCO \rightarrow HO\text{-}C^{CC}_{CC}C(\cdot)NCO$$
$$HO\text{-}C^{CC}_{CC}C(\cdot)NCO + O_2 \rightarrow HO\text{-}C^{CC}_{CC}C(OO\cdot)NCO \rightarrow HO\text{-}C^{CC}_{CC}C{=}0 + NO + CO$$

(where C^{CC}_{CC} refers to the other 5 carbons in what was originally the aromatic ring, and where non-interacting groups are not shown). This process, if it occurred to a sufficient extent, would not only inhibit radicals by removing OH without regenerating other radicals, but would also slow down the rate of O_3 formation because of the reaction of O_3 with NO. On the other hand, it would release NO_x into the system, which would tend towards enhancing O_3 formation under NO_x-limited conditions.

Given the lack of photooxidation product data for TDI, the significant uncertainties concerning the atmospheric reactions of even the simplest aromatics and the fact that nothing is known about the mechanisms of the atmospheric reactions of the isocyanate group in even simple molecules, any mechanism developed for the atmospheric reactions of TDI would necessarily be pure speculation. Therefore, no attempt was made to derive a detailed or explicit mechanism for the atmospheric reactions of TDI. Instead, parameterized models, showing the overall processes in as simple a manner as is chemically reasonable and consistent with the data, are used. This is analogous to the approach used for representing the unknown ring-opening reactions of aromatic hydrocarbons, and for representing the atmospheric reactions of phenols, cresols, and the uncharacterized aromatic ring fragmentation products in the mechanisms currently used for air quality modeling (Carter, 1990; Gery et al, 1988; Stockwell et al, 1990). In all these cases, our current knowledge does not justify any greater level of detail, which may not give any more reliable predictions of ozone impacts than a simpler, parameterized approach.

In view of these considerations, and of the types of parameterized mechanisms used to model the ozone impacts of other aromatics, the reaction of TDI with OH radicals under atmospheric conditions was represented by the following parameterization,

$$OH + TDI \rightarrow y_{OH}\ OH + y_{NO\rightarrow NO2}\ R2O2. + y_{NO}\ NO + y_{NO\rightarrow NPHE}\ RO2\text{-}NP. + y_{CRES}\ CRES + y_{AFG2}\ AFG2$$

where, based on the data of Becker et al. (1988),

$$k(OH + TDI) = 7.4 \times 10^{-12} \text{ cm}^3 \text{ molec}^{-1} \text{ s}^{-1}.$$

Here, the "y" parameters refer to the yields of various product species, radicals or "chemical operators" used in the base mechanism. The assumed product yield parameters, which together represent a variety of possible overall photooxidation mechanisms, are as follows:

- The parameter y_{OH} is the amount of OH radicals regenerated without any NO to NO_2 conversions. Note that $1-y_{OH}$ is the amount of radical inhibition involved in the overall OH + TDI photooxidation process.

- The parameter $y_{NO \rightarrow NO2}$ is the number of NO to NO_2 conversions involved in the reactions of TDI, which are represented in the base mechanism by the chemical operator "R2O2." (Carter, 1990). In the presence of NO_x this species reacts with NO to form NO_2. In the absence of NO_x, this species reacts with other peroxy radicals to form no products.

- The parameter y_{NO} is the amount of NO generated from the isocyanate group, by processes such as the speculative reactions shown above.

- The parameter $y_{NO \rightarrow NPHE}$ is the yield of organic nitrates from the reactions of peroxy radicals with NO. In the case of aromatics, the organic nitrates are represented by the nitrophenol, or NPHE, model species (Carter, 1990). Organic nitrate formation from the peroxy + NO reaction is important in the photooxidations of the higher molecular weight alkanes (Carter and Atkinson, 1989b), though it is somewhat less important a factor in the current mechanisms assumed for aromatics (Carter, 1990). However, this possibility was considered for completeness. In the presence of NO_x the operator RO2-NP. reacts with NO to form nitrophenols, while when NO_x is absent it reacts with other peroxy radicals to form nothing.

- The parameter y_{CRES} is the yield of products which react like phenols or cresols. These are represented by the model species "CRES" in the base mechanism. Formation of this product is an important factor affecting reactivity under NO_x-limited conditions, because in the presence of O_3 and NO_x it reacts rapidly with NO_3 radicals via a mechanism which is assumed to remove NO_x from the system.

- The parameter y_{AFG2} is the yield of products which are highly photoreactive and tend to initiate radical formation. It is necessary to assume significant formation of such species in aromatic ring fragmentation processes in order to account for the relatively high reactivities of aromatic hydrocarbons such as toluene or the xylenes (Carter, 1990). The model species "AFG2" is the most reactive of the several model species used to represent photoreactive aromatic products, so it is used to represent the possible formation of such products in the photooxidation of TDI.

The specific reactions and rate constants for the various assumed products or operators are given in Appendix A along with the listing of the rest of the mechanism. The values of these various product yield

parameters for TDI were varied in the simulations of the chamber experiments to determine the set which best fit the data. The results of these adjustments are discussed in the Results section. Note that the data were best fit by assuming that some of these parameters were zero, so they are not all incorporated in the mechanisms used in the final calculations discussed here.

Although reaction with OH radicals is the only significant known gas-phase atmospheric reaction process for the aromatic hydrocarbons, the possibility of other modes of reaction need to be considered. For example, phenol and cresols react significantly with NO_3 radicals, and the possibility that this reaction may be non-negligible in the case of TDI cannot be ruled out. This was examined in several test simulations of some of the chamber experiments, but the data were best fit if this reaction were assumed not to be significant. Based on the Batelle data (Holdren et al, 1985), direct photolysis of TDI is assumed not to be significant.

The Batelle data (Holdren et al, 1985), as well as the experiments and tests for this study, indicate that TDI also undergoes negligible loss on the walls. This is represented in the model by a simple first-order loss, with no gas-phase product formation. The rate of this loss was determined based on the simulations of the chamber data, as discussed in the Results section. This unimolecular decay was assumed to be a wall loss process, and thus was assumed not to be significant in the atmospheric reactivity simulations

Environmental Chamber Modeling Methods

The ability of the chemical mechanisms to appropriately simulate the atmospheric impacts of the TDI isomers was evaluated by conducting model simulations of the environmental chamber experiments from this study. This requires including in the model appropriate representations of chamber-dependent effects such as wall reactions and characteristics of the light source. The methods used are based on those discussed in detail by Carter and Lurmann (1990, 1991), updated as discussed by Carter et al. (1995c,d 1997a). Tables A-1 in Appendix A show the reactions used to represent the chamber effects in the simulations of the experiments for this program, and Table A-4 show the values of the chamber-dependent parameters which were used, and indicate how they were derived.

Results of the characterization experiments carried out for this program indicated that exposure to TDI had non-negligible effects on the chamber radical source and other chamber wall effects, such as NO_x offgasing. Because of this, as shown on Table A-4, the model simulations of experiments in Side A, which was the only side exposed to TDI until run DTC462, used different radical source and NO_x offgasing parameters than model simulations of Side B. This was tested by modeling side equivalency test runs, and is discussed further in the Results section.

The photolysis rates were derived from results of NO_2 actinometry experiments and measurements of the relative spectra of the light source. In the case of the blacklight light source used in these experiments, where the spectrum of the light source appears to be relatively constant, the general blacklight spectrum derived by Carter et al (1995d) was used. (Separate assignments of overall light intensities (as measured by NO_2 photolysis rates) were made for experiments prior to and after run DTC-472, when both the reactors and the light banks were changed.) The thermal rate constants were calculated using the temperatures measured during the experiments, with the small variations in temperature with time during the experiment being taken into account. The computer programs and modeling methods employed are discussed in more detail elsewhere (Carter et al, 1995d). The specific values of the chamber-dependent parameters used in the model simulations of the experiments for this study are given in Table A-4 in Appendix A.

The initial reactant concentrations used when modeling the experiments were based on the measured initial concentrations except as indicated otherwise. The amount of TDI assumed to be present in the experiments was based on the results of the HPLC analyses, except for run DTC459, where the HPLC measurements appear to be anomalously high compared with the THC data. Note that the initial gas-phase TDI as measured by HPLC or THC indicated that only about half of the nominally injected TDI made it to the gas phase. This is discussed further in the Results section. In the case of Run DTC447, which had no valid TDI data of any type, the initial gas-phase TDI was assumed to be the same as in run DTC453, where the same amount was injected.

Atmospheric Reactivity Modeling Methods

To estimate the effects of TDI emissions on ozone formation under conditions more representative of polluted urban atmospheres, incremental reactivities, defined as the change in O_3 caused by adding small amounts of test compounds the emissions, were calculated for ethane, TDI and the mixture representing the VOCs emitted from all sources (the base ROG). The modeling approach and scenarios is the same as used as described in detail elsewhere (Carter, 1994a,b, Carter et al, 1993b), and is only briefly summarized here.

Scenarios Used for Reactivity Assessment

The scenarios employed were those used by Carter (1994a,b) to develop various reactivity scales to quantify impacts of VOCs on ozone formation in various environments. These were based on a series of single-day EKMA box model scenarios (EPA, 1984) derived by the EPA for assessing how various ROG and NO_x control strategies would affect ozone nonattainment in various areas of the country (Baugues, 1990). The characteristics of these scenarios and the methods used to derive their input data are described in more detail elsewhere (Baugues, 1990; Carter, 1994b). Briefly, 39 urban areas in the United States were selected based on geographical representativeness of ozone nonattainment areas and data availability, and a representative high ozone episode was selected for each. The initial non-methane

organic carbon (NMOC) and NO_x concentrations, the aloft O_3 concentrations, and the mixing height inputs were based on measurement data for the various areas, the hourly emissions in the scenarios were obtained from the National Acid Precipitation Assessment Program emissions inventory (Baugues, 1990), and biogenic emissions were also included. Table 1 gives a summary of the urban areas represented and other selected characteristics of the scenarios.

Several changes to the scenario inputs were made based on discussions with the California ARB staff and others (Carter, 1994b). Two percent of the initial NO_x and 0.1% of the emitted NO_x in all the scenarios was assumed to be in the form of HONO. The photolysis rates were calculated using solar light intensities and spectra calculated by Jeffries (1991) for 640 meters, the approximate mid-point of the mixed layer during daylight hours. The composition of the VOCs entrained from aloft was based on the analysis of Jeffries et al. (1989). The composition of the initial and emitted reactive organics (referred to as the "base ROG" mixture) was derived based on analyses of air quality data (Carter, 1994a, Jeffries et al, 1989). Complete listings of the input data for the scenarios are given elsewhere (Carter, 1994b). These are referred to as "base case" scenarios, to distinguish them from those where NO_x inputs are adjusted as discussed below.

In addition to these 39 base case scenarios, three adjusted NO_x scenarios were developed to represent different conditions of NO_x availability. NO_x levels were found to be the most important factor affecting differences in relative ozone impacts among most VOCs (Carter and Atkinson, 1989; Carter, 1994a), and for such compounds the ranges of relative reactivities under various conditions can be reasonably well represented by ranges in relative reactivities in three "averaged conditions" scenarios representing three different NO_x conditions. These scenarios were derived by averaging the inputs to the 39 EPA scenarios, except for the NO_x emissions. In the "Maximum Incremental Reactivity" (MIR) scenario, the NO_x inputs were adjusted such that the final O_3 level is most sensitive to changes in VOC emissions; in the "Maximum Ozone Incremental Reactivity" (MOIR) scenario the NO_x inputs were adjusted to yield the highest maximum O_3 concentration; and in the "Equal Benefit Incremental Reactivity" (EBIR) scenario the NO_x inputs were adjusted such that relative changes in VOC and NO_x emissions had equal effect on ozone formation. As discussed by Carter (1994a), there represent respectively the high, medium and low ranges of NO_x conditions which are of relevance when assessing VOC control strategies for reducing ozone.

The use of averaged conditions, adjusted NO_x scenarios in this work is slightly different than the approach used by Carter (1994a), where the MIR, MOIR, and EBIR scales were derived by adjusting NO_x conditions separately for each of the 39 base case scenarios, and then averaging the reactivities derived from them. However, Carter (1994a) showed that both approaches yield essentially the same results.

Table 1. Summary of conditions of base case scenarios used for atmospheric reactivity assessment.

City, State	Calc. Max O_3 (ppb)	ROG /NO_x	NO_x /NO_x^{MOR}	Final Height (km)	Init.+Emit Base ROG (mmol m^{-2})	Aloft O_3 (ppb)
Atlanta, GA	178	7.3	0.7	2.1	12	63
Austin, TX	174	9.3	0.5	2.1	11	85
Baltimore, MD	323	5.2	1.1	1.2	17	84
Baton Rouge, LA	245	6.8	1.0	1.0	11	62
Birmingham, AL	237	6.9	0.6	1.8	13	81
Boston, MA	194	6.5	0.6	2.6	14	105
Charlotte, NC	143	7.8	0.3	3.0	7	92
Chicago, IL	280	11.6	0.5	1.4	25	40
Cincinnati, OH	197	6.4	0.8	2.8	17	70
Cleveland, OH	250	6.6	1.0	1.7	16	89
Dallas, TX	210	4.7	1.3	2.3	18	75
Denver, CO	209	6.3	1.2	3.4	29	57
Detroit, MI	236	6.8	0.8	1.8	17	68
El Paso, TX	186	6.6	1.1	2.0	12	65
Hartford, CT	169	8.4	0.5	2.3	11	78
Houston, TX	305	6.1	1.0	1.7	25	65
Indianapolis, IN	210	6.6	0.9	1.7	12	52
Jacksonville, FL	156	7.6	0.7	1.5	8	40
Kansas City, MO	154	7.1	0.6	2.2	9	65
Lake Charles, LA	290	7.4	0.7	0.5	7	40
Los Angeles, CA	576	7.6	1.0	0.5	23	100
Louisville, KY	209	5.5	0.9	2.5	14	75
Memphis, TN	224	6.8	0.7	1.8	15	58
Miami, FL	133	9.6	0.4	2.7	9	57
Nashville, TN	165	8.1	0.5	1.6	7	50
New York, NY	361	8.1	0.8	1.5	39	103
Philadelphia, PA	240	6.2	1.0	1.8	19	53
Phoenix, AZ	273	7.6	1.0	3.3	40	60
Portland, OR	164	6.5	0.7	1.6	6	66
Richmond, VA	232	6.2	0.8	1.9	16	64
Sacramento, CA	201	6.6	0.9	1.1	7	60
St Louis, MO	319	6.1	1.1	1.6	26	82
Salt Lake City, UT	183	8.5	0.6	2.2	11	85
San Antonio, TX	131	3.9	1.1	2.3	6	60
San Diego, CA	195	7.1	1.0	0.9	8	90
San Francisco, CA	308	4.8	1.8	0.7	25	70
Tampa, FL	230	4.4	1.1	1.0	8	68
Tulsa, OK	224	5.3	0.9	1.8	15	70
Washington, DC	275	5.3	0.9	1.4	13	99

[a] Ratio of NO_x inputs to NO_x inputs which yield the highest ozone concentrations for the conditions of the scenario This provides a useful measure of NO_x availability (Carter, 1994a).

Quantification of Atmospheric Reactivity

The reactivity of a VOC in an airshed scenario is measured by the change in ozone caused by adding the VOC to the emissions, divided by the amount of VOC added, calculated for sufficiently small amounts of added VOC that the incremental reactivity is independent of the amount added. The specific calculation procedure is discussed in detail elsewhere (Carter, 1994a,b). The incremental reactivities depend on how the amounts of VOC added and amounts of ozone formed are quantified. In this work, the amount of added VOC is quantified on a mass basis, since this is how VOCs are regulated. Two different ozone quantification methods were used, as follows:

- "Ozone Yield" incremental reactivities measure the effect of the VOC on the total amount of ozone formed in the scenario at the time of its maximum concentration. This is quantified as grams O_3 formed per gram VOC added. Most previous recent studies of incremental reactivity (Dodge, 1984; Carter and Atkinson, 1987, 1989, Chang and Rudy, 1990; Jeffries and Crouse, 1991) have been based on this quantification method.

- "IntO_3>0.12" reactivities measure the effect of the VOC on the sum of the hourly ozone concentrations for the hours when ozone 0.12 ppm in the base case scenarios (Carter 1994a). This provides a measure on the effect of the VOC on exposure to unacceptable levels of ozone, with 0.12 ppm being the previous Federal one-hour ozone standard. Carter (1994a) has shown that this quantification can result in different reactivity ratios for some VOCs.

Since ratios of reactivities are generally more relevant to control strategy applications and are usually less sensitive to scenario conditions, the calculated atmospheric reactivity results in this work are given in terms of relative reactivities. This is defined as the incremental reactivity of the VOC divided by the incremental reactivity of the base ROG mixture, i.e., the mixture used to represent VOC emissions from all sources in the scenarios. These relative reactivities can also be thought of as the relative effect on O_3 of controlling emissions of the particular VOC by itself, compared to controlling emissions from all VOC sources equally.

Chemical Models and Mechanisms Used

The models used to represent the reactions of TDI in the atmospheric reactivity simulations were the same as used in modeling the chamber data, except that the unimolecular wall loss process was assumed to be negligible. All emitted TDI was assumed to be available for gas-phase reaction, and possible dry deposition processes, which may be non-negligible, were ignored. The mechanisms for the other species were also the same as employed in the chamber simulations, except that the reactions representing chamber effects were removed, and the reactions for the full variety of VOCs emitted into the scenarios (Carter, 1994a) were included. Most of the emitted VOCs are not represented in the model explicitly, but are represented using lumped model species whose rate constants and product yield parameters are derived based on the mixture of compounds they represent. The rate constants and mechanistic parameters for the emitted species in the scenarios were the same as those used previously

(Carter et al, 1993b), except for the aromatics, whose unknown photoreactive product yields were reoptimized in a manner analogous to that discussed above for toluene and m-xylene (Carter et al. 1997a). The mechanism listing in Appendix A gives the reactions of the model species used in the atmospheric simulations to represent various types of anthropogenic and biogenic emissions, indicating the types of compounds each is used to represent, and giving their rate constants and product yield parameters.

RESULTS AND DISCUSSION

Summary of Experiments and Characterization Results

Summary of Experiments

Table 2 gives a chronological listing of all the experiments carried out for this program. In addition to the reactivity experiments, several TDI dark decay experiments were conducted (though only one had usable TDI data), characterization experiments were conducted to measure chamber wall effects, side equivalency tests were conducted to determine differences between results of experiments in different chamber sides caused by TDI exposure, and control experiments were carried out for comparison with results of similar experiments carried out previously. Table 2 includes characterization and control experiments carried out previously for other programs which are relevant to characterizing conditions of runs for this program. Relevant results of the control and characterization runs are summarized on the table, and are discussed below.

Table 3 summarizes the incremental reactivity experiments which were carried out for TDI. As discussed in more detail below, it can be seen that TDI injection inhibited rates of NO oxidation and O_3 formation, final O_3 yields, and IntOH levels in all the reactivity experiments carried out for this program. Because of evidence that TDI exposure affects results of characterization experiments (see below), for all experiments prior to DTC462 the TDI was only injected into Side A. In run DTC462 the effect of side on the reactivity results were evaluated by repeating the low NO_x full surrogate run DTC454 with the TDI injected into Side B. In addition, that irradiation was carried out for two days (~18 hours), to assess whether the apparent inhibiting effects of TDI persisted over longer time periods. Most of the experiments employed 2,4-TDI, though two final experiments, one employing the mini-surrogate and one employing the low NO_x full surrogate, employed the 2,6 isomer. The results of these experiments, and of the model evaluation using these data, are discussed in detail later in this report.

TDI Analysis Tests and Dark Decay Experiments

Prior to conducting any irradiation experiments with TDI, several dark decay and analysis tests experiments were carried out where ~1-4 ppm (nominal) TDI was injected into Side A of the chamber, and analyzed as a function of time in the absence of other reactants and in the dark. Unfortunately, it was subsequently discovered that the sampling time used in the HPLC analyses for these initial experiments was too long, and that the filters were saturated. Therefore, there were no valid HPLC data for TDI for any of these initial experiments. However, it was determined that the total hydrocarbon (THC) analyzer responded quantitatively to TDI, and data from this method were available in one experiment to monitor the dark decay rate of TDI, and were also used to supplement the HPLC data in most of the reactivity experiments. The problems with the HPLC method were corrected prior to

Table 2. Chronological listing of the environmental chamber experiments carried out for

RunID	Date (s)	Title	Comments [a]
DTC429	10/14/96	NO2 Actinometry	The NO_2 photolysis rate was measured using the quartz tube method was 0.18 min^{-1}, in good agreement with slightly downward trend of previous actinometry results in this chamber.
DTC435	10/22/96	pure air irradiation	After 6 hours of irradiation, approximately 24 ppb O_3 formed on side A and 22 on side B. Results are within the normal range, and were consistent with the predictions of the chamber effects model.
DTC436	10/23/96	Ozone decay	Measured O_3 decay rate was ~1% per hour, in good agreement with the default value used in the chamber model.
DTC443	11/12/96	Propene + NOx	Control run for comparison with other propene runs carried out in this and other chambers. The results were consistent with previous propene runs. Good side equivalency observed.
DTC444	11/13/96	n-Butane + NOx	Control run to measure the chamber radical source. Results were in good agreement with predictions of the standard chamber model.
DTC445	11/14/96	Ozone dark decay	The ozone dark decay rate, after correction for dilution, was ~1.2%/hour on both sides, in good agreement with the standard chamber effects model. Dilution on both sides was ~0.5%/hour, within the normal range for these reactors.
DTC446	1/14/97 thru 2/11/97	TDI injection and analysis testing	A number of tests were carried out where TDI was injected on Side A for purposes of testing the analysis methods or monitoring dark decay. See text.
DTC447	2/21/97	Mini-Surrogate + TDI	Nominal 4 ppm TDI injected in Side A, though the measured gas-phase TDI concentration was ~1.7 ppm. Large inhibition of NO oxidation and O3 formation observed. See

Table 2 (continued)

RunID	Date (s)	Title	Comments [a]
DTC448	2/25/97	n-Butane + NOx	Control run to measure the chamber radical source. Results for side B were in normal range, but NO oxidation rate in Side A indicated the radical source was 2-3 times higher than normal, indicating a probable TDI contamination effect.
DTC449	2/26/97	Mini-Surrogate Side Comparison Test	Control run to evaluate side inequivalency. Side A had a somewhat higher ozone formation and NO oxidation rate, consistent with the higher radical source indicated by run DTC448. See Figure 3.
DTC450	2/27/97	Mini-Surrogate + TDI (A)	Nominal 1 ppm TDI added to Side A, 0.5 ppm observed in gas phase. See Table 2 and Figure 4.
DTC451	2/28/97	Low NOx Full Surrogate Side Comparison Test	Only minor differences between sides, with peak ozone in TDI-exposed Side A being slightly less than on Side B. Results are consistent with predictions of model with radical sources adjusted to fit DTC448. See Figure 3.
DTC452	3/3/97	NO2 Actinometry	The NO_2 photolysis rate was measured using the quartz tube method was 0.18 min^{-1}, somewhat lower than predicted by the trend of previous actinometry results in this chamber. An increase in the rate of decline in light intensity was assumed.
DTC453	3/4/97	Low NOx Full Surrogate + TDI	Nominal 4 ppm TDI injected into Side A, 1.7 ppm observed in the gas phase. Results on Table 2 and Figure 4.
DTC454	3/5/97	Low NOx Full Surrogate + TDI (1 ppm)	Nominal 1 ppm TDI injected into Side A, 0.45 ppm observed in gas phase. Results on Table 2 and Figure 11.

Table 2 (continued)

RunID	Date (s)	Title	Comments [a]
DTC455	3/6/97	Full Surrogate Side Comparison Test	Only minor differences between sides, with the initial rate of NO oxidation being slightly more on the TDI exposed side A. Results are consistent with predictions of model with radical sources adjusted to fit DTC448. See Figure 3.
DTC456	3/7/97	Full Surrogate + TDI	Nominal 1 ppm TDI added to Side A, 0.5 ppm observed in the gas phase. Results on Table 2 and Figure 8.
DTC457	3/11/97	CO + NOx	Control run to test chamber radical source. The radical source rate which fit the TDI-exposed Side A was ~50% higher than observed in Run DTC448. Radical source rate on other side was in normal range.
DTC458	3/12/97	Propene + NOx Control Run	The NO oxidation and O3 formation rate on the TDI-exposed Side A was faster than on Side B. Difference was greater than predicted based on difference in radical source rate. See Figure 3.
DTC459	3/13/97	Full Surrogate + TDI	Nominal 0.5 ppm TDI added to Side A, 0.4 ppm observed in gas phase by HPLC. Results on Table 2 and Figure 9.
DTC460	3/14/97	Propylene Glycol Kinetics and Analysis Tests	Propylene glycol was injected into the chamber for another program, with OH radicals being generated by reaction of ozone with olefins.
DTC461	3/18/97	n-Butane + NOx	Control run to test the chamber radical source. The radical source was about two times greater than previous runs on both sides, with the TDI-exposed side again having twice the radical source as the other side.
DTC462	3/19/97 through 3/20/97	Low NOx Full Surrogate + TDI. TDI in Side B. Two Day run	Nominal 1 ppm TDI added to Side B, 0.45 ppm observed in the gas phase. Lights on for 6 hours for Day 1, off at night, and on for 6 hours for Day 2. Results on Table 2 and Figure 13.

Table 2 (continued)

RunID	Date (s)	Title	Comments [a]
DTC463	3/21/97	n-Butane + NOx	Control run to test the chamber radical source. The radical source on Side A was comparable to those in Runs DTC448 and DTC457. The radical source in Side B higher than normal, being comparable to that in DTC461.
DTC464	3/25/97	Pure Air Irradiation	Run to evaluate background effects 40 and 25 ppb O3 formed on Sides A and B, respectively after 6 hours. Results on Side B consistent with standard chamber model. Results on Side A indicate NOx offgasing rate which is ~2 times normal.
DTC465	3/27/97	Acetaldehyde - Air Irradiation	Run for evaluating NOx offgasing effects, but non-negligible amounts of initial NOx found to be present, so run was not useful for that purpose. Ozone and PAN formation about the same on both sides, which model predicted is sensitive to the initial NOx.
DTC466	4/1/97	Low NOx Full Surrogate + 2,6-TDI	Nominal 1 ppm 2,6-TDI added to Side A, 0.33 ppm observed in the gas phase. Results on Table 2 and Figure 12.
DTC467	4/2/97	Mini-Surrogate + 2,6-TDI	Nominal 1 ppm 2,6-TDI added to Side A, 0.45 ppm observed in the gas phase. Results on Table 2 and Figure 7.
DTC468	4/3/97	n-butane + NOx	Control run to test the chamber radical source. Results were very similar to DTC463.
DTC469	4/4/97	NO2 Actinometry	The NO_2 photolysis rate was measured using the quartz tube method was 0.15 min^{-1}, also lower than predicted by the trend of previous actinometry results, and suggesting a more rapid rate of decline in light intensity than was the case before run DTC429.

[a] Unless indicated otherwise, the TDI isomer injected was 2,4-TDI

Table 3. Summary of conditions and results of the incremental reactivity experiments.

Run	Initial Reactants (ppm)					t=6 d(O_3-NO) (ppm)			t=5 IntOH (10^{-6} min)		
	NO_x	Surg [a]	TDI			Base	Test	IR [b]	Base	Test	IR
			Inj [c]	HPLC	THC						
Mini-Surrogate + 2,4-TDI											
DTC-447(A)	0.44	6.2	4.0	1.66 [d]		0.48	0.15	-0.20	12	4	-5
DTC-450(A)	0.39	5.7	1.0	0.48	0.35	0.57	0.42	-0.31	13	10	-7
Mini-Surrogate + 2,6-TDI											
DTC-467(A)	0.39	5.2	1.0	0.46	0.37	0.39	0.28	-0.23	11	6	-10
High NO_x Full Surrogate + 2,4-TDI											
DTC-456(A)	0.29	3.8	1.0	0.48	0.37	0.50	0.39	-0.22	23	17	-11
DTC-459(A) [e]	0.29	3.9	0.5	(0.38)	0.13	0.51	0.46	-0.13	22	20	-5
Low NO_x Full Surrogate + 2,4-TDI											
DTC-453(A)	0.17	3.9	4.0	1.66	1.88	0.35	0.21	-0.08	24	10	-8
DTC-462(B)	0.14	4.0	1.0	0.44	0.40	0.35	0.29	-0.15	27	20	-16
DTC-454(A)	0.14	4.0	1.0	0.41	0.45	0.33	0.26	-0.19	24	20	-10
Low NO_x Full Surrogate + 2,6-TDI											
DTC-466(A)	0.16	3.6	1.0	0.33	0.39	0.34	0.27	-0.20	27	20	-22

[a] Total base ROG surrogate in ppmC.

[b] Incremental reactivity

[c] Calculated concentration from volume of liquid TDI injected.

[d] No TDI data. Initial TDI assumed to be same as DTC456, which had same amount injected.

[e] The initial TDI as measured by HPLC is high compared to the THC data and the amount injected and injection efficiencies for other runs. The Initial gas-phase TDI used for modeling was 0.14 ppm, derived based on the THC data and the ratio of the HPLC/THC measurements for the other runs.

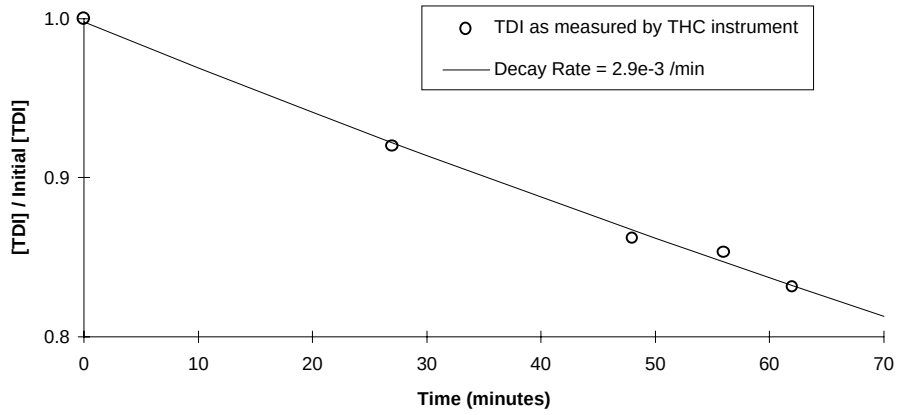

Figure 2.. Results of the TDI dark decay experiment.

carrying out most of the TDI reactivity experiments, and only one experiment, DTC447, lacked useable TDI data.

Table 3 compares the initial TDI in the reactivity experiments as determined by the HPLC and the THC methods, and also as determined by the nominal amount injected. It can be seen that the HPLC and THC methods were in qualitative agreement, except for run DTC459, where the HPLC measurements were ~3 times higher than indicated by the THC data. In addition, for method evaluation purposes, several TDI sampling cartridges taken during run DTC462 were sent to Dow Chemical for analysis. Dow Chemical's results indicated that the initial gas-phase TDI in that experiment was 0.35 ppm, in fair agreement with the 0.44 ppm obtained in our HPLC analysis. Based on these data, the initial gas-phase TDI concentrations should be considered to have about a ±25% uncertainty.

Table 3 also shows that the gas-phase TDI measurements as obtained by HPLC or THC were consistently lower than the nominal amounts of TDI added to the chamber, as calculated from the volumes of liquid TDI which were injected. The apparent gas-phase TDI was about half the calculated amount injected for all experiments except for the run (DTC459) where the THC and HPLC TDI analyses disagreed. In that run the ratio of gas phase to injected TDI derived from the HPLC data ~75%, but the ratio derived from the THC data was consistent with that observed for the other runs, suggesting that it is the HPLC data for that run which is anomalous. In view of the agreement between the two very different gas-phase measurements for all runs except for DTC449, this discrepancy between measured gas-phase and injected TDI is attributed to incomplete TDI injection rather than to an analysis problem. The TDI has quite a low volatility and it appears to have a large affinity for surface absorption, and it is probable that a significant fraction of the injected TDI condensed on the walls of the injection system or the chamber during the injection process.

Consistent with the Batelle results, the TDI was also observed to undergo dark decay at significant rates, presumably due to wall loss. Figure 2 shows the results of the single dark decay experiment where usable TDI data were obtained, which was carried out prior to the reactivity experiments. As shown on the figure, the data were well fit by a first order decay plot, with the decay rate being 2.9×10^{-3} min^{-1}, or 17.4 % per hour. This is quite similar to the ~15% per hour decay rate observed in the Batelle study (Holdren et al, 1985). However, the TDI dark decay rate which best fit the data in the model simulations of the reactivity experiments was only 1×10^{-3} min^{-1} (or 6% per hour), which was only 1/3 as much. This is shown in Figure 3, which shows the experimental and calculated TDI decay rates for all the reactivity experiments where apparently valid HPLC TDI data were available. (The TDI model used was that which best fit the O_3 and other chamber data, as discussed later.) This may be due to a conditioning effect, since the dark decay experiment Figure 2 was carried out prior to the reactivity experiments. (Note also that the TDI decay rate in the first few hours of run DTC642, the first run where TDI is exposed to Side B, is better fit by the higher decay rate indicated by the initial dark decay experiment.

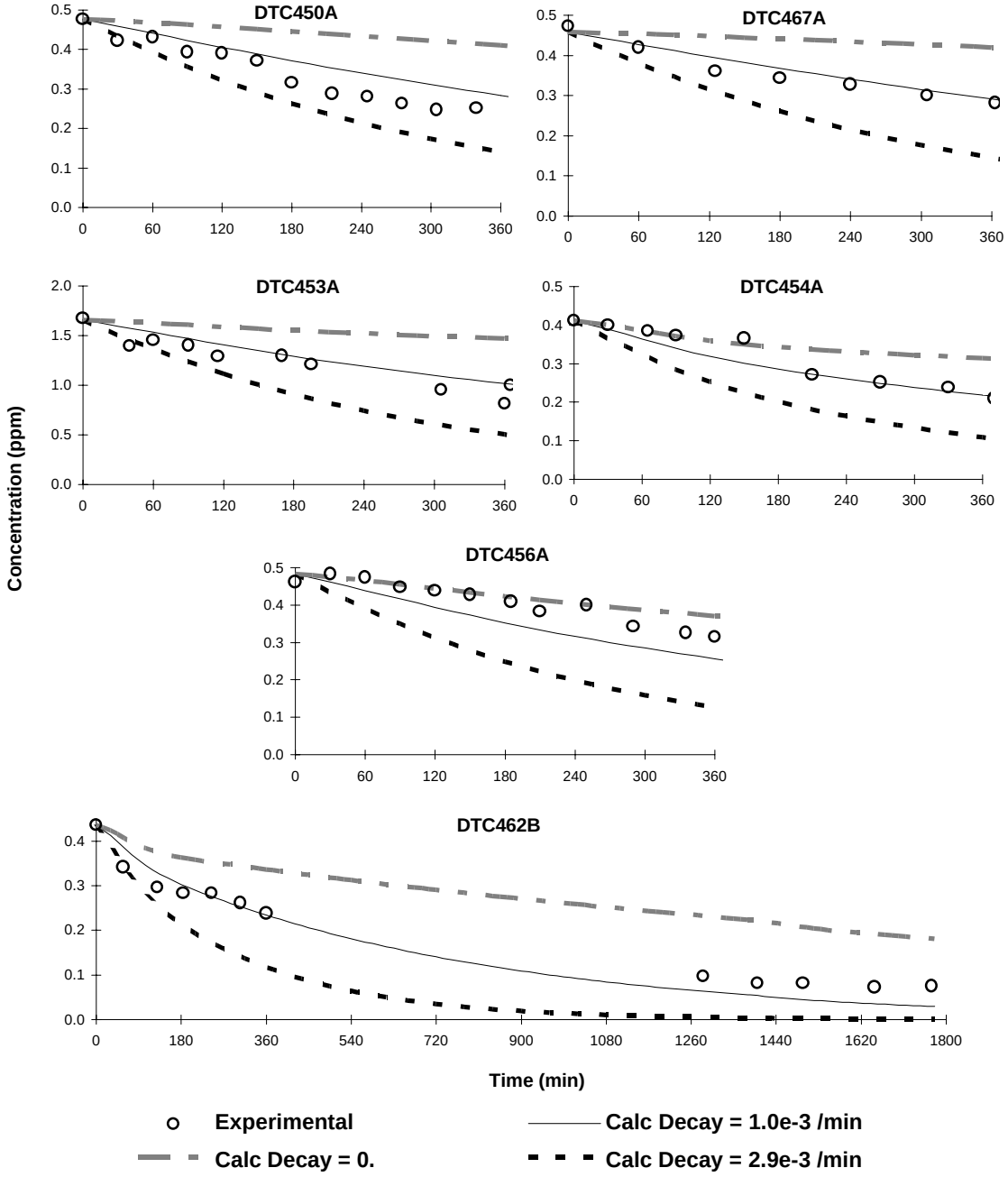

Figure 3. Experimental and calculated concentration-time plots for TDI in the TDI reactivity irradiations.

The data on Figure 3 also suggest that there is run to run variability in the apparent TDI dark decay rate.) In any case, a TDI unimolecular decay rate of 6% per hour was used in the model evaluation simulations of the TDI reactivity experiments which are discussed below.

Characterization Results and Derivation and Evaluation of Modified Chamber Effects Model

Table 2 gives a summary of the characterization and control runs carried out in association with the reactivity experiments for this program. These consisted of the following: n-butane - NO_x and CO - NO_x irradiations to measure the chamber radical source (see Carter et al, 1982, 1995c,d); pure air irradiations to measure background effects; acetaldehyde - air experiments to measure NO_x offgasing effects; ozone dark decay experiments to measure wall losses of O_3; standard propene - NO_x runs for comparison with similar standard propene runs in this and other chambers; and side equivalency tests to assess possible differences between chamber sides in reactivity experiments. The results are discussed in this section.

Runs DTC435 - DTC445 listed on Table 2 consist of relevant characterization runs carried out prior to the introduction of TDI in the chamber. As indicated on Table 2, the results were in good agreement with the predictions of the standard chamber effects model used when simulating experiments in this chamber (Carter et al, 1995c,d, 1997a), indicating that the chamber was in its normal condition. However, n-butane - NO_x run DTC448, which was carried out after TDI had been injected into Side A for various analysis tests and for the mini-surrogate + TDI reactivity experiment Run DTC447, indicated that the radical source in Side A was 2-3 times higher than normal. The radical source in Side B, which had not at that time been exposed to TDI, was in the normal range. A subsequent CO - NO_x experiment, DTC457, also indicated a higher than normal radical source in Side A, while the results in Side B, which still had not been exposed to TDI, were still in the normal range. The n-butane - NO_x run DTC461, carried out after several attempts to measure the propylene glycol + OH rate constant by forming OH radicals by reacting O_3 with alkenes in the dark, showed radical source rates higher than the levels in previous and subsequent on both sides, and may be anomalous. However, consistent with the previous n-butane or CO - NO_x runs, the radical source rate on the TDI-exposed side was twice that on the unexposed side. Immediately after that, a two day run (DTC462) was carried out where the TDI was injected onto Side B, exposing the Side B reactor to TDI for the first time. A n-butane - NO_x run (DTC463) was carried out immediately after that experiment. The radical source rate fitting the data for Side A was consistent with the previous determinations, while the radical source in Side B was about two times higher than previously, in both cases excluding the anomalously high run DTC461 from the comparisons. The n-butane - NO_x experiment carried out around the end of the program (DTC468) gave results which were very similar to those for DTC463.

Pure air and acetaldehyde - air runs were carried out to evaluate NO_x offgasing effects, but only data from the pure air runs were usable because of small amounts of initial NO_x in the chamber, which

significantly affect results of acetaldehyde - air runs. The pure air carried out prior to the TDI exposure on Side A gave results showing that background effects were similar on both sides, and were in the range predicted by the standard chamber model. However, the pure air run carried out around the end of the program, after numerous runs where TDI was in Side A and one two day run where it was in Side B, indicated that the background NO_x offgasing rate on Side A was ~2 times higher than normal, though the results for Side B were still in the normal range.

The results of these experiments were used to derive modified parameters for the chamber effects models for simulating experiments carried out in the different chamber sides after they were exposed to TDI. These parameters are given in Table A-4. As indicated there, for modeling all runs carried out in Side A after the first TDI run, the radical source and NO_x offgasing rates used were respectively 2.6 and 2 times higher than the standard chamber model. The standard chamber model was used when modeling runs carried out in Side B prior to run DTC462, while for DTC462B and following runs in Side B, the radical source parameter was increased by a factor of 1.6. These modified parameters were obtained based on the results of the n-butane - NO_x, CO - NO_x and pure air runs discussed above, excluding the apparently anomalous n-butane - NO_x run DTC461.

The implication of the apparent TDI contamination effects on the results and analysis of the TDI reactivity experiments can be evaluated by examining the data from the side equivalency tests, where the same surrogate - NO_x mixture were irradiated simultaneously on each side. One such run was carried out for each of the three types of surrogate runs, and the results are shown on Figure 4. Note that all three of these runs were carried out after runs where TDI was injected into Side A, but before any TDI exposure for Side B. The "Differences in d(O_3-NO)" and "Differences in IntOH" data can be compared with d(O_3-NO) and IntOH reactivities for experiments where 1 ppm of test compound were added. Results of model simulations, using the modified, side-specific chamber effects model derived as discussed above (and given in Table A-4), are also shown.

Figure 4 shows that the TDI exposure causes a measurable increase in the d(O_3-NO) and IntOH formation rate in the mini-surrogate experiments, and that this increase is reasonably well fit by the model simulations using the modified chamber effect parameters for Side A. Although the model slightly underpredicts the total d(O_3-NO) in both sides, it gives a good simulation of the side differences. The effect of the TDI exposure on the d(O_3-NO) in the high and low NO_x full surrogate runs is relatively small, being only slightly larger than measurement uncertainty. The IntOH effect in the higher NO_x full surrogate run is comparable to that observed in the mini-surrogate run, but the IntOH differences in the low NO_x full surrogate run are too low to measure. These relatively small side differences for the full surrogate runs are all consistent with predictions of the modified chamber effects model. Therefore, any side differences caused by TDI exposure can be taken into account in the model simulations of these runs by using the appropriately adjusted chamber effects model. The data from these side comparison tests

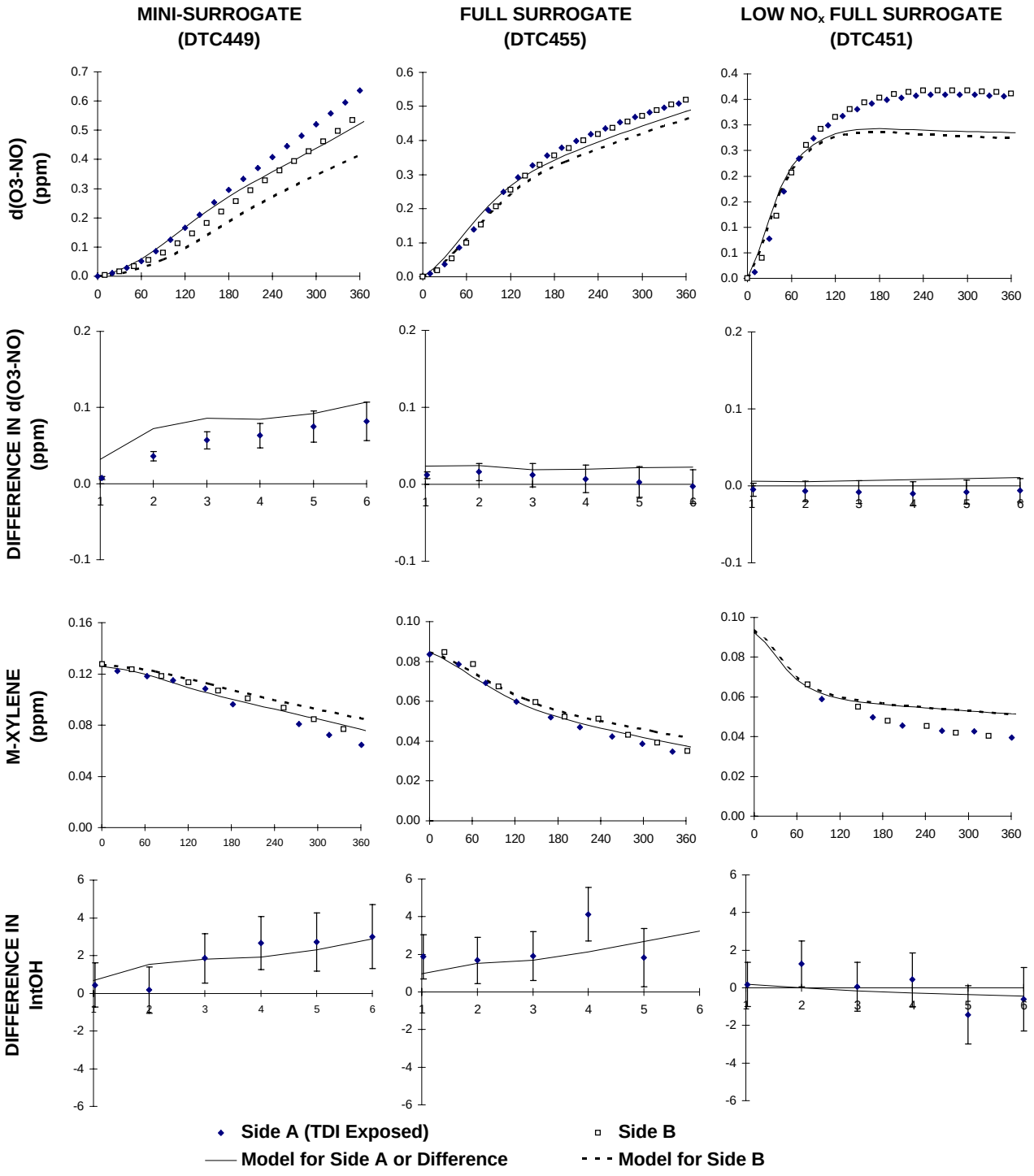

Figure 4. Plots of selected results of the side comparison tests.

indicate that these corrections will be non-negligible in the case of the mini-surrogate runs but minor for the high and low NO_x full surrogate runs.

Results of The Reactivity Experiments

Experimental Results

Summaries of the conditions and results of the incremental reactivity experiments were given on Table 3, above, and Figures 5-13 show concentration-time plots of the major results from all of these experiments. Note that a total of seven runs, two or three each for each type of surrogate, were carried out for 2,4-TDI, and two runs, one mini-surrogate and one low NO_x full surrogate, were carried out for 2,6-TDI. In addition, as shown on Figure 13, one of the low NO_x full surrogate runs with 2,4-TDI was carried out for a ~18 hour time period, to determine if the apparent inhibition of O_3 by TDI persisted over longer time periods.

Figures 4-6 show the results of the three mini-surrogate + TDI experiments. It can be seen that both TDI isomers significantly slow down the rates of NO oxidation and O_3 formation (i.e., $d(O_3\text{-NO})$ formation) and of m-xylene consumption, indicating negative $d(O_3\text{-NO})$ and IntOH reactivities. Note that the inhibiting effects of TDI in the mini-surrogate experiments are in the opposite direction than expected based on the fact that TDI exposure apparently causes the chamber radical source to increase. The relatively large negative IntOH reactivities indicate that TDI has significant radical inhibition processes in its mechanism. Since $d(O_3\text{-NO})$ reactivities in mini-surrogate runs tend to be highly sensitive to radical inhibition effects (Carter et al, 1995b), this is probably the main reason that the $d(O_3\text{-NO})$ reactivities are also negative. Note Runs DTC450 and DTC467, carried out by adding comparable amounts of 2,4- or 2,6-TDI, give very similar results, indicating that the two TDI isomers have very similar radical inhibition effects.

Figures 7 and 8 show the results of the high NO_x full surrogate experiments. Again TDI addition is seen to significantly inhibit both IntOH and $d(O_3\text{-NO})$ levels. The IntOH inhibition is consistent with the results of the mini-surrogate runs, and again indicate its radical inhibiting effect. The fact that TDI also inhibits $d(O_3\text{-NO})$ to almost the same extent that it does in the mini-surrogate runs is of interest, since $d(O_3\text{-NO})$ reactivities in the full surrogate runs are relatively less sensitive to radical inhibition/initiation effects, and more sensitive to direct NO to NO_2 conversions by the test compound, than is the case for the mini-surrogate runs. For example, the n-alkanes, which also act as radical inhibitors, have negative $d(O_3\text{-NO})$ reactivities in the mini-surrogate runs, but have small and often slightly positive $d(O_3\text{-NO})$ reactivities in the full surrogate runs due to the compensating effect of the relatively large number of NO to NO_2 conversions in their mechanisms (Carter et al, 1995b, 1996). The fact that TDI has almost as large negative $d(O_3\text{-NO})$ reactivities with the full surrogate as it does with the mini-surrogate suggests that TDI may not have large amounts of NO to NO_2 conversions involved in its photooxidations, at least compared to other compounds such as alkanes.

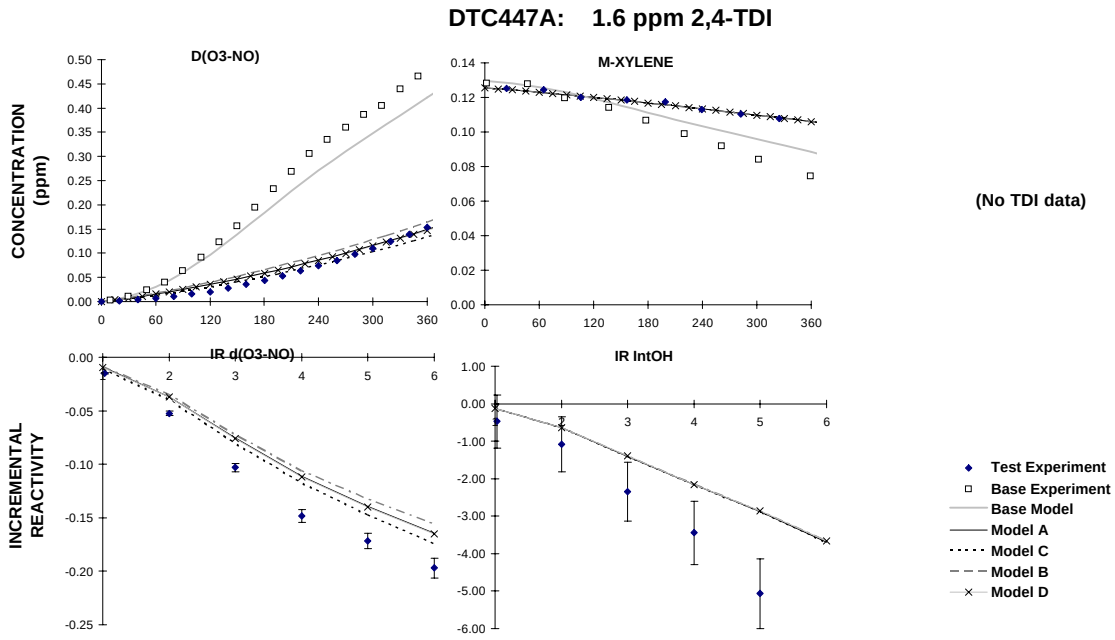

Figure 5. Plots of selected results of the mini-surrogate +2,4-TDI run DTC-447.

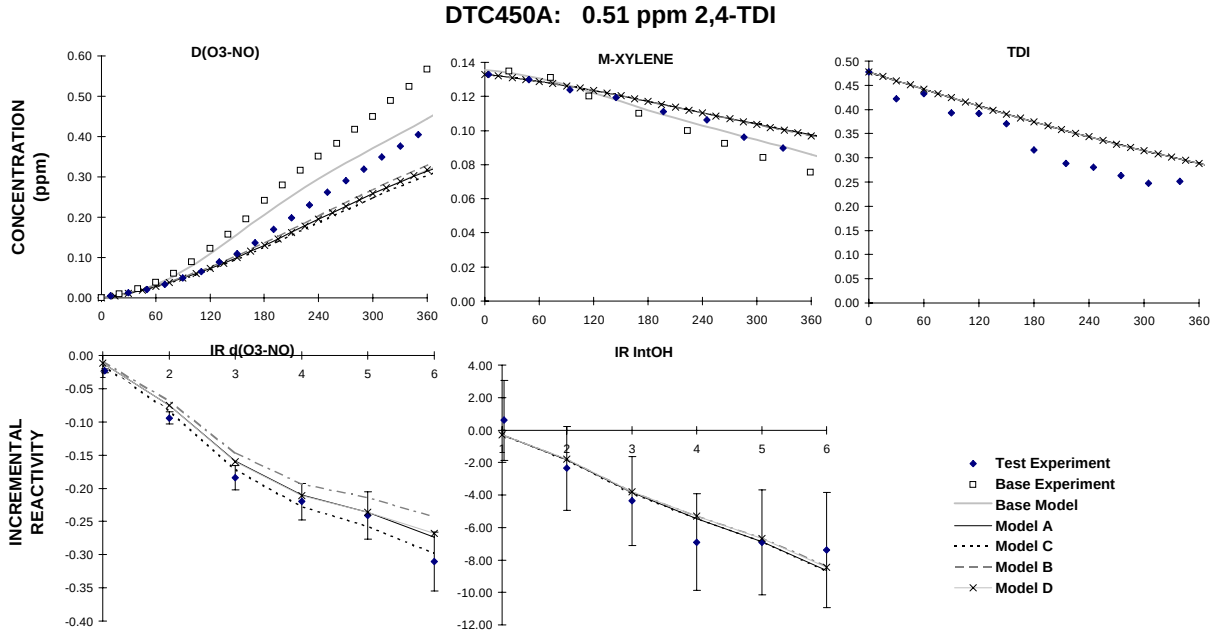

Figure 6. Plots of selected results of the mini-surrogate + 2,4-TDI run DTC-450.

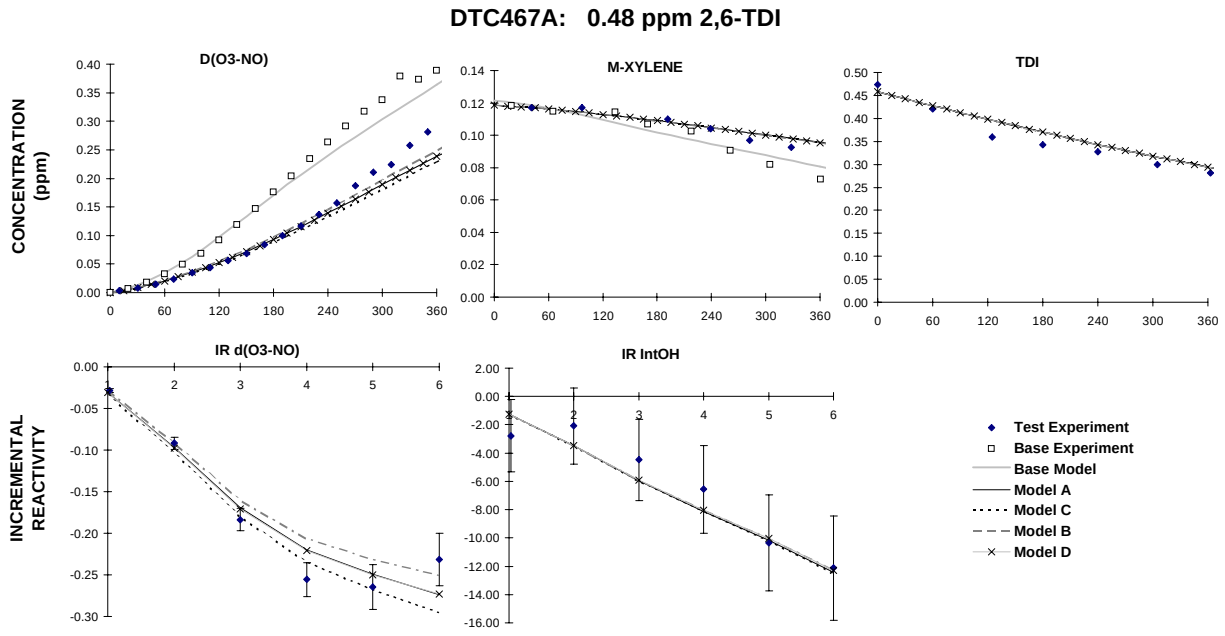

Figure 7. Plots of selected results of the mini-surrogate + 2,6-TDI run DTC-467.

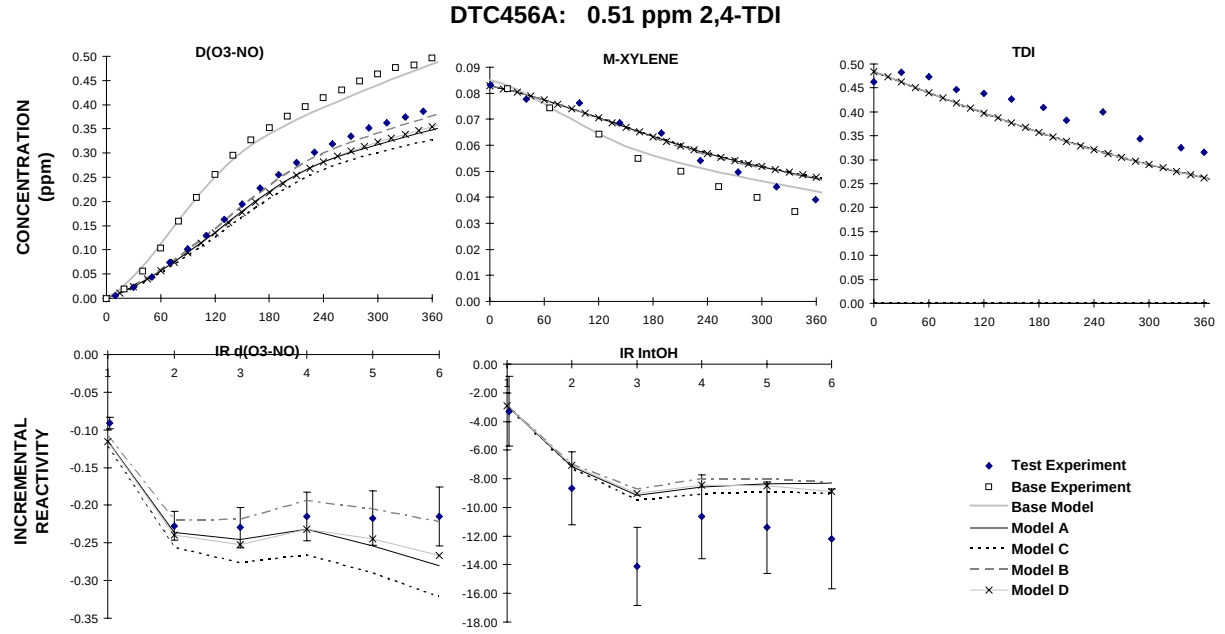

Figure 8. Plots of selected results of the full surrogate + 2,4-TDI run DTC-456.

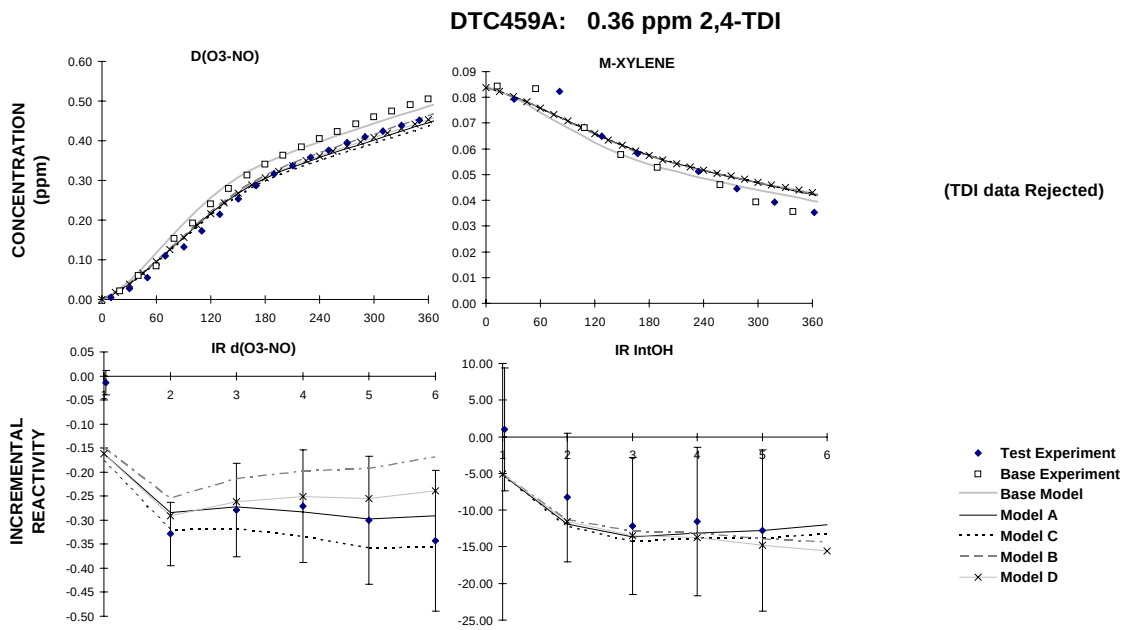

Figure 9. Plots of selected results of the full surrogate + 2,4-TDI run DTC-459.

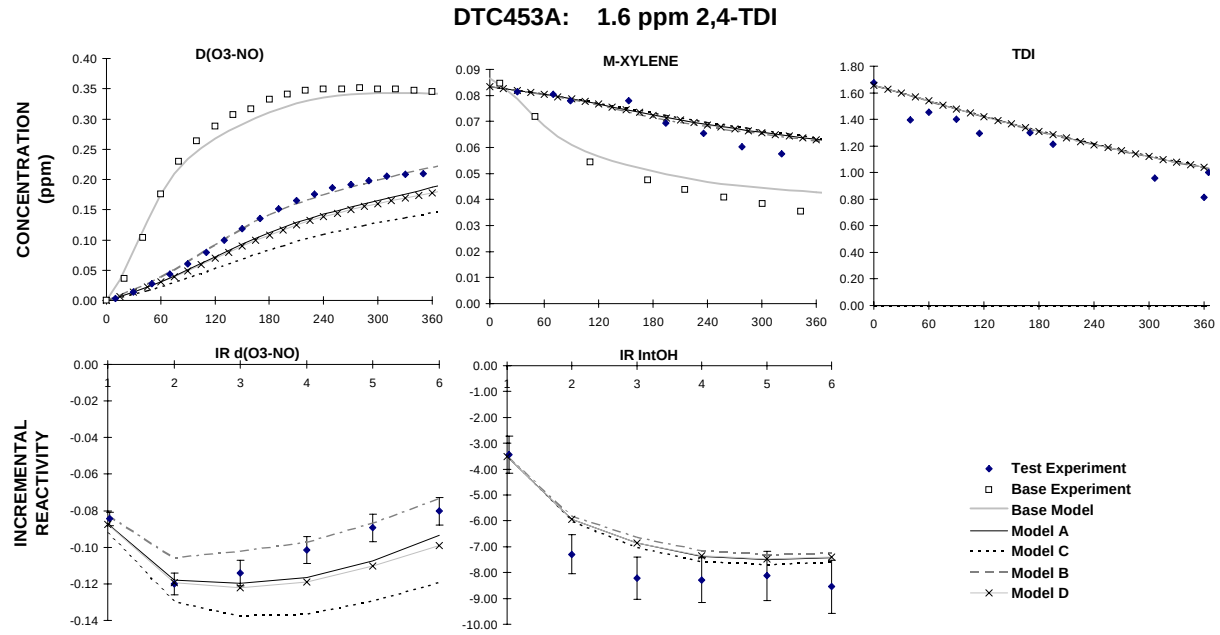

Figure 10 Plots of selected results of the low NO_x full surrogate + 2,4-TDI run DTC-453.

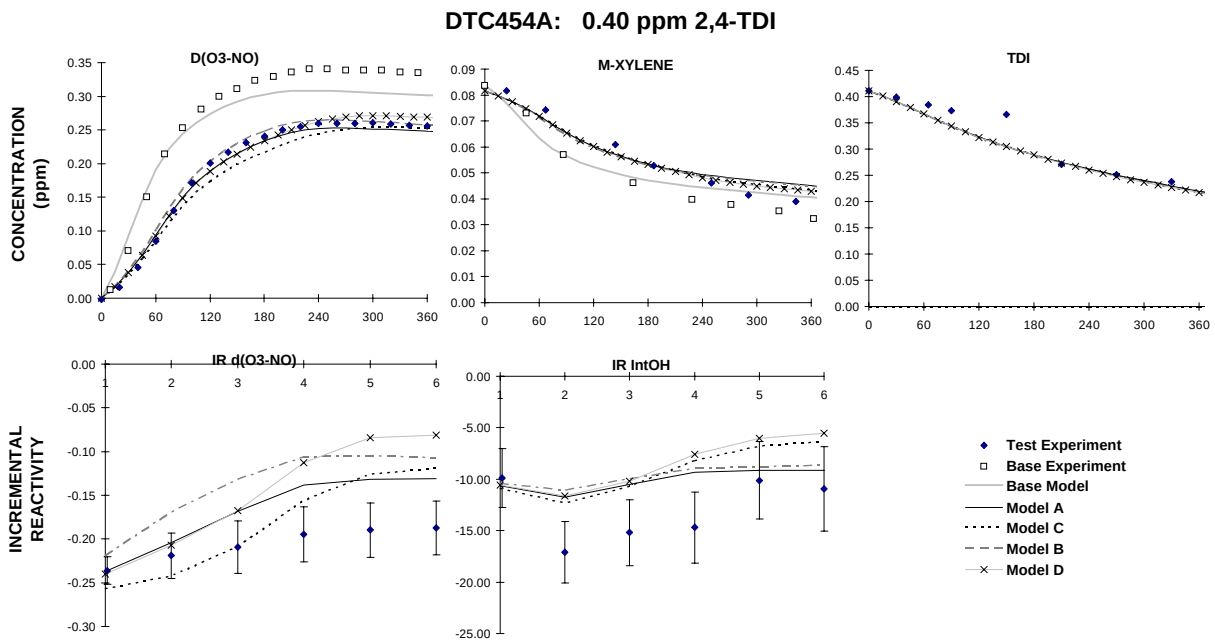

Figure 11. Plots of selected results of the low NO_x full surrogate + 2,4-TDI run DTC-454.

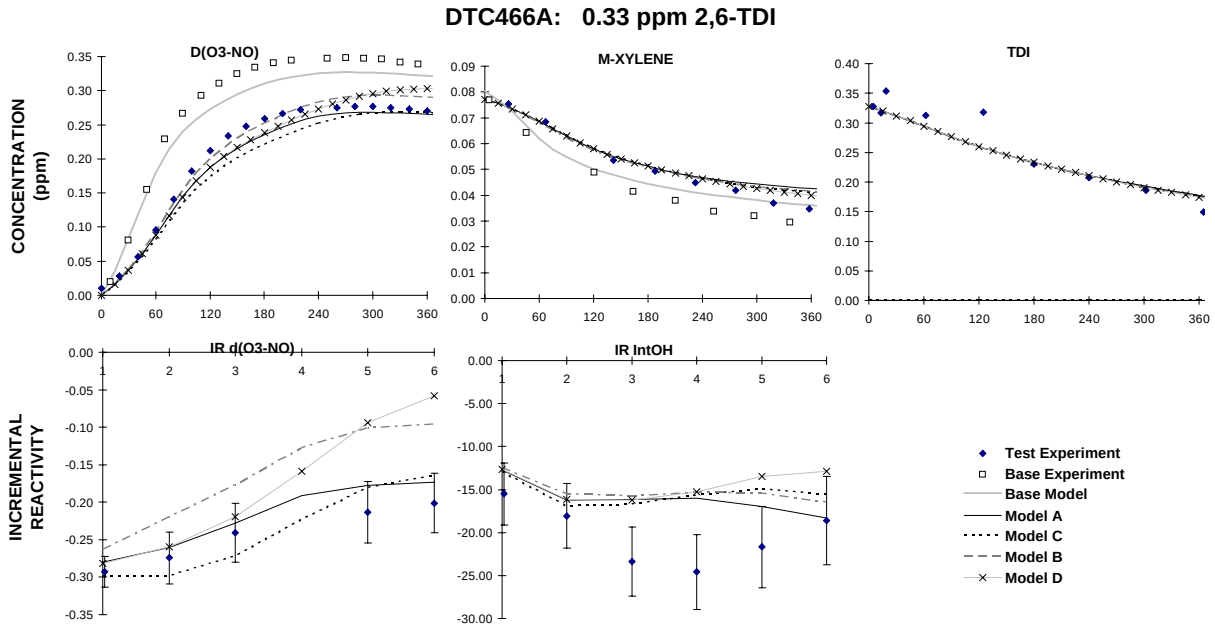

Figure 12. Plots of selected results of the low NO_x full surrogate + 2,6-TDI run DTC-466

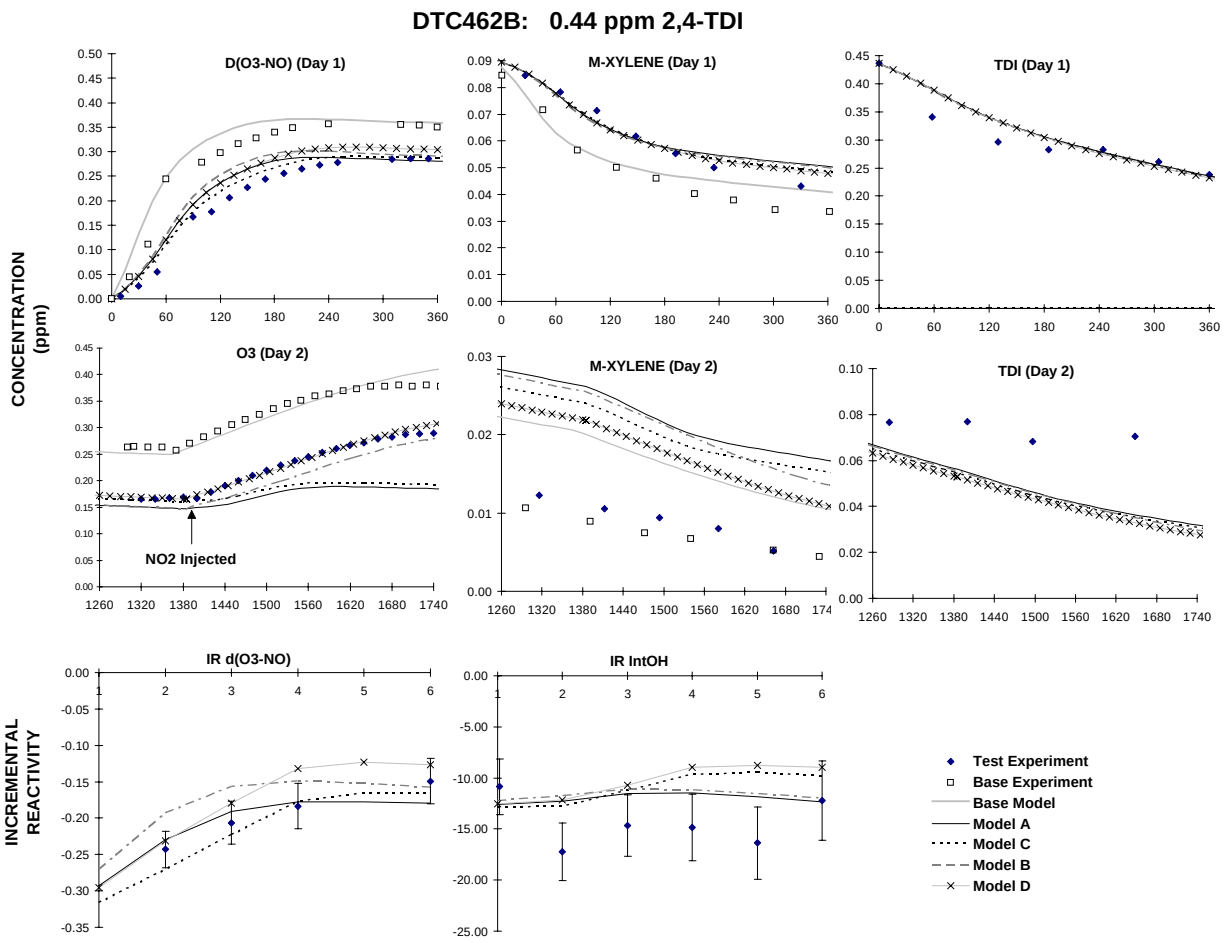

Figure 13. Plots of selected results of the two-day low NO_x full surrogate + 2,4-TDI run DTC-462. (Reactivity data shown only for first day.)

Figures 10-13 show the results of the low NO_x full surrogate experiments. Again, the TDI inhibited both IntOH and d(O_3-NO) levels. Very similar results were obtained in the comparable experiments with the 2,4- and 2,6-TDI isomers (Runs DTC454 and DTC466, respectively), again indicating no significant isomeric differences in the major TDI reactivity characteristics. The negative d(O_3-NO) reactivities during the initial stages of the experiments are consistent with the results of the high NO_x full surrogate runs, since generally they are sensitive to the same mechanistic factors. However, the low NO_x full surrogate runs are also useful in indicating effect of the test compound on peak O_3 yields under conditions which are NO_x limited, which are sensitive to aspects of the mechanism affecting NO_x removal rates. The fact that TDI still has a significantly negative d(O_3-NO) incremental reactivity at the end of these experiments means that the TDI photooxidation process must involve significant NO_x sinks as well as radical sinks. This is despite the fact that speculative reactions can be derived where oxidation of the isocyanate groups may possibly result in releasing NO into the system. If TDI oxidation involved NO_x formation and had no counter-balancing NO_x sinks, then it would be expected to have a positive effect on the ultimate O_3 yield by the end of these low NO_x experiments. This clearly is not the case. NO may indeed be formed, but if so there must be stronger NO_x sinks in the overall photooxidation which counteracts its effect.

To evaluate whether the inhibiting effects of TDI would persist over time periods longer than a day, the irradiation was continued for a ~18 hours in the low NO_x full surrogate run DTC462. Since the O_3 formation had stopped by the end of the first ~5 hours of the run, additional NO_2 was injected after ~12 hours. The addition of NO_2 caused O_3 formation to resume, at approximately the same rate on both sides. However, since the initial O_3 was lower on the TDI side, the final O_3 on the TDI side was also lower. This suggests that TDI apparently does not form significant amounts of reactive products whose reactions may cause higher ozone levels in the long run. On the other hand, the fact that O_3 formation rate on the second day was not significantly slower on the TDI-exposed side than the base case side suggest that TDI also doesn't form persistent products which tend to cause continued O_3 inhibition in multi-day scenarios. This observation may be useful in evaluating several of the alternative models for TDI's atmospheric reactions, as discussed below.

Model Adjustments and Alternative Models Considered

As discussed above, the TDI photooxidation reactions were modeled using a parameterized single-step mechanism with the net effect of the OH + TDI reactions being represented as regenerating an adjustable amount (y_{OH}) of OH radicals, with an adjustable number ($y_{NO\rightarrow NO2}$) of NO to NO_2 conversions, and forming adjustable yields of various products, including y_{NO} NO, y_{CRES} cresols, $y_{NO\rightarrow NPHE}$ nitrophenols, and y_{AFG2} photoreactive fragmentation products. The following adjustments were made based on the experimental observations discussed above. These were found to be necessary to obtain model predictions which are even approximately consistent with the data:

- Since the results of the mini-surrogate experiments indicate that TDI has strong radical inhibition characteristics, we assume that photoreactive radical initiators such as AFG2 are not formed to a significant extent (i.e, that $y_{AFG2} = 0$). If this is assumed, the results of the mini-surrogate experiments are best fit by assuming ~70% radical inhibition, i.e., $y_{OH} = 0.3$. An alternative would be to assume non-negligible yields of initiating products such as AFG2, and compensate for this by assuming lower levels of y_{OH}. However, this type of model would predict a greater degree of initiation at the very beginning of the experiment than is the case later on, which is not indicated by the data.

- As discussed above, the fact that TDI is almost as much an inhibitor of $d(O_3\text{-NO})$ in the full surrogate experiments as it is in the mini-surrogate runs suggests that there are relatively few NO to NO_2 conversions in the TDI photooxidation process. Consistent with this, the inhibition of $d(O_3\text{-NO})$ in the full surrogate experiments are indeed significantly overpredicted if any net NO consumption or NO to NO_2 conversion is assumed in the model. Best fits are obtained if it is assumed that $y_{NO\rightarrow NO2} = 0$.

- The fact that TDI inhibits final O_3 yields in the low NO_x full surrogate runs indicates that TDI probably has overall NO_x sinks in its mechanism. Consistent with this, the inhibition by TDI of the peak O_3 levels in these runs are significantly underpredicted unless the model either assumes formation of significant yields of cresols (with the data being best fit by $y_{CRES} = 1$), or assumes other significant net NO_x-sink processes such as nitrophenol formation via peroxy + NO reactions.

The simplest overall process for the reaction of TDI with OH radicals which is consistent with these observations and adjustments is as follows:

$$\text{OH + TDI} \rightarrow \rightarrow \text{0.3 OH + CRES} \qquad \text{(Model A)}$$

As indicated, this is referred to as Model A in the subsequent discussion. However, the NO_x sinks needed to fit the low NO_x reactivity data can also be represented by formation of products such as nitrophenols from the reactions of NO with peroxy radicals formed in the TDI photooxidation. To conserve radicals, the maximum value of $y_{NO\rightarrow NPHE}$ which is consistent with the best fit value of y_{OH} is 0.7, but the data are best fit by assuming that $y_{NO\rightarrow NPHE} \approx 0.5$. Therefore, an alternative TDI model which takes these observations into account is

$$\text{OH + TDI} \rightarrow \rightarrow \text{0.3 OH + 0.5 RO2-NP.} \qquad \text{(Model B)}$$

where, as shown on Table A-1 in Appendix A, RO2-NP. reacts in the presence of NO_x to form nitrophenols.

$$\text{RO2-NP.} + \text{NO} \rightarrow \text{NPHE.}$$

As indicated, this alternative is referred to as Model B in the subsequent discussion. Note that the NPHE model species, like CRES, is also assumed to remove NO_x via NO_3 radicals reaction (see Table A-1 in Appendix A). Alternative models which assume that the peroxy + NO reaction forms alkyl nitrate species (RNO3), as is used in the mechanisms for the alkanes and other saturated compounds (Carter, 1990), do not provide a sufficient NO_x sink to correctly simulate the TDI reactivities in the low NO_x surrogate runs. This is because the RNO3 model species does not react to provide the NO_x sinks required for the model to simulate these data.

As suggested above, the possibility that NO might be generated as a product of oxidation at the isocyanate group needs to be considered. To be consistent with radical balance and the regeneration of 0.3 moles of OH as assumed in the models, the maximum overall yield of NO would be 0.7, though an NO yield of 0.5 was used in the test calculations. The impact of this reaction on the model simulations was evaluated by considering two alternative versions of Models A and B, where 0.5 moles of NO is also assumed to be a product, i.e.:

$$\text{OH + TDI} \rightarrow \rightarrow \text{0.3 OH + CRES + 0.5 NO} \qquad \text{(Model C)}$$

$$\text{OH + TDI} \rightarrow \rightarrow \text{0.3 OH + 0.5 RO2-NP. + 0.5 NO} \qquad \text{(Model D)}$$

As indicated, these are referred to as Models C and D, respectively.

Results of Model Simulations of the Chamber Experiments

Figures 5 - 13 show the results of the model simulations of all the reactivity experiments using the four alternative TDI photooxidation models. The data for the four mini-surrogate runs are shown on Figures 5-7. All four models give about the same predictions, and, as expected since they were adjusted to do so, fit the $d(O_3\text{-NO})$ reactivity data reasonably well. The slight underprediction of the inhibition for run DTC447 is well within the uncertainty due to the uncertainty in the initial TDI concentration, which had to be estimated because there were no valid TDI data. Note that although the model was adjusted to fit the $d(O_3\text{-NO})$ reactivity data, it also fit the IntOH reactivity data quite well. Note also that the model is consistent with the data in predicting that the relative rate of inhibition does not change significantly with time, as might be the case if either the inhibition were due primarily to the formation of a highly inhibiting product, or if larger inhibition in the primary TDI reaction was being partially offset by formation of radical initiating products.

Figures 8 and 9 show the results of the model simulations of the two high NO_x full surrogate runs. Although the differences between the $d(O_3\text{-NO})$ predictions of the four models was somewhat greater than was the case for the mini-surrogate runs (there were no differences in the IntOH predictions), the differences are within the experimental uncertainties of the reactivity data. The fact four alternative TDI mechanisms give very similar predictions in the simulations of the high NO_x reactivity experiments is

expected, since the differences between them primarily concern NO_x sources and sinks, or yields of products which are NO_x sinks. The d(O_3-NO) and IntOH reactivity data in the high NO_x full surrogate runs are well fit by all models. This is in part due to the adjustment of the NO to NO_2 conversion parameter, $y_{NO \rightarrow NO2}$, to a low value to fit these data. Note that acceptable fits to the data for run DTC459 could not be obtained if the high initial TDI based on the HPLC data were used; model predictions which are much more consistent with the simulations of the other run (DTC456A) are obtained if the initial TDI is derived based on the THC data, as indicated in Footnote [e] to Table 3.

Figures 10-13 show the results of the model simulations of the four low NO_x full surrogate runs. Although as expected the differences between the predictions of the four models is somewhat greater than in the simulations of the lower NO_x runs, the differences between the simulations of the Day 1 reactivity results are also probably within the uncertainty of the data. (However, this is not the case for the Day 2 data for run DTC462, as discussed below.) All four models give reasonably good fits to the Day 1 reactivity data. This good fit is due in part to the inclusion of the NO_x sink processes in the models (either cresol formation in Models A and C or nitrophenol formation from peroxy + NO reactions in Models B and D). Without assuming these NO_x-sink processes, the models predict that TDI will not inhibit the final O_3 at the end of the runs to the extent that is observed, and instead predict that the d(O_3-NO) reactivities will approach zero or even become slightly positive by the end of the runs, contrary to the observation that they remain almost constant at relatively large negative values throughout the latter part of the experiments.

It is only on the simulations of the second day of the two-day run DTC462 that the differences between the alternative mechanisms become apparent. When fresh NO_2 is injected into the chamber after ~24 hours of irradiation, the O_3 is observed to increase on both the added TDI and the control side at about the same rate. This rate of increase on the base case side is reasonably well fit by the base case model, and the rate of increase on the added TDI side is reasonably well fit by the predictions of Models B and D, which represent the NO_x sink by the formation of nitrophenols from peroxy + NO reactions. On the other hand, Models A and C, which represent the NO_x sink by the formation of cresol-like products, predicts that only slight O_3 increases result when NO_2 is added to TDI side with TDI, much less than observed. This predicted continued inhibition of O_3 is caused by the added NO_x being removed relatively rapidly by the reactions of cresols with the NO_3 radicals formed from the reaction of NO_2 with O_3. Apparently, any TDI products which react with NO_3 radicals do not persist to the extent that is predicted by Models A or C.

Note that the precision of the data is not sufficient to permit conclusions about the relative performances of Models A *vs* C or Models B *vs* D. In other words, the data are inconclusive about whether the reactions of TDI may involve the release of NO. The effect of this NO_x source and O_3 sink (since NO reacts with O_3) on the results of the simulations of the experiments is apparently not as

important as the effects of varying the uncertain parameters in the mechanism which are adjusted to fit the data. However, the effects may be non-negligible in affecting predicted atmospheric reactivity, as discussed in the following section.

Atmospheric Reactivity Calculations

Since incremental reactivities in environmental chamber experiments are not necessarily the same as those in the atmosphere (Carter and Atkinson, 1989a; Carter et al, 1995b), atmospheric reactivity simulations are needed to assess the atmospheric implications of our results. Table 4 shows the relative ozone impacts, in terms of ozone formed per gram of mixture or compound added, calculated for various types of atmospheric conditions for each of the four models for TDI's atmospheric reactions. For comparison purposes, the relative impacts of ethane, the compound the EPA has used as the basis for determining VOC exemptions (Dimitriades, 1996), are also shown. The ozone impacts are quantified both in terms of peak ozone (ozone yield) and in terms of integrated ozone over 0.12 ppm ($IntO_3$>0.12). The ozone impacts are shown relative to the ozone impact caused by increasing the mass emissions of all VOCs, so the numbers shown are the relative effects of controlling emissions of the mixture or compound compared to controlling emissions of VOCs from all sources equally. The data are shown for each of the 39 "base case" EKMA scenarios, together with the corresponding averages and standard deviations, and for the three adjusted NO_x scenarios.

Table 4 shows that all four TDI models predict it will have a negative ozone impact in all of the EKMA model scenarios. The calculations for the adjusted NO_x scenarios indicate that the amount of ozone inhibition, relative to the incremental reactivity of the base ROG mixture, is highly sensitive to NO_x conditions, with the magnitude of the relative O_3 inhibition increasing markedly as the NO_x is reduced. However, part of this increase in relative inhibition with decreasing NO_x could be due to the fact that the denominator, the base ROG reactivity, decreases with decreasing NO_x levels. The absolute incremental reactivities of the TDI models and the base ROG mixture, quantified by ozone yield, is shown on Table 5. It shows that the for Models A-C the absolute amount of inhibition of peak O_3 yields caused by TDI still increases as NO_x is reduced, though to a much lesser extent than the O_3 inhibition relative to the base ROG reactivity In addition, the absolute TDI incremental reactivities predicted by Model D are almost independent of NO_x levels. There is also somewhat less variability of the absolute TDI reactivity among the base case scenarios, compared to the relative reactivities, particularly for Model D. This greater variability of relative compared to absolute reactivities is unusual, and indicates that the ozone impacts of TDI are affected quite differently by varying atmospheric conditions than those for the positively reactive VOCs such as those in the base ROG mixture.

Tables 4 and 5 show that none of the four alternative TDI mechanisms predict that TDI is positively reactive in any of the EKMA scenarios. However, the four alternative TDI mechanisms do differ somewhat in their predictions of how much O_3 inhibition is caused by TDI in the various scenarios.

Table 4. Summary of calculated incremental reactivities (gram basis) for the four alternative TDI models and ethane, relative to the average of all VOC emissions.

Scenario	O_3 Yield Relative Reactivities					$IntO_3$ >0.12 Relative Reactivities				
	Ethane	TDI				Ethane	TDI			
		A	B	C	D		A	B	C	D
Adjusted NO_x										
Max React	0.08	-0.04	-0.11	-0.15	-0.22	0.07	-0.07	-0.12	-0.16	-0.22
Max Ozone	0.15	-0.98	-0.69	-0.87	-0.59	0.10	-0.52	-0.43	-0.52	-0.43
Equal Benefit	0.20	-2.59	-1.79	-1.98	-1.19	0.13	-1.60	-1.17	-1.22	-0.80
Base Case										
Average	**0.18**	**-2.09**	**-1.40**	**-1.63**	**-0.94**	**0.12**	**-1.20**	**-0.91**	**-0.93**	**-0.64**
St.Dev	**0.04**	**1.70**	**0.83**	**1.44**	**0.50**	**0.03**	**0.80**	**0.53**	**0.61**	**0.25**
ATL GA	0.17	-1.36	-1.24	-0.89	-0.76	0.12	-0.96	-0.91	-0.62	-0.57
AUS TX	0.20	-2.58	-1.92	-1.70	-1.05	0.14	-1.92	-1.46	-1.22	-0.77
BAL MD	0.16	-1.61	-0.84	-1.46	-0.69	0.09	-0.62	-0.40	-0.63	-0.41
BAT LA	0.16	-1.50	-1.12	-1.24	-0.86	0.11	-0.98	-0.80	-0.84	-0.66
BIR AL	0.24	-4.05	-2.35	-3.27	-1.56	0.14	-2.21	-1.37	-1.80	-0.95
BOS MA	0.21	-1.88	-1.39	-1.38	-0.89	0.13	-1.10	-0.85	-0.83	-0.59
CHA NC	0.21	-2.35	-2.04	-1.15	-0.84	0.17	-1.91	-1.69	-0.87	-0.65
CHI IL	0.28	-9.59	-4.97	-7.82	-3.19	0.14	-4.54	-2.55	-3.67	-1.68
CIN OH	0.20	-1.81	-1.25	-1.41	-0.86	0.13	-1.01	-0.74	-0.82	-0.56
CLE OH	0.15	-1.72	-1.05	-1.48	-0.81	0.09	-0.77	-0.54	-0.73	-0.49
DAL TX	0.12	-0.40	-0.34	-0.44	-0.39	0.09	-0.30	-0.29	-0.37	-0.36
DEN CO	0.11	-1.05	-0.75	-0.91	-0.61	0.08	-0.50	-0.41	-0.50	-0.41
DET MI	0.20	-2.10	-1.33	-1.73	-0.96	0.12	-0.99	-0.70	-0.87	-0.58
ELP TX	0.12	-1.08	-0.82	-0.90	-0.63	0.08	-0.67	-0.55	-0.60	-0.49
HAR CT	0.21	-2.19	-1.85	-1.39	-1.06	0.15	-1.49	-1.32	-0.91	-0.74
HOU TX	0.19	-1.76	-1.01	-1.55	-0.81	0.12	-0.99	-0.64	-0.93	-0.58
IND IN	0.16	-1.36	-1.06	-1.10	-0.81	0.11	-0.78	-0.66	-0.69	-0.57
JAC FL	0.17	-1.29	-1.41	-0.67	-0.80	0.14	-1.07	-1.23	-0.51	-0.66
KAN MO	0.20	-1.32	-1.26	-0.79	-0.73	0.15	-0.90	-0.89	-0.55	-0.54
LAK LA	0.23	-3.34	-2.31	-2.65	-1.62	0.14	-2.31	-1.74	-1.79	-1.22
LOS CA	0.15	-3.85	-1.51	-3.51	-1.17	0.09	-1.71	-0.78	-1.62	-0.69
LOU KY	0.19	-1.11	-0.92	-0.88	-0.70	0.14	-0.78	-0.69	-0.64	-0.55
MEM TN	0.21	-2.20	-1.59	-1.71	-1.09	0.14	-1.41	-1.07	-1.10	-0.76
MIA FL	0.19	-2.25	-2.23	-0.94	-0.91	0.18	-2.13	-2.13	-0.83	-0.83
NAS TN	0.24	-2.33	-2.11	-1.40	-1.18	0.20	-2.08	-1.93	-1.12	-0.98
NEW NY	0.18	-6.92	-2.94	-6.03	-2.05	0.09	-2.46	-1.15	-2.22	-0.91
PHI PA	0.18	-1.44	-1.05	-1.20	-0.81	0.12	-0.79	-0.63	-0.70	-0.55
PHO AZ	0.17	-2.34	-1.22	-2.06	-0.94	0.10	-1.08	-0.65	-1.01	-0.58
POR OR	0.18	-1.19	-1.19	-0.75	-0.75	0.15	-0.93	-0.97	-0.56	-0.60
RIC VA	0.19	-2.00	-1.38	-1.61	-0.98	0.12	-1.02	-0.76	-0.86	-0.60
SAC CA	0.18	-1.24	-1.08	-0.95	-0.80	0.12	-0.79	-0.75	-0.64	-0.60
SAI MO	0.15	-1.78	-0.93	-1.61	-0.76	0.09	-0.73	-0.46	-0.72	-0.45
SAL UT	0.19	-2.54	-1.69	-1.89	-1.05	0.12	-1.46	-1.02	-1.11	-0.68
SAN TX	0.13	-0.39	-0.44	-0.33	-0.39	0.12	-0.36	-0.42	-0.32	-0.38
SDO CA	0.12	-1.40	-1.02	-1.14	-0.76	0.10	-0.94	-0.73	-0.80	-0.60
SFO CA	0.06	-0.08	-0.12	-0.16	-0.20	0.05	-0.12	-0.14	-0.20	-0.22
TAM FL	0.14	-0.69	-0.59	-0.64	-0.54	0.10	-0.45	-0.42	-0.47	-0.44
TUL OK	0.18	-1.22	-0.90	-1.00	-0.69	0.12	-0.64	-0.52	-0.58	-0.46
WAS DC	0.20	-2.08	-1.20	-1.79	-0.91	0.12	-1.08	-0.70	-0.98	-0.60

Table 5. Summary of calculated absolute incremental reactivities (gram basis) for the four alternative TDI models and for the average of all VOC emissions.

Scenario	O_3 Yield Incremental Reactivities (g O_3 / g VOC)				
	Base	TDI			
	ROG	A	B	C	D
Adjusted NO_x					
Max React	1.25	-0.05	-0.14	-0.18	-0.27
Max Ozone	0.45	-0.44	-0.31	-0.39	-0.27
Equal Benefit	0.24	-0.62	-0.43	-0.47	-0.28
Base Case					
Average	**0.32**	**-0.52**	**-0.36**	**-0.41**	**-0.25**
St.Dev	**0.12**	**0.19**	**0.09**	**0.17**	**0.05**
ATL GA	0.27	-0.37	-0.34	-0.24	-0.21
AUS TX	0.22	-0.56	-0.42	-0.37	-0.23
BAL MD	0.41	-0.66	-0.34	-0.59	-0.28
BAT LA	0.25	-0.38	-0.28	-0.31	-0.22
BIR AL	0.24	-0.96	-0.56	-0.78	-0.37
BOS MA	0.24	-0.45	-0.33	-0.33	-0.21
CHA NC	0.19	-0.44	-0.38	-0.22	-0.16
CHI IL	0.09	-0.89	-0.46	-0.73	-0.30
CIN OH	0.34	-0.61	-0.43	-0.48	-0.29
CLE OH	0.34	-0.59	-0.36	-0.51	-0.28
DAL TX	0.60	-0.24	-0.21	-0.26	-0.23
DEN CO	0.41	-0.43	-0.31	-0.37	-0.25
DET MI	0.30	-0.64	-0.40	-0.52	-0.29
ELP TX	0.39	-0.43	-0.32	-0.35	-0.25
HAR CT	0.26	-0.58	-0.49	-0.37	-0.28
HOU TX	0.32	-0.57	-0.33	-0.50	-0.26
IND IN	0.39	-0.53	-0.42	-0.43	-0.32
JAC FL	0.24	-0.31	-0.34	-0.16	-0.19
KAN MO	0.34	-0.45	-0.43	-0.27	-0.25
LAK LA	0.16	-0.53	-0.37	-0.42	-0.26
LOS CA	0.17	-0.65	-0.25	-0.59	-0.20
LOU KY	0.40	-0.44	-0.37	-0.35	-0.28
MEM TN	0.26	-0.57	-0.41	-0.45	-0.29
MIA FL	0.19	-0.42	-0.41	-0.17	-0.17
NAS TN	0.24	-0.56	-0.51	-0.34	-0.29
NEW NY	0.11	-0.78	-0.33	-0.68	-0.23
PHI PA	0.33	-0.48	-0.35	-0.40	-0.27
PHO AZ	0.37	-0.86	-0.45	-0.76	-0.35
POR OR	0.32	-0.39	-0.39	-0.24	-0.24
RIC VA	0.33	-0.66	-0.45	-0.53	-0.32
SAC CA	0.37	-0.45	-0.40	-0.35	-0.29
SAI MO	0.35	-0.63	-0.33	-0.56	-0.27
SAL UT	0.28	-0.72	-0.48	-0.54	-0.30
SAN TX	0.51	-0.20	-0.23	-0.17	-0.20
SDO CA	0.25	-0.35	-0.26	-0.29	-0.19
SFO CA	0.70	-0.06	-0.08	-0.12	-0.14
TAM FL	0.46	-0.32	-0.27	-0.29	-0.25
TUL OK	0.37	-0.45	-0.33	-0.37	-0.25
WAS DC	0.31	-0.65	-0.37	-0.56	-0.28

The sensitivity to chemical mechanism differences appears to be the highest in the relatively high NO_x MIR scenario, and tends to decline as the relative NO_x levels decrease. The issue of whether NO is formed in the TDI photooxidation process (as assumed in Models C and D but not A and B) appears to a factor affecting how O_3 inhibition by TDI is affected by NO_x levels. The models assuming NO is generated predict greater inhibition at high NO_x levels (because of the reaction of NO with O_3) and lower inhibition at low NO_x levels (because it counteracts the other NO_x sinks in the TDI mechanism), with the net result being that the sensitivity of the ozone inhibition to NO_x levels is reduced. Note that the chamber data are somewhat more consistent with the predictions of the models which assume the NO_x sink is due to nitrophenol formation (i.e., Models C and D), and that these models also tend to predict lower sensitivity of TDI inhibition to NO_x levels then is the case for the alternative models.

An EKMA scenario modified to run over a five day period, with equal emissions and conditions on each day, was run to determine if TDI's inhibiting effects may be different under multi-day stagnation conditions. TDI model "D" was used, since it gave the best fit to the results of the 18 hour chamber experiment. The results indicated that TDI's inhibition of O_3 was essentially the same on each day of the simulation. Similar results were obtained in other multi-day scenario calculations, such as those described by Carter and Atkinson (1989a).

CONCLUSIONS

The decision whether it is appropriate to regulate a compound as an ozone precursor requires a qualitative assessment of its ozone impacts under a variety of environmental conditions. This involves developing a chemical mechanism or model for the compound's atmospheric reactions which can be used in airshed models to predict its atmospheric reactivity. Until this study, there was no information concerning the atmospheric reactions of TDI isomers or any related compound, and thus atmospheric ozone impacts for such compounds were unknown. The objective of this study was to provide the data needed to develop models which can be used to predict the ozone impacts of the TDI isomers under atmospheric conditions. We believe this program was successful in achieving this objective.

Consistent with previous data, TDI was found to have a high affinity for surface absorption, and tended to undergo a first order wall loss in large Teflon reactors at rates ranging from 5-15% per hour. Despite use of a heated injection system, only about half of the liquid TDI could be introduced into the gas phase, with the rest apparently condensing onto the walls of the chamber or injector. Exposure of the chamber walls to TDI was also found to enhance chamber artifacts such as excess radical sources and apparent NO_x offgasing artifacts in the irradiation experiments. However, these wall effects could be accounted for in the chamber effects model, and in most experiments the wall effects were small compared to the effects of TDI's gas phase reactions. Therefore, these wall effects do not significantly affect the major conclusions of this work.

The major conclusion of this study is that the net effect of the atmospheric gas-phase reactions of the TDI is to inhibit ozone formation. This inhibition was observed in all chamber experiments carried out for this program. It is attributed to the presence of both significant radical sinks and significant NO_x sinks in TDI's atmospheric reactions. The radical sinks slow down ozone formation under high NO_x conditions, and the NO_x sinks inhibit peak ozone yields under low NO_x conditions. In addition, TDI apparently does not form significant amounts of reactive products which cause increased O_3 formation after the first day. Furthermore, unlike most VOCs, the overall process of TDI photooxidation apparently does not cause significant amounts of NO to NO_2 conversion, which is the major process by which VOCs cause ozone formation. This means that TDI would not appreciably promote ozone formation even under conditions which are not sensitive to its radical and NO_x inhibition effects.

There is insufficient information concerning the details of the atmospheric reactions of aromatics in general, and isocyanates in particular, to develop explicit mechanisms for TDI's atmospheric reactions. However, relatively simple parameterized models for the overall effects of TDI's reactions were found to give quite good simulations of all of the experiments carried out for this program. Both 2,4-TDI and 2,6-

TDI were simulated with essentially the same mechanism, indicating no significant isomeric differences affecting TDI's reactivity. The experiments used to evaluate the TDI models were carried out under three quite different chemical conditions. Modeling the experiments most sensitive to radical initiation/inhibition effects indicated that only ~30% of the OH radicals reacting with TDI are regenerated in the overall photooxidation process, experiments sensitive to NO to NO_2 conversions are best fit using models assuming no such conversion occur in TDI's overall reactions, and results of TDI reactivity experiments carried out under low NO_x conditions are simulated only if it is assumed that TDI forms significant yields of products, such as cresols or nitrophenols, which have significant NO_x sinks in their mechanism. Note that the ~70% overall radical inhibition makes TDI a more effective radical inhibitor than the volatile silicone compounds, which were found to have no more than ~50% radical inhibition in their overall mechanisms (Carter et al., 1992).

The TDI models which fit the chamber data predicted that TDI emissions would cause reduced ozone formation in all of the EKMA scenarios used by Carter (1994a) to calculate various VOC reactivity scales. Models with differing mechanistic assumptions concerning the NO_x sink processes yielded somewhat different predictions of the how the TDI inhibition effects are affected by changing NO_x conditions, but none indicated that TDI had positive ozone impacts under any conditions. While these were all one-day simulations, a limited number of multi-day scenario calculations suggested that TDI is likely to have similar inhibiting effects under multi-day conditions.

Therefore, it is concluded that emissions of TDI are unlikely to have a positive effect on ozone formation under any atmospheric conditions. While the exact chemical processes responsible for TDI's inhibiting effects are unknown, the fact that this inhibition occurs, and that it is effective under a variety of atmospheric conditions, has been clearly established by these chamber data.

REFERENCES

Atkinson, R. (1989): "Kinetics and Mechanisms of the Gas-Phase Reactions of the Hydroxyl Radical with Organic Compounds," J. Phys. Chem. Ref. Data, Monograph no 1.

Atkinson, R. (1990): "Gas-Phase Tropospheric Chemistry of Organic Compounds: A Review," Atmos. Environ., 24A, 1-24.

Baugues, K. (1990): "Preliminary Planning Information for Updating the Ozone Regulatory Impact Analysis Version of EKMA," Draft Document, Source Receptor Analysis Branch, Technical Support Division, U. S. Environmental Protection Agency, Research Triangle Park, NC, January.

Becker, K. H., V. Bastian, and Th. Klein (1988): "The Reactions of OH Radicals with Toluene Diisocyanate, Toluenediamine and Methylenedianiline Under Simulated Atmospheric Conditions," J. Photochem. Photobiol A., 45 195-205.

Carter, W. P. L. (1990): "A Detailed Mechanism for the Gas-Phase Atmospheric Reactions of Organic Compounds," Atmos. Environ., 24A, 481-518.

Carter, W. P. L. (1994a): "Development of Ozone Reactivity Scales for Volatile Organic Compounds," J. Air & Waste Manage. Assoc., 44, 881-899.

Carter, W. P. L. (1995): "Computer Modeling of Environmental Chamber Measurements of Maximum Incremental Reactivities of Volatile Organic Compounds," Atmos. Environ., 29, 2513-2517.

Carter, W. P. L., R. Atkinson, A. M. Winer, and J. N. Pitts, Jr. (1982): "Experimental Investigation of Chamber-Dependent Radical Sources," Int. J. Chem. Kinet., 14, 1071.

Carter, W. P. L. and R. Atkinson (1987): "An Experimental Study of Incremental Hydrocarbon Reactivity," Environ. Sci. Technol., 21, 670-679

Carter, W. P. L. and R. Atkinson (1989a): "A Computer Modeling Study of Incremental Hydrocarbon Reactivity", Environ. Sci. Technol., 23, 864.

Carter, W. P. L. and R. Atkinson (1989b): "Alkyl Nitrate Formation from the Atmospheric Photooxidation of Alkanes; a Revised Estimation Method," J. Atm. Chem. 8, 165-173.

Carter, W. P. L., and F. W. Lurmann (1990): "Evaluation of the RADM Gas-Phase Chemical Mechanism," Final Report, EPA-600/3-90-001.

Carter, W. P. L. and F. W. Lurmann (1991): "Evaluation of a Detailed Gas-Phase Atmospheric Reaction Mechanism using Environmental Chamber Data," Atm. Environ. 25A, 2771-2806.

Carter, W. P. L., J. A. Pierce, I. L. Malkina, and D. Luo (1992): "Investigation of the Ozone Formation Potential of Selected Volatile Silicone Compounds," Final Report to Dow Corning Corporation, Midland, MI, November.

Carter, W. P. L., J. A. Pierce, I. L. Malkina, D. Luo and W. D. Long (1993a): "Environmental Chamber Studies of Maximum Incremental Reactivities of Volatile Organic Compounds," Report to Coordinating Research Council, Project No. ME-9, California Air Resources Board Contract No. A032-0692; South Coast Air Quality Management District Contract No. C91323, United States Environmental Protection Agency Cooperative Agreement No. CR-814396-01-0, University Corporation for Atmospheric Research Contract No. 59166, and Dow Corning Corporation. April 1.

Carter, W. P. L, D. Luo, I. L. Malkina, and J. A. Pierce (1993b): "An Experimental and Modeling Study of the Photochemical Ozone Reactivity of Acetone," Final Report to Chemical Manufacturers Association Contract No. KET-ACE-CRC-2.0. December 10.

Carter, W. P. L., J. A. Pierce, D. Luo, and I. L. Malkina (1995a): "Environmental Chamber Study of Maximum Incremental Reactivities of Volatile Organic Compounds," Atmos. Environ. 29, 2499-2511.

Carter, W. P. L., D. Luo, I. L. Malkina, and J. A. Pierce (1995b): "Environmental Chamber Studies of Atmospheric Reactivities of Volatile Organic Compounds. Effects of Varying ROG Surrogate and NO_x," Final report to Coordinating Research Council, Inc., Project ME-9, California Air Resources Board, Contract A032-0692, and South Coast Air Quality Management District, Contract C91323. March 24.

Carter, W. P. L., D. Luo, I. L. Malkina, and D. Fitz (1995c): "The University of California, Riverside Environmental Chamber Data Base for Evaluating Oxidant Mechanism. Indoor Chamber Experiments through 1993," Report submitted to the U. S. Environmental Protection Agency, EPA/AREAL, Research Triangle Park, NC., March 20..

Carter, W. P. L., D. Luo, I. L. Malkina, and J. A. Pierce (1995d): "Environmental Chamber Studies of Atmospheric Reactivities of Volatile Organic Compounds. Effects of Varying Chamber and Light Source," Final report to National Renewable Energy Laboratory, Contract XZ-2-12075, Coordinating Research Council, Inc., Project M-9, California Air Resources Board, Contract A032-0692, and South Coast Air Quality Management District, Contract C91323, March 26.

Carter, W. P. L., D. Luo, and I. L. Malkina (1996): "Investigation of the Atmospheric Ozone Formation Potentials of C_{12} - C_{16} n-alkanes," Report to the Aluminum Association, Contract AA1345, October 28.

Carter, W. P. L., D. Luo, and I. L. Malkina (1997a): "Environmental Chamber Studies for Development of an Updated Photochemical Mechanism for VOC Reactivity Assessment," Draft final report to California Air Resources Board Contract 92-345, Coordinating Research Council Project M-9, and National Renewable Energy Laboratory Contract ZF-2-12252-07. March 10.

Chang, T. Y. and S. J. Rudy (1990): "Ozone-Forming Potential of Organic Emissions from Alternative-Fueled Vehicles," Atmos. Environ., 24A, 2421-2430.

Dimitriades, B. (1996): "Scientific Basis for the VOC Reactivity Issues Raised by Section 183(e) of the Clean Air Act Amendments of 1990," J. Air Waste Manage. Assoc. 46, 963-970.

Dodge, M. C. (1984): "Combined effects of organic reactivity and NMHC/NOx ratio on photochemical oxidant formation -- a modeling study," Atmos. Environ., 18, 1657.

Duff, P. B. (1984): "Fate of Toluene Diisocyanate in Air. Phase II Study," Proceedings of the SPI 29th Annual Technical/Marketing Conference. 9-24.

EPA (1984): "Guideline for Using the Carbon Bond Mechanism in City-Specific EKMA," EPA-450/4-84-005, February.

Gery, M. W., G. Z. Whitten, and J. P. Killus (1988): "Development and Testing of the CBM-IV For Urban and Regional Modeling,", EPA-600/ 3-88-012, January.

Gilbert, D. S. (1987): "Fate of TDI and MDI in Air, Soil, and Water," Proceedings of the SPI/FSK Polyurethanes World Conference, 166-172.

Holdren, M. W., C. W. Spicer and R. M. Riggin (1985): "Report on the Fate of TDI in the Atmosphere," Battelle Columbus Laboratories, Columbus, OH.

Johnson, G. M. (1983): "Factors Affecting Oxidant Formation in Sydney Air," in "The Urban Atmosphere -- Sydney, a Case Study." Eds. J. N. Carras and G. M. Johnson (CSIRO, Melbourne), pp. 393-408.

Jeffries, H. E. (1991): "UNC Solar Radiation Models," unpublished draft report for EPA Cooperative Agreements CR813107, CR813964 and CR815779". Undated.

Jeffries, H. E., K. G. Sexton, J. R. Arnold, and T. L. Kale (1989): "Validation Testing of New Mechanisms with Outdoor Chamber Data. Volume 2: Analysis of VOC Data for the CB4 and CAL Photochemical Mechanisms," Final Report, EPA-600/3-89-010b.

Jeffries, H. E. and R. Crouse (1991): "Scientific and Technical Issues Related to the Application of Incremental Reactivity. Part II: Explaining Mechanism Differences," Report prepared for Western States Petroleum Association, Glendale, CA, October.

Pitts, J. N., Jr., E. Sanhueza, R. Atkinson, W. P. L. Carter, A. M. Winer, G. W. Harris, and C. N. Plum (1984): "An Investigation of the Dark Formation of Nitrous Acid in Environmental Chambers," Int. J. Chem. Kinet., 16, 919-939.

Stockwell, W. R., P. Middleton, J. S. Chang, and X. Tang (1990): "The Second Generation Regional Acid Deposition Model Chemical Mechanism for Regional Air Quality Modeling," J. Geophys. Res. 95, 16343- 16376.

Tuazon, E. C., R. Atkinson, C. N. Plum, A. M. Winer, and J. N. Pitts, Jr. (1983): "The Reaction of Gas-Phase N_2O_5 with Water Vapor," Geophys. Res. Lett. 10, 953-956.

Zafonte, L., P. L. Rieger, and J. R. Holmes (1977): "Nitrogen Dioxide Photolysis in the Los Angeles Atmosphere," Environ. Sci. Technol. 11, 483-487.

APPENDIX A
LISTING OF THE CHEMICAL MECHANISM

The chemical mechanism used in the environmental chamber and atmospheric model simulations discussed in this report is given in Tables A-1 through A-4. Table A-1 lists the species used in the mechanism, Table A-2 gives the reactions and rate constants, Table A-3 gives the parameters used to calculate the rates of the photolysis reactions, and Table A-4 gives the values and derivations of the chamber-dependent parameters used when modeling the environmental chamber experiments. Footnotes to Table A-2 indicate the format used for the reaction listing.

Table A-1. List of species in the chemical mechanism used in the model simulations for this study.

Name	Description
Constant Species.	
O2	Oxygen
M	Air
H2O	Water
Active Inorganic Species.	
O3	Ozone
NO	Nitric Oxide
NO2	Nitrogen Dioxide
NO3	Nitrate Radical
N2O5	Nitrogen Pentoxide
HONO	Nitrous Acid
HNO3	Nitric Acid
HNO4	Peroxynitric Acid
HO2H	Hydrogen Peroxide
Active Radical Species and Operators.	
HO2.	Hydroperoxide Radicals
RO2.	Operator to Calculate Total Organic Peroxy Radicals
RCO3.	Operator to Calculate Total Acetyl Peroxy Radicals
Active Reactive Organic Product Species.	
CO	Carbon Monoxide
HCHO	Formaldehyde
CCHO	Acetaldehyde
RCHO	Lumped C3+ Aldehydes
ACET	Acetone
MEK	Lumped Ketones
PHEN	Phenol

Table A-1, (continued)

Name	Description
CRES	Cresols
BALD	Aromatic aldehydes (e.g., benzaldehyde)
GLY	Glyoxal
MGLY	Methyl Glyoxal
BACL	Biacetyl or other lumped α-dicarbonyls, including α-keto esters
AFG1	Reactive Aromatic Fragmentation Products from benzene and naphthalene
AFG2	Other Reactive Aromatic Fragmentation Products
AFG3	Aromatic Fragmentation Products used in adjusted m-xylene mechanism
RNO3	Organic Nitrates
NPHE	Nitrophenols
ISOPROD	Lumped isoprene product species
PAN	Peroxy Acetyl Nitrate
PPN	Peroxy Propionyl Nitrate
GPAN	PAN Analogue formed from Glyoxal
PBZN	PAN Analogues formed from Aromatic Aldehydes
-OOH	Operator Representing Hydroperoxy Groups
Non-Reacting Species	
CO2	Carbon Dioxide
-C	"Lost Carbon"
-N	"Lost Nitrogen"
H2	Hydrogen
Steady State Species and Operators.	
HO.	Hydroxyl Radicals
O	Ground State Oxygen Atoms
O*1D2	Excited Oxygen Atoms
RO2-R.	Peroxy Radical Operator representing NO to NO_2 conversion with HO_2 formation.
RO2-N.	Peroxy Radical Operator representing NO consumption with organic nitrate formation.
RO2-NP.	Peroxy Radical Operator representing NO consumption with nitrophenol formation
R2O2.	Peroxy Radical Operator representing NO to NO_2 conversion.
CCO-O2.	Peroxy Acetyl Radicals
C2CO-O2.	Peroxy Propionyl Radicals
HCOCO-O2.	Peroxyacyl Radical formed from Glyoxal
BZ-CO-O2.	Peroxyacyl Radical formed from Aromatic Aldehydes
HOCOO.	Intermediate formed in Formaldehyde + HO_2 reaction
BZ-O.	Phenoxy Radicals
BZ(NO2)-O.	Nitratophenoxy Radicals
HOCOO.	Radical Intermediate formed in the HO_2 + Formaldehyde system.
(HCHO2)	Excited Criegee biradicals formed from $=CH_2$ groups
(CCHO2)	Excited Criegee biradicals formed from $=CHCH_3$ groups
(RCHO2)	Excited Criegee biradicals formed from =CHR groups, where R not CH_3
(C(C)CO2)	Excited Criegee biradicals formed from $=C(CH_3)_2$ groups
(C(R)CO2)	Excited Criegee biradicals formed from $=C(CH_3)R$ or CR_2 groups
(BZCHO2)	Excited Criegee biradicals formed from styrenes
(C:CC(C)O2)	Excited Criegee biradicals formed from isoprene
(C:C(C)CHO2)	Excited Criegee biradicals formed from isoprene
(C2(O2)CHO)	Excited Criegee biradicals formed from isoprene products

Table A-1, (continued)

Name	Description
(HOCCHO2)	Excited Criegee biradicals formed from isoprene products
(HCOCHO2)	Excited Criegee biradicals formed from isoprene products
(C2(O2)COH)	Excited Criegee biradicals formed from isoprene products
Primary Organics Represented explicitly	
CH4	Methane
ETHANE	Ethane
N-C4	n-Butane
N-C6	n-Hexane
N-C8	n-Octane
TOLUENE	Toluene
M-XYLENE	m-Xylene
ETHE	Ethene
PROPENE	Propene
T-2-BUTE	trans-2-Butene
ISOP	Isoprene
APIN	α-Pinene
UNKN	Unknown biogenics.
TDI	2,4- or 2,6-Toluene Diisocyanate
Lumped species used to represent the Base ROG mixture in the EKMA model simulations.	
ALK1	Alkanes and other saturated compounds with $k_{OH} < 10^4$ ppm^{-1} min^{-1}.
ALK2	Alkanes and other saturated compounds with $k_{OH} \geq 10^4$ ppm^{-1} min^{-1}.
ARO1	Aromatics with $k_{OH} < 2x10^4$ ppm^{-1} min^{-1}.
ARO2	Aromatics with $k_{OH} \geq 2x10^4$ ppm^{-1} min^{-1}.
OLE2	Alkenes (other than ethene) with $k_{OH} < 7x10^4$ ppm^{-1} min^{-1}.
OLE3	Alkenes with $k_{OH} \geq 7x10^4$ ppm^{-1} min^{-1}.

Table A-2. List of reactions in the chemical mechanism used in the model simulations for this study.

Rxn. Label	Kinetic Parameters [a] k(300)	A	Ea	B	Reactions [b]
Inorganic Reactions					
1	(Phot. Set = NO2)				NO2 + HV = NO + O
2	6.00E-34	6.00E-34	0.00	-2.30	O + O2 + M = O3 + M
3A	9.69E-12	6.50E-12	-0.24	0.00	O + NO2 = NO + O2
3B	1.55E-12	(Falloff Kinetics)			O + NO2 = NO3 + M
	k0 =	9.00E-32	0.00	-2.00	
	kINF =	2.20E-11	0.00	0.00	
		F= 0.60	n= 1.00		
4	1.88E-14	2.00E-12	2.78	0.00	O3 + NO = NO2 + O2
5	3.36E-17	1.40E-13	4.97	0.00	O3 + NO2 = O2 + NO3
6	2.80E-11	1.70E-11	-0.30	0.00	NO + NO3 = 2 NO2
7	1.92E-38	3.30E-39	-1.05	0.00	NO + NO + O2 = 2 NO2
8	1.26E-12	(Falloff Kinetics)			NO2 + NO3 = N2O5
	k0 =	2.20E-30	0.00	-4.30	
	kINF =	1.50E-12	0.00	-0.50	
		F= 0.60	n= 1.00		
9	5.53E+10	9.09E+26	22.26	0.00	N2O5 + #RCON8 = NO2 + NO3
10	1.00E-21	(No T Dependence)			N2O5 + H2O = 2 HNO3
11	4.17E-16	2.50E-14	2.44	0.00	NO2 + NO3 = NO + NO2 + O2
12A	(Phot. Set = NO3NO)				NO3 + HV = NO + O2
12B	(Phot. Set = NO3NO2)				NO3 + HV = NO2 + O
13A	(Phot. Set = O3O3P)				O3 + HV = O + O2
13B	(Phot. Set = O3O1D)				O3 + HV = O*1D2 + O2
14	2.20E-10	(No T Dependence)			O*1D2 + H2O = 2 HO.
15	2.92E-11	1.92E-11	-0.25	0.00	O*1D2 + M = O + M
16	4.81E-12	(Falloff Kinetics)			HO. + NO = HONO
	k0 =	7.00E-31	0.00	-2.60	
	kINF =	1.50E-11	0.00	-0.50	
		F= 0.60	n= 1.00		
17	(Phot. Set = HONO)				HONO + HV = HO. + NO
18	1.13E-11	(Falloff Kinetics)			HO. + NO2 = HNO3
	k0 =	2.60E-30	0.00	-3.20	
	kINF =	2.40E-11	0.00	-1.30	
		F= 0.60	n= 1.00		
19	1.03E-13	6.45E-15	-1.65	0.00	HO. + HNO3 = H2O + NO3
21	2.40E-13	(No T Dependence)			HO. + CO = HO2. + CO2
22	6.95E-14	1.60E-12	1.87	0.00	HO. + O3 = HO2. + O2
23	8.28E-12	3.70E-12	-0.48	0.00	HO2. + NO = HO. + NO2
24	1.37E-12	(Falloff Kinetics)			HO2. + NO2 = HNO4
	k0 =	1.80E-31	0.00	-3.20	
	kINF =	4.70E-12	0.00	-1.40	
		F= 0.60	n= 1.00		
25	7.92E+10	4.76E+26	21.66	0.00	HNO4 + #RCON24 = HO2. + NO2
27	4.61E-12	1.30E-12	-0.75	0.00	HNO4 + HO. = H2O + NO2 + O2
28	2.08E-15	1.10E-14	0.99	0.00	HO2. + O3 = HO. + 2 O2
29A	1.73E-12	2.20E-13	-1.23	0.00	HO2. + HO2. = HO2H + O2
29B	5.00E-32	1.90E-33	-1.95	0.00	HO2. + HO2. + M = HO2H + O2
29C	3.72E-30	3.10E-34	-5.60	0.00	HO2. + HO2. + H2O = HO2H + O2 + H2O
29D	2.65E-30	6.60E-35	-6.32	0.00	HO2. + HO2. + H2O = HO2H + O2 + H2O
30A	1.73E-12	2.20E-13	-1.23	0.00	NO3 + HO2. = HNO3 + O2
30B	5.00E-32	1.90E-33	-1.95	0.00	NO3 + HO2. + M = HNO3 + O2
30C	3.72E-30	3.10E-34	-5.60	0.00	NO3 + HO2. + H2O = HNO3 + O2 + H2O
30D	2.65E-30	6.60E-35	-6.32	0.00	NO3 + HO2. + H2O = HNO3 + O2 + H2O
31	(Phot. Set = H2O2)				HO2H + HV = 2 HO.
32	1.70E-12	3.30E-12	0.40	0.00	HO2H + HO. = HO2. + H2O
33	9.90E-11	4.60E-11	-0.46	0.00	HO. + HO2. = H2O + O2
Peroxy Radical Operators					
B1	7.68E-12	4.20E-12	-0.36	0.00	RO2. + NO = NO
B2	2.25E-11	(Falloff Kinetics)			RCO3. + NO = NO
	k0 =	5.65E-28	0.00	-7.10	
	kINF =	2.64E-11	0.00	-0.90	
		F= 0.27	n= 1.00		
B4	1.04E-11	(Falloff Kinetics)			RCO3. + NO2 = NO2
	k0 =	2.57E-28	0.00	-7.10	
	kINF =	1.20E-11	0.00	-0.90	
		F= 0.30	n= 1.00		
B5	4.90E-12	3.40E-13	-1.59	0.00	RO2. + HO2. = HO2. + RO2-HO2-PROD
B6	4.90E-12	3.40E-13	-1.59	0.00	RCO3. + HO2. = HO2. + RO2-HO2-PROD
B8	1.00E-15	(No T Dependence)			RO2. + RO2. = RO2-RO2-PROD
B9	1.09E-11	1.86E-12	-1.05	0.00	RO2. + RCO3. = RO2-RO2-PROD

Table A-2 (continued)

Rxn. Label	Kinetic Parameters [a] k(300)	A	Ea	B	Reactions [b]
B10	1.64E-11	2.80E-12	-1.05	0.00	RCO3. + RCO3. = RO2-RO2-PROD
B11	(Same k as for RO2.)				RO2-R. + NO = NO2 + HO2.
B12	(Same k as for RO2.)				RO2-R. + HO2. = -OOH
B13	(Same k as for RO2.)				RO2-R. + RO2. = RO2. + 0.5 HO2.
B14	(Same k as for RO2.)				RO2-R. + RCO3. = RCO3. + 0.5 HO2.
B19	(Same k as for RO2.)				RO2-N. + NO = RNO3
B20	(Same k as for RO2.)				RO2-N. + HO2. = -OOH + MEK + 1.5 -C
B21	(Same k as for RO2.)				RO2-N. + RO2. = RO2. + 0.5 HO2. + MEK + 1.5 -C
B22	(Same k as for RO2.)				RO2-N. + RCO3. = RCO3. + 0.5 HO2. + MEK + 1.5 -C
B15	(Same k as for RO2.)				R2O2. + NO = NO2
B16	(Same k as for RO2.)				R2O2. + HO2. =
B17	(Same k as for RO2.)				R2O2. + RO2. = RO2.
B18	(Same k as for RO2.)				R2O2. + RCO3. = RCO3.
B23	(Same k as for RO2.)				RO2-XN. + NO = -N
B24	(Same k as for RO2.)				RO2-XN. + HO2. = -OOH
B25	(Same k as for RO2.)				RO2-XN. + RO2. = RO2. + 0.5 HO2.
B26	(Same k as for RO2.)				RO2-XN. + RCO3. = RCO3. + HO2.
G2	(Same k as for RO2.)				RO2-NP. + NO = NPHE
G3	(Same k as for RO2.)				RO2-NP. + HO2. = -OOH + 6 -C
G4	(Same k as for RO2.)				RO2-NP. + RO2. = RO2. + 0.5 HO2. + 6 -C
G5	(Same k as for RO2.)				RO2-NP. + RCO3. = RCO3. + HO2. + 6 -C
Excited Criegee Biradicals					
RZ1	(fast)				(HCHO2) = 0.7 HCOOH + 0.12 "HO. + HO2. + CO" + 0.18 "H2 + CO2"
RZ2	(fast)				(CCHO2) = 0.25 CCOOH + 0.15 "CH4 + CO2" + 0.6 HO. + 0.3 "CCO-O2. + RCO3." + 0.3 "RO2-R. + HCHO + CO + RO2."
RZ3	(fast)				(RCHO2) = 0.25 CCOOH + 0.15 CO2 + 0.6 HO. + 0.3 "C2CO-O2. + RCO3." + 0.3 "RO2-R. + CCHO + CO + RO2." + 0.55 -C
RZ4	(fast)				(C(C)CO2) = HO. + R2O2. + HCHO + CCO-O2. + RCO3. + RO2.
RZ5	(fast)				(C(R)CO2) = HO. + CCO-O2. + CCHO + R2O2. + RCO3. + RO2.
RZ6	(fast)				(CYCCO2) = 0.3 "HO. + C2CO-O2. + R2O2. + RCO3. + RO2." + 0.3 RCHO + 4.2 -C
RZ8	(fast)				(BZCHO2) = 0.5 "BZ-O. + R2O2. + CO + HO."
ISZ1	(fast)				(C:CC(C)O2) = HO. + R2O2. + HCHO + C2CO-O2. + RO2. + RCO3.
ISZ2	(fast)				(C:C(C)CHO2) = 0.75 RCHO + 0.25 ISOPROD + 0.5 -C
MAZ1	(fast)				(C2(O2)CHO) = HO. + R2O2. + HCHO + HCOCO-O2. + RO2. + RCO3.
M1Z1	(fast)				(HOCCHO2) = 0.6 HO. + 0.3 "CCO-O2. + RCO3." + 0.3 "RO2-R. + HCHO + CO + RO2." + 0.8 -C
M2Z1	(fast)				(HCOCHO2) = 0.12 "HO2. + 2 CO + HO." + 0.74 -C + 0.51 "CO2 + HCHO"
M2Z2	(fast)				(C2(O2)COH) = HO. + MGLY + HO2. + R2O2. + RO2.
Organic Product Species					
B7	(Phot. Set = CO2H)				-OOH + HV = HO2. + HO.
B7A	1.81E-12	1.18E-12	-0.25	0.00	HO. + -OOH = HO.
B7B	3.71E-12	1.79E-12	-0.44	0.00	HO. + -OOH = RO2-R. + RO2.
C1	(Phot. Set = HCHONEWR)				HCHO + HV = 2 HO2. + CO
C2	(Phot. Set = HCHONEWM)				HCHO + HV = H2 + CO
C3	9.76E-12	1.13E-12	-1.29	2.00	HCHO + HO. = HO2. + CO + H2O
C4	7.79E-14	9.70E-15	-1.24	0.00	HCHO + HO2. = HOCOO.
C4A	1.77E+02	2.40E+12	13.91	0.00	HOCOO. = HO2. + HCHO
C4B	(Same k as for RO2.)				HOCOO. + NO = -C + NO2 + HO2.
C9	6.38E-16	2.80E-12	5.00	0.00	HCHO + NO3 = HNO3 + HO2. + CO
C10	1.57E-11	5.55E-12	-0.62	0.00	CCHO + HO. = CCO-O2. + H2O + RCO3.
C11A	(Phot. Set = CCHOR)				CCHO + HV = CO + HO2. + HCHO + RO2-R. + RO2.
C12	2.84E-15	1.40E-12	3.70	0.00	CCHO + NO3 = HNO3 + CCO-O2. + RCO3.
C25	1.97E-11	8.50E-12	-0.50	0.00	RCHO + HO. = C2CO-O2. + RCO3.
C26	(Phot. Set = RCHO)				RCHO + HV = CCHO + RO2-R. + RO2. + CO + HO2.
C27	2.84E-15	1.40E-12	3.70	0.00	NO3 + RCHO = HNO3 + C2CO-O2. + RCO3.
C38	2.23E-13	4.81E-13	0.46	2.00	ACET + HO. = R2O2. + HCHO + CCO-O2. + RCO3. + RO2.

Table A-2 (continued)

Rxn. Label	Kinetic Parameters [a] k(300)	A	Ea	B	Reactions [b]
C39	(Phot. Set = ACET-93C)				ACET + HV = CCO-O2. + HCHO + RO2-R. + RCO3. + RO2.
C44	1.16E-12	2.92E-13	-0.82	2.00	MEK + HO. = H2O + 0.5 "CCHO + HCHO + CCO-O2. + C2CO-O2." + RCO3. + 1.5 "R2O2. + RO2."
C57	(Phot. Set = KETONE)				MEK + HV + #0.1 = CCO-O2. + CCHO + RO2-R. + RCO3. + RO2.
C95	2.07E-12	2.19E-11	1.41	0.00	RNO3 + HO. = NO2 + 0.155 MEK + 1.05 RCHO + 0.48 CCHO + 0.16 HCHO + 0.11 -C + 1.39 "R2O2. + RO2."
C58A	(Phot. Set = GLYOXAL1)				GLY + HV = 0.8 HO2. + 0.45 HCHO + 1.55 CO
C58B	(Phot. Set = GLYOXAL2)				GLY + HV + #0.029 = 0.13 HCHO + 1.87 CO
C59	1.14E-11 (No T Dependence)				GLY + HO. = 0.6 HO2. + 1.2 CO + 0.4 "HCOCO-O2. + RCO3."
C60	(Same k as for CCHO)				GLY + NO3 = HNO3 + 0.6 HO2. + 1.2 CO + 0.4 "HCOCO-O2. + RCO3."
C68A	(Phot. Set = MEGLYOX1)				MGLY + HV = HO2. + CO + CCO-O2. + RCO3.
C68B	(Phot. Set = MEGLYOX2)				MGLY + HV + 0.107 = HO2. + CO + CCO-O2. + RCO3.
C69	1.72E-11 (No T Dependence)				MGLY + HO. = CO + CCO-O2. + RCO3.
C70	(Same k as for CCHO)				MGLY + NO3 = HNO3 + CO + CCO-O2. + RCO3.
G7	1.14E-11 (No T Dependence)				HO. + AFG1 = HCOCO-O2. + RCO3.
G8	(Phot. Set = ACROLEIN)				AFG1 + HV + #0.029 = HO2. + HCOCO-O2. + RCO3.
U2OH	1.72E-11 (No T Dependence)				HO. + AFG2 = C2CO-O2. + RCO3.
U2HV	(Phot. Set = ACROLEIN)				AFG2 + HV = HO2. + CO + CCO-O2. + RCO3.
G46	2.63E-11 (No T Dependence)				HO. + PHEN = 0.15 RO2-NP. + 0.85 RO2-R. + 0.2 GLY + 4.7 -C + RO2.
G51	3.60E-12 (No T Dependence)				NO3 + PHEN = HNO3 + BZ-O.
G52	4.20E-11 (No T Dependence)				HO. + CRES = 0.15 RO2-NP. + 0.85 RO2-R. + 0.2 MGLY + 5.5 -C + RO2.
G57	2.10E-11 (No T Dependence)				NO3 + CRES = HNO3 + BZ-O. + -C
G30	1.29E-11 (No T Dependence)				BALD + HO. = BZ-CO-O2. + RCO3.
G31	(Phot. Set = BZCHO)				BALD + HV + #0.05 = 7 -C
G32	2.61E-15	1.40E-12	3.75	0.00	BALD + NO3 = HNO3 + BZ-CO-O2.
G58	3.60E-12 (No T Dependence)				NPHE + NO3 = HNO3 + BZ(NO2)-O.
G59	(Same k as for BZ-O.)				BZ(NO2)-O. + NO2 = 2 -N + 6 -C
G60	(Same k as for RO2.)				BZ(NO2)-O. + HO2. = NPHE
G61	(Same k as for BZ-O.)				BZ(NO2)-O. = NPHE
C13	(Same k as for RCO3.)				CCO-O2. + NO = CO2 + NO2 + HCHO + RO2-R. + RO2.
C14	(Same k as for RCO3.)				CCO-O2. + NO2 = PAN
C15	(Same k as for RCO3.)				CCO-O2. + HO2. = -OOH + CO2 + HCHO
C16	(Same k as for RCO3.)				CCO-O2. + RO2. = RO2. + 0.5 HO2. + CO2 + HCHO
C17	(Same k as for RCO3.)				CCO-O2. + RCO3. = RCO3. + HO2. + CO2 + HCHO
C18	6.50E-04 (Falloff Kinetics)				PAN = CCO-O2. + NO2 + RCO3.
	k0 =	4.90E-03	23.97	0.00	
	kINF =	4.00E+16	27.08	0.00	
		F= 0.30	n= 1.00		
C28	(Same k as for RCO3.)				C2CO-O2. + NO = CCHO + RO2-R. + CO2 + NO2 + RO2.
C29	8.40E-12 (No T Dependence)				C2CO-O2. + NO2 = PPN
C30	(Same k as for RCO3.)				C2CO-O2. + HO2. = -OOH + CCHO + CO2
C31	(Same k as for RCO3.)				C2CO-O2. + RO2. = RO2. + 0.5 HO2. + CCHO + CO2
C32	(Same k as for RCO3.)				C2CO-O2. + RCO3. = RCO3. + HO2. + CCHO + CO2
C33	6.78E-04	1.60E+17	27.97	0.00	PPN = C2CO-O2. + NO2 + RCO3.
C62	(Same k as for RCO3.)				HCOCO-O2. + NO = NO2 + CO2 + CO + HO2.
C63	(Same k as for RCO3.)				HCOCO-O2. + NO2 = GPAN
C65	(Same k as for RCO3.)				HCOCO-O2. + HO2. = -OOH + CO2 + CO
C66	(Same k as for RCO3.)				HCOCO-O2. + RO2. = RO2. + 0.5 HO2. + CO2 + CO
C67	(Same k as for RCO3.)				HCOCO-O2. + RCO3. = RCO3. + HO2. + CO2 + CO
C64	(Same k as for PAN)				GPAN = HCOCO-O2. + NO2 + RCO3.
G33	(Same k as for RCO3.)				BZ-CO-O2. + NO = BZ-O. + CO2 + NO2 + R2O2. + RO2.
G43	3.53E-11	1.30E-11	-0.60	0.00	BZ-O. + NO2 = NPHE
G44	(Same k as for RO2.)				BZ-O. + HO2. = PHEN
G45	1.00E-03 (No T Dependence)				BZ-O. = PHEN
G34	8.40E-12 (No T Dependence)				BZ-CO-O2. + NO2 = PBZN
G36	(Same k as for RCO3.)				BZ-CO-O2. + HO2. = -OOH + CO2 + PHEN
G37	(Same k as for RCO3.)				BZ-CO-O2. + RO2. = RO2. + 0.5 HO2. + CO2 + PHEN

Table A-2 (continued)

Rxn. Label	Kinetic Parameters [a] k(300)	A	Ea	B	Reactions [b]
G38	(Same k as for RCO3.)				BZ-CO-O2. + RCO3. = RCO3. + HO2. + CO2 + PHEN
G35	2.17E-04	1.60E+15	25.90	0.00	PBZN = BZ-CO-O2. + NO2 + RCO3.
IPOH	3.36E-11	(No T Dependence)			ISOPROD + HO. = 0.293 CO + 0.252 CCHO + 0.126 HCHO + 0.041 GLY + 0.021 RCHO + 0.168 MGLY + 0.314 MEK + 0.503 RO2-R. + 0.21 CCO-O2. + 0.288 C2CO-O2. + 0.21 R2O2. + 0.713 RO2. + 0.498 RCO3. + -0.112 -C
IPO3	7.11E-18	(No T Dependence)			ISOPROD + O3 = 0.02 CCHO + 0.04 HCHO + 0.01 GLY + 0.84 MGLY + 0.09 MEK + 0.66 (HCHO2) + 0.09 (HCOCHO2) + 0.18 (HOCCHO2) + 0.06 (C2(O2)CHO) + 0.01 (C2(O2)COH) + -0.39 -C
IPHV	(Phot. Set = ACROLEIN)				ISOPROD + HV + 0.0036 = 0.333 CO + 0.067 CCHO + 0.9 HCHO + 0.033 MEK + 0.333 HO2. + 0.7 RO2-R. + 0.267 CCO-O2. + 0.7 C2CO-O2. + 0.7 RO2. + 0.967 RCO3. + -0.133 -C
IPN3	1.00E-15	(No T Dependence)			ISOPROD + NO3 = 0.643 CO + 0.282 HCHO + 0.85 RNO3 + 0.357 RCHO + 0.925 HO2. + 0.075 C2CO-O2. + 0.075 R2O2. + 0.925 RO2. + 0.075 RCO3. + 0.075 HNO3 + -2.471 -C
Hydrocarbon Species Represented Explicitly					
	8.71E-15	6.25E-13	2.55	2.00	METHANE + HO. = RO2-R. + HCHO + RO2.
	2.74E-13	1.28E-12	0.92	2.00	ETHANE + HO. = RO2-R. + CCHO + RO2.
	2.56E-12	1.36E-12	-0.38	2.00	N-C4 + HO. = 0.076 RO2-N. + 0.924 RO2-R. + 0.397 R2O2. + 0.001 HCHO + 0.571 CCHO + 0.14 RCHO + 0.533 MEK + -0.076 -C + 1.397 RO2.
	5.63E-12	1.35E-11	0.52	0.00	N-C6 + HO. = 0.185 RO2-N. + 0.815 RO2-R. + 0.738 R2O2. + 0.02 CCHO + 0.105 RCHO + 1.134 MEK + 0.186 -C + 1.738 RO2.
	8.76E-12	3.15E-11	0.76	0.00	N-C8 + HO. = 0.333 RO2-N. + 0.667 RO2-R. + 0.706 R2O2. + 0.002 RCHO + 1.333 MEK + 0.998 -C + 1.706 RO2.
	5.91E-12	1.81E-12	-0.70	0.00	TOLUENE + HO. = 0.085 BALD + 0.26 CRES + 0.118 GLY + 0.964 MGLY + 0.259 AFG2 + 0.74 RO2-R. + 0.26 HO2. + 0.681 -C + 0.74 RO2.
	2.36E-11	(No T Dependence)			M-XYLENE + HO. = 0.04 BALD + 0.18 CRES + 0.108 GLY + 1.599 MGLY + 0.461 AFG2 + 0.82 RO2-R. + 0.18 HO2. + 0.063 -C + 0.82 RO2. 0.82 RO2.
	8.43E-12	1.96E-12	-0.87	0.00	ETHENE + HO. = RO2-R. + RO2. + 1.56 HCHO + 0.22 CCHO
	1.68E-18	9.14E-15	5.13	0.00	ETHENE + O3 = HCHO + (HCHO2)
	2.18E-16	4.39E-13	4.53	2.00	ETHENE + NO3 = R2O2. + RO2. + 2 HCHO + NO2
	7.42E-13	1.04E-11	1.57	0.00	ETHENE + O = RO2-R. + HO2. + RO2. + HCHO + CO
	2.60E-11	4.85E-12	-1.00	0.00	PROPENE + HO. = RO2-R. + RO2. + HCHO + CCHO
	1.05E-17	5.51E-15	3.73	0.00	PROPENE + O3 = 0.6 HCHO + 0.4 CCHO + 0.4 (HCHO2) + 0.6 (CCHO2)
	9.74E-15	4.59E-13	2.30	0.00	PROPENE + NO3 = R2O2. + RO2. + HCHO + CCHO + NO2
	4.01E-12	1.18E-11	0.64	0.00	PROPENE + O = 0.4 HO2. + 0.5 RCHO + 0.5 MEK + -0.5 -C
	6.30E-11	1.01E-11	-1.09	0.00	T-2-BUTE + HO. = RO2-R. + RO2. + 2 CCHO
	1.95E-16	6.64E-15	2.10	0.00	T-2-BUTE + O3 = CCHO + (CCHO2)
	3.92E-13	1.10E-13	-0.76	2.00	T-2-BUTE + NO3 = R2O2. + RO2. + 2 CCHO + NO2
	2.34E-11	2.26E-11	-0.02	0.00	T-2-BUTE + O = 0.4 HO2. + 0.5 RCHO + 0.5 MEK + 0.5 -C
Models for TDI Reactions [c]					
A	7.40E-12	7.40E-12	0.00	0.00	TDI + HO. = 0.3 HO. + CRES
B	7.40E-12	7.40E-12	0.00	0.00	TDI + HO. = 0.3 HO. + 0.5 {RO2-NP. + RO2.}
C	7.40E-12	7.40E-12	0.00	0.00	TDI + HO. = 0.3 HO. + CRES + 0.5 NO
D	7.40E-12	7.40E-12	0.00	0.00	TDI + HO. = 0.3 HO. + 0.5 {RO2-NP. + RO2.} + 0.5 NO
Lumped Species used in EKMA Simulations [d]					
A1OH	3.46E-12	2.56E-12	-0.18	0.00	ALK1 + HO. = 0.911 RO2-R. + 0.074 RO2-N. + 0.005 RO2-XN. + 0.011 HO2. + 0.575 R2O2. + 1.564 RO2. + 0.065 HCHO + 0.339 CCHO + 0.196 RCHO + 0.322 ACET + 0.448 MEK + 0.024 CO + 0.025 GLY + 0.051 -C

Table A-2 (continued)

Rxn. Label	Kinetic Parameters [a] k(300)	A	Ea	B	Reactions [b]
A2OH	9.14E-12	5.12E-12	-0.35	0.00	ALK2 + HO. = 0.749 RO2-R. + 0.249 RO2-N. + 0.002 RO2-XN. + 0.891 R2O2. + 1.891 RO2. + 0.029 HCHO + 0.048 CCHO + 0.288 RCHO + 0.028 ACET + 1.105 MEK + 0.043 CO + 0.018 CO2 + 1.268 -C
B1OH	5.87E-12	(No T Dependence)			ARO1 + HO. = 0.742 RO2-R. + 0.258 HO2. + 0.742 RO2. + 0.015 PHEN + 0.244 CRES + 0.08 BALD + 0.124 GLY + 0.681 MGLY + 0.11 AFG1 + 0.244 AFG2 + 1.857 -C
B2OH	3.22E-11	1.20E-11	-0.59	0.00	ARO2 + HO. = 0.82 RO2-R. + 0.18 HO2. + 0.82 RO2. + 0.18 CRES + 0.036 BALD + 0.068 GLY + 1.02 MGLY + 0.532 AFG2 + 2.588 -C
O2OH	3.17E-11	2.22E-12	-1.59	0.00	OLE2 + HO. = 0.858 RO2-R. + 0.142 RO2-N. + RO2. + 0.858 HCHO + 0.252 CCHO + 0.606 RCHO + 1.267 -C
O2O3	1.08E-17	1.42E-15	2.91	0.00	OLE2 + O3 = 0.6 HCHO + 0.635 RCHO + 0.981 -C + 0.4 (HCHO2) + 0.529 (CCHO2) + 0.071 (RCHO2)
O2N3	1.16E-14	1.99E-13	1.69	0.00	OLE2 + NO3 = R2O2. + RO2. + HCHO + 0.294 CCHO + 0.706 RCHO + 1.451 -C + NO2
O2OA	4.11E-12	4.51E-12	0.06	0.00	OLE2 + O = 0.4 HO2. + 0.5 RCHO + 0.5 MEK + 1.657 -C
O3OH	6.23E-11	4.54E-12	-1.56	0.00	OLE3 + HO. = 0.861 RO2-R. + 0.139 RO2-N. + RO2. + 0.24 HCHO + 0.661 CCHO + 0.506 RCHO + 0.113 ACET + 0.086 MEK + 0.057 BALD + 0.848 -C
O3O3	1.70E-16	1.77E-15	1.40	0.00	OLE3 + O3 = 0.203 HCHO + 0.358 CCHO + 0.309 RCHO + 0.061 MEK + 0.027 BALD + 0.976 -C + 0.076 (HCHO2) + 0.409 (CCHO2) + 0.279 (RCHO2) + 0.158 (C(C)CO2 + 0.039 (C(R)CO2 + 0.04 (BZCHO2)
O3N3	1.07E-12	3.19E-13	-0.72	0.00	OLE3 + NO3 = R2O2. + RO2. + 0.278 HCHO + 0.767 CCHO + 0.588 RCHO + 0.131 ACET + 0.1 MEK + 0.066 BALD + 0.871 -C + NO2
O3OA	2.52E-11	8.66E-12	-0.64	0.00	OLE3 + O = 0.4 HO2. + 0.5 RCHO + 0.5 MEK + 2.205 -C 0.001 RCHO + 1.223 MEK + 5.004 -C + 1.644 RO2.
Reactions used to Represent Chamber-Dependent Processes [e]					
O3W	(varied)	(No T Dependence)			O3 =
N25I	(varied)	(No T Dependence)			N2O5 = 2 NOX-WALL
N25S	(varied)	(No T Dependence)			N2O5 + H2O = 2 NOX-WALL
NO2W	(varied)	(No T Dependence)			NO2 = (yHONO) HONO + (1-yHONO) NOX-WALL
XSHC	(varied)	(No T Dependence)			HO. = HO2.
RSI	(Phot. Set = NO2)				HV + #RS/K1 = HO.
ONO2	(Phot. Set = NO2)				HV + #E-NO2/K1 = NO2 + #-1 NOX-WALL

[a] Except as noted, the expression for the rate constant is $k = A\ e^{Ea/RT}\ (T/300)^{B}$. Rate constants and A factor are in cm, molecule, sec. units. Units of Ea is kcal $mole^{-1}$. "Phot Set" means this is a photolysis reaction, with the absorption coefficients and quantum yields given in Table A-3. In addition, if "#(number)" or "#(parameter)" is given as a reactant, then the value of that number or parameter is multiplied by the result in the "rate constant expression" columns to obtain the rate constant used. Furthermore, "#RCONnn" as a reactant means that the rate constant for the reaction is obtained by multiplying the rate constant given by that for reaction "nn". Thus, the rate constant given is actually an equilibrium constant.

[b] The format of the reaction listing is the same as that used in the documentation of the detailed mechanism (Carter 1990).

[c] First column gives model designation for alternative TDI mechanisms which were examined. See text.

[d] The rate constants and product yield parameters are based on the mixture of species in the base ROG mixture which are being represented.

[e] See Table A-4 for the values of the parameters used for the specific chambers modeled in this study.

Table A-3. Absorption cross sections and quantum yields for photolysis reactions.

WL (nm)	Abs (cm^2)	QY	WL (nm)	Abs (cm^2)	QY	WL (nm)	Abs (cm^2)	QY	WL (nm)	Abs (cm^2)	QY	WL (nm)	Abs (cm^2)	QY
Photolysis File = NO2														
250.0	2.83E-20	1.000	255.0	1.45E-20	1.000	260.0	1.90E-20	1.000	265.0	2.05E-20	1.000	270.0	3.13E-20	1.000
275.0	4.02E-20	1.000	280.0	5.54E-20	1.000	285.0	6.99E-20	1.000	290.0	8.18E-20	0.999	295.0	9.67E-20	0.998
300.0	1.17E-19	0.997	305.0	1.66E-19	0.996	310.0	1.76E-19	0.995	315.0	2.25E-19	0.994	320.0	2.54E-19	0.993
325.0	2.79E-19	0.992	330.0	2.99E-19	0.991	335.0	3.45E-19	0.990	340.0	3.88E-19	0.989	345.0	4.07E-19	0.988
350.0	4.10E-19	0.987	355.0	5.13E-19	0.986	360.0	4.51E-19	0.984	365.0	5.78E-19	0.983	370.0	5.42E-19	0.981
375.0	5.35E-19	0.979	380.0	5.99E-19	0.975	381.0	5.98E-19	0.974	382.0	5.97E-19	0.973	383.0	5.96E-19	0.972
384.0	5.95E-19	0.971	385.0	5.94E-19	0.969	386.0	5.95E-19	0.967	387.0	5.96E-19	0.966	388.0	5.98E-19	0.964
389.0	5.99E-19	0.962	390.0	6.00E-19	0.960	391.0	5.98E-19	0.959	392.0	5.96E-19	0.957	393.0	5.93E-19	0.953
394.0	5.91E-19	0.950	395.0	5.89E-19	0.942	396.0	6.06E-19	0.922	397.0	6.24E-19	0.870	398.0	6.41E-19	0.820
399.0	6.59E-19	0.760	400.0	6.76E-19	0.695	401.0	6.67E-19	0.635	402.0	6.58E-19	0.560	403.0	6.50E-19	0.485
404.0	6.41E-19	0.425	405.0	6.32E-19	0.350	406.0	6.21E-19	0.290	407.0	6.10E-19	0.225	408.0	5.99E-19	0.185
409.0	5.88E-19	0.153	410.0	5.77E-19	0.130	411.0	5.88E-19	0.110	412.0	5.98E-19	0.094	413.0	6.09E-19	0.083
414.0	6.19E-19	0.070	415.0	6.30E-19	0.059	416.0	6.29E-19	0.048	417.0	6.27E-19	0.039	418.0	6.26E-19	0.030
419.0	6.24E-19	0.023	420.0	6.23E-19	0.018	421.0	6.18E-19	0.012	422.0	6.14E-19	0.008	423.0	6.09E-19	0.004
424.0	6.05E-19	0.000	425.0	6.00E-19	0.000									
Photolysis File = NO3NO														
585.0	2.77E-18	0.000	590.0	5.14E-18	0.250	595.0	4.08E-18	0.400	600.0	2.83E-18	0.250	605.0	3.45E-18	0.200
610.0	1.48E-18	0.200	615.0	1.96E-18	0.100	620.0	3.58E-18	0.100	625.0	9.25E-18	0.050	630.0	5.66E-18	0.050
635.0	1.45E-18	0.030	640.0	1.11E-18	0.000									
Photolysis File = NO3NO2														
400.0	0.00E+00	1.000	405.0	3.00E-20	1.000	410.0	4.00E-20	1.000	415.0	5.00E-20	1.000	420.0	8.00E-20	1.000
425.0	1.00E-19	1.000	430.0	1.30E-19	1.000	435.0	1.80E-19	1.000	440.0	1.90E-19	1.000	445.0	2.20E-19	1.000
450.0	2.80E-19	1.000	455.0	3.30E-19	1.000	460.0	3.70E-19	1.000	465.0	4.30E-19	1.000	470.0	5.10E-19	1.000
475.0	6.00E-19	1.000	480.0	6.40E-19	1.000	485.0	6.90E-19	1.000	490.0	8.80E-19	1.000	495.0	9.50E-19	1.000
500.0	1.01E-18	1.000	505.0	1.10E-18	1.000	510.0	1.32E-18	1.000	515.0	1.40E-18	1.000	520.0	1.45E-18	1.000
525.0	1.48E-18	1.000	530.0	1.94E-18	1.000	535.0	2.04E-18	1.000	540.0	1.81E-18	1.000	545.0	1.81E-18	1.000
550.0	2.36E-18	1.000	555.0	2.68E-18	1.000	560.0	3.07E-18	1.000	565.0	2.53E-18	1.000	570.0	2.54E-18	1.000
575.0	2.74E-18	1.000	580.0	3.05E-18	1.000	585.0	2.77E-18	1.000	590.0	5.14E-18	0.750	595.0	4.08E-18	0.600
600.0	2.83E-18	0.550	605.0	3.45E-18	0.400	610.0	1.45E-18	0.300	615.0	1.96E-18	0.250	620.0	3.58E-18	0.200
625.0	9.25E-18	0.150	630.0	5.66E-18	0.050	635.0	1.45E-18	0.000						
Photolysis File = O3O3P														
280.0	3.97E-18	0.100	281.0	3.60E-18	0.100	282.0	3.24E-18	0.100	283.0	3.01E-18	0.100	284.0	2.73E-18	0.100
285.0	2.44E-18	0.100	286.0	2.21E-18	0.100	287.0	2.01E-18	0.100	288.0	1.76E-18	0.100	289.0	1.58E-18	0.100
290.0	1.41E-18	0.100	291.0	1.26E-18	0.100	292.0	1.10E-18	0.100	293.0	9.89E-19	0.100	294.0	8.59E-19	0.100
295.0	7.70E-19	0.100	296.0	6.67E-19	0.100	297.0	5.84E-19	0.100	298.0	5.07E-19	0.100	299.0	4.52E-19	0.100
300.0	3.92E-19	0.100	301.0	3.42E-19	0.100	302.0	3.06E-19	0.100	303.0	2.60E-19	0.100	304.0	2.37E-19	0.100
305.0	2.01E-19	0.112	306.0	1.79E-19	0.149	307.0	1.56E-19	0.197	308.0	1.38E-19	0.259	309.0	1.25E-19	0.339
310.0	1.02E-19	0.437	311.0	9.17E-20	0.546	312.0	7.88E-20	0.652	313.0	6.77E-20	0.743	314.0	6.35E-20	0.816
315.0	5.10E-20	0.872	316.0	4.61E-20	0.916	317.0	4.17E-20	0.949	318.0	3.72E-20	0.976	319.0	2.69E-20	0.997
320.0	3.23E-20	1.000	330.0	6.70E-21	1.000	340.0	1.70E-21	1.000	350.0	4.00E-22	1.000	355.0	0.00E+00	1.000
400.0	0.00E+00	1.000	450.0	1.60E-22	1.000	500.0	1.34E-21	1.000	550.0	3.32E-21	1.000	600.0	5.06E-21	1.000
650.0	2.45E-21	1.000	700.0	8.70E-22	1.000	750.0	3.20E-22	1.000	800.0	1.60E-22	1.000	900.0	0.00E+00	1.000
Photolysis File = O3O1D														
280.0	3.97E-18	0.900	281.0	3.60E-18	0.900	282.0	3.24E-18	0.900	283.0	3.01E-18	0.900	284.0	2.73E-18	0.900
285.0	2.44E-18	0.900	286.0	2.21E-18	0.900	287.0	2.01E-18	0.900	288.0	1.76E-18	0.900	289.0	1.58E-18	0.900
290.0	1.41E-18	0.900	291.0	1.26E-18	0.900	292.0	1.10E-18	0.900	293.0	9.89E-19	0.900	294.0	8.59E-19	0.900
295.0	7.70E-19	0.900	296.0	6.67E-19	0.900	297.0	5.84E-19	0.900	298.0	5.07E-19	0.900	299.0	4.52E-19	0.900
300.0	3.92E-19	0.900	301.0	3.42E-19	0.900	302.0	3.06E-19	0.900	303.0	2.60E-19	0.900	304.0	2.37E-19	0.900
305.0	2.01E-19	0.888	306.0	1.79E-19	0.851	307.0	1.56E-19	0.803	308.0	1.38E-19	0.741	309.0	1.25E-19	0.661
310.0	1.02E-19	0.563	311.0	9.17E-20	0.454	312.0	7.88E-20	0.348	313.0	6.77E-20	0.257	314.0	6.35E-20	0.184
315.0	5.10E-20	0.128	316.0	4.61E-20	0.084	317.0	4.17E-20	0.051	318.0	3.72E-20	0.024	319.0	2.69E-20	0.003
320.0	3.23E-20	0.000												
Photolysis File = HONO														
311.0	0.00E+00	1.000	312.0	2.00E-21	1.000	313.0	4.20E-21	1.000	314.0	4.60E-21	1.000	315.0	4.20E-21	1.000
316.0	3.00E-21	1.000	317.0	4.60E-21	1.000	318.0	3.60E-20	1.000	319.0	6.10E-20	1.000	320.0	2.10E-20	1.000
321.0	4.27E-20	1.000	322.0	4.01E-20	1.000	323.0	3.93E-20	1.000	324.0	4.01E-20	1.000	325.0	4.04E-20	1.000
326.0	3.13E-20	1.000	327.0	4.12E-20	1.000	328.0	7.55E-20	1.000	329.0	6.64E-20	1.000	330.0	7.29E-20	1.000
331.0	8.70E-20	1.000	332.0	1.38E-19	1.000	333.0	5.91E-20	1.000	334.0	5.91E-20	1.000	335.0	6.45E-20	1.000
336.0	5.91E-20	1.000	337.0	4.58E-20	1.000	338.0	1.91E-19	1.000	339.0	1.63E-19	1.000	340.0	1.05E-19	1.000
341.0	8.70E-20	1.000	342.0	3.35E-19	1.000	343.0	2.01E-19	1.000	344.0	1.02E-19	1.000	345.0	8.54E-20	1.000
346.0	8.32E-20	1.000	347.0	8.20E-20	1.000	348.0	7.49E-20	1.000	349.0	7.13E-20	1.000	350.0	6.83E-20	1.000
351.0	1.74E-19	1.000	352.0	1.14E-19	1.000	353.0	3.71E-19	1.000	354.0	4.96E-19	1.000	355.0	2.46E-19	1.000
356.0	1.19E-19	1.000	357.0	9.35E-20	1.000	358.0	7.78E-20	1.000	359.0	7.29E-20	1.000	360.0	6.83E-20	1.000
361.0	6.90E-20	1.000	362.0	7.32E-20	1.000	363.0	9.00E-20	1.000	364.0	1.21E-19	1.000	365.0	1.33E-19	1.000
366.0	2.13E-19	1.000	367.0	3.52E-19	1.000	368.0	4.50E-19	1.000	369.0	2.93E-19	1.000	370.0	1.19E-19	1.000
371.0	9.46E-20	1.000	372.0	8.85E-20	1.000	373.0	7.44E-20	1.000	374.0	4.77E-20	1.000	375.0	2.70E-20	1.000
376.0	1.90E-20	1.000	377.0	1.50E-20	1.000	378.0	1.90E-20	1.000	379.0	5.80E-20	1.000	380.0	7.78E-20	1.000
381.0	1.14E-19	1.000	382.0	1.40E-19	1.000	383.0	1.72E-19	1.000	384.0	1.99E-19	1.000	385.0	1.90E-19	1.000
386.0	1.19E-19	1.000	387.0	5.65E-20	1.000	388.0	3.20E-20	1.000	389.0	1.90E-20	1.000	390.0	1.20E-20	1.000
391.0	5.00E-21	1.000	392.0	0.00E+00	1.000									
Photolysis File = H2O2														
250.0	8.30E-20	1.000	255.0	6.70E-20	1.000	260.0	5.20E-20	1.000	265.0	4.20E-20	1.000	270.0	3.20E-20	1.000
275.0	2.50E-20	1.000	280.0	2.00E-20	1.000	285.0	1.50E-20	1.000	290.0	1.13E-20	1.000	295.0	8.70E-21	1.000
300.0	6.60E-21	1.000	305.0	4.90E-21	1.000	310.0	3.70E-21	1.000	315.0	2.80E-21	1.000	320.0	2.00E-21	1.000
325.0	1.50E-21	1.000	330.0	1.20E-21	1.000	335.0	9.00E-22	1.000	340.0	7.00E-22	1.000	345.0	5.00E-22	1.000
350.0	3.00E-22	1.000	355.0	0.00E+00	1.000									

Table A-3. (continued)

WL (nm)	Abs (cm^2)	QY	WL (nm)	Abs (cm^2)	QY	WL (nm)	Abs (cm^2)	QY	WL (nm)	Abs (cm^2)	QY	WL (nm)	Abs (cm^2)	QY
Photolysis File = CO2H														
210.0	3.75E-19	1.000	220.0	2.20E-19	1.000	230.0	1.38E-19	1.000	240.0	8.80E-20	1.000	250.0	5.80E-20	1.000
260.0	3.80E-20	1.000	270.0	2.50E-20	1.000	280.0	1.50E-20	1.000	290.0	9.00E-21	1.000	300.0	5.80E-21	1.000
310.0	3.40E-21	1.000	320.0	1.90E-21	1.000	330.0	1.10E-21	1.000	340.0	6.00E-22	1.000	350.0	4.00E-22	1.000
360.0	0.00E+00	1.000												
Photolysis File = HCHONEWR														
280.0	2.49E-20	0.590	280.5	1.42E-20	0.596	281.0	1.51E-20	0.602	281.5	1.32E-20	0.608	282.0	9.73E-21	0.614
282.5	6.76E-21	0.620	283.0	5.82E-21	0.626	283.5	9.10E-21	0.632	284.0	3.71E-20	0.638	284.5	4.81E-20	0.644
285.0	3.95E-20	0.650	285.5	2.87E-20	0.656	286.0	2.24E-20	0.662	286.5	1.74E-20	0.668	287.0	1.13E-20	0.674
287.5	1.10E-20	0.680	288.0	2.62E-20	0.686	288.5	4.00E-20	0.692	289.0	3.55E-20	0.698	289.5	2.12E-20	0.704
290.0	1.07E-20	0.710	290.5	1.35E-20	0.713	291.0	1.99E-20	0.717	291.5	1.56E-20	0.721	292.0	8.65E-21	0.724
292.5	5.90E-21	0.727	293.0	1.11E-20	0.731	293.5	6.26E-20	0.735	294.0	7.40E-20	0.738	294.5	5.36E-20	0.741
295.0	4.17E-20	0.745	295.5	3.51E-20	0.749	296.0	2.70E-20	0.752	296.5	1.75E-20	0.755	297.0	1.16E-20	0.759
297.5	1.51E-20	0.763	298.0	3.69E-20	0.766	298.5	4.40E-20	0.769	299.0	3.44E-20	0.773	299.5	2.02E-20	0.776
300.0	1.06E-20	0.780	300.4	7.01E-21	0.780	300.6	8.63E-21	0.779	300.8	1.47E-20	0.779	301.0	2.01E-20	0.779
301.2	2.17E-20	0.779	301.4	1.96E-20	0.779	301.6	1.54E-20	0.778	301.8	1.26E-20	0.778	302.0	1.03E-20	0.778
302.2	8.53E-21	0.778	302.4	7.13E-21	0.778	302.6	6.61E-21	0.777	302.8	1.44E-20	0.777	303.0	3.18E-20	0.777
303.2	3.81E-20	0.777	303.4	5.57E-20	0.777	303.6	6.91E-20	0.776	303.8	6.58E-20	0.776	304.0	6.96E-20	0.776
304.2	5.79E-20	0.776	304.4	5.24E-20	0.776	304.6	4.30E-20	0.775	304.8	3.28E-20	0.775	305.0	3.60E-20	0.775
305.2	5.12E-20	0.775	305.4	4.77E-20	0.775	305.6	4.43E-20	0.774	305.8	4.60E-20	0.774	306.0	4.01E-20	0.774
306.2	3.28E-20	0.774	306.4	2.66E-20	0.774	306.6	2.42E-20	0.773	306.8	1.95E-20	0.773	307.0	1.58E-20	0.773
307.2	1.37E-20	0.773	307.4	1.19E-20	0.773	307.6	1.01E-20	0.772	307.8	9.01E-21	0.772	308.0	8.84E-21	0.772
308.2	2.08E-20	0.772	308.4	2.39E-20	0.772	308.6	3.08E-20	0.771	308.8	3.39E-20	0.771	309.0	3.18E-20	0.771
309.2	3.06E-20	0.771	309.4	2.84E-20	0.771	309.6	2.46E-20	0.770	309.8	1.95E-20	0.770	310.0	1.57E-20	0.770
310.2	1.26E-20	0.767	310.4	9.26E-21	0.764	310.6	7.71E-21	0.761	310.8	6.05E-21	0.758	311.0	5.13E-21	0.755
311.2	4.82E-21	0.752	311.4	4.54E-21	0.749	311.6	6.81E-21	0.746	311.8	1.04E-20	0.743	312.0	1.43E-20	0.740
312.2	1.47E-20	0.737	312.4	1.35E-20	0.734	312.6	1.13E-20	0.731	312.8	9.86E-21	0.728	313.0	7.82E-21	0.725
313.2	6.48E-21	0.722	313.4	1.07E-20	0.719	313.6	2.39E-20	0.716	313.8	3.80E-20	0.713	314.0	5.76E-20	0.710
314.2	6.14E-20	0.707	314.4	7.45E-20	0.704	314.6	5.78E-20	0.701	314.8	5.59E-20	0.698	315.0	4.91E-20	0.695
315.2	4.37E-20	0.692	315.4	3.92E-20	0.689	315.6	2.89E-20	0.686	315.8	2.82E-20	0.683	316.0	2.10E-20	0.680
316.2	1.66E-20	0.677	316.4	2.05E-20	0.674	316.6	4.38E-20	0.671	316.8	5.86E-20	0.668	317.0	6.28E-20	0.665
317.2	5.07E-20	0.662	317.4	4.33E-20	0.659	317.6	4.17E-20	0.656	317.8	3.11E-20	0.653	318.0	2.64E-20	0.650
318.2	2.24E-20	0.647	318.4	1.70E-20	0.644	318.6	1.24E-20	0.641	318.8	1.11E-20	0.638	319.0	7.70E-21	0.635
319.2	6.36E-21	0.632	319.4	5.36E-21	0.629	319.6	4.79E-21	0.626	319.8	6.48E-21	0.623	320.0	1.48E-20	0.620
320.2	1.47E-20	0.614	320.4	1.36E-20	0.608	320.6	1.69E-20	0.601	320.8	1.32E-20	0.595	321.0	1.49E-20	0.589
321.2	1.17E-20	0.583	321.4	1.15E-20	0.577	321.6	9.64E-21	0.570	321.8	7.26E-21	0.564	322.0	5.94E-21	0.558
322.2	4.13E-21	0.552	322.4	3.36E-21	0.546	322.6	2.39E-21	0.539	322.8	2.01E-21	0.533	323.0	1.76E-21	0.527
323.2	2.82E-21	0.521	323.4	4.65E-21	0.515	323.6	7.00E-21	0.508	323.8	7.80E-21	0.502	324.0	7.87E-21	0.496
324.2	6.59E-21	0.490	324.4	5.60E-21	0.484	324.6	4.66E-21	0.477	324.8	4.21E-21	0.471	325.0	7.77E-21	0.465
325.2	2.15E-20	0.459	325.4	3.75E-20	0.453	325.6	4.10E-20	0.446	325.8	6.47E-20	0.440	326.0	7.59E-20	0.434
326.2	6.51E-20	0.428	326.4	5.53E-20	0.422	326.6	5.76E-20	0.415	326.8	4.43E-20	0.409	327.0	3.44E-20	0.403
327.2	3.22E-20	0.397	327.4	2.13E-20	0.391	327.6	1.91E-20	0.384	327.8	1.42E-20	0.378	328.0	9.15E-21	0.372
328.2	6.79E-21	0.366	328.4	4.99E-21	0.360	328.6	4.77E-21	0.353	328.8	1.75E-20	0.347	329.0	3.27E-20	0.341
329.2	3.99E-20	0.335	329.4	5.13E-20	0.329	329.6	4.00E-20	0.322	329.8	3.61E-20	0.316	330.0	3.38E-20	0.310
330.2	3.08E-20	0.304	330.4	2.16E-20	0.298	330.6	2.09E-20	0.291	330.8	1.41E-20	0.285	331.0	9.95E-21	0.279
331.2	7.76E-21	0.273	331.4	6.16E-21	0.267	331.6	4.06E-21	0.260	331.8	3.03E-21	0.254	332.0	2.41E-21	0.248
332.2	1.74E-21	0.242	332.4	1.33E-21	0.236	332.6	2.70E-21	0.229	332.8	1.65E-21	0.223	333.0	1.17E-21	0.217
333.2	9.84E-22	0.211	333.4	8.52E-22	0.205	333.6	6.32E-22	0.198	333.8	5.21E-22	0.192	334.0	1.46E-21	0.186
334.2	1.80E-21	0.180	334.4	1.43E-21	0.174	334.6	1.03E-21	0.167	334.8	7.19E-22	0.161	335.0	4.84E-22	0.155
335.2	2.73E-22	0.149	335.4	1.34E-22	0.143	335.6	-1.62E-22	0.136	335.8	1.25E-22	0.130	336.0	4.47E-22	0.124
336.2	1.23E-21	0.118	336.4	2.02E-21	0.112	336.6	3.00E-21	0.105	336.8	2.40E-21	0.099	337.0	3.07E-21	0.093
337.2	2.29E-21	0.087	337.4	2.46E-21	0.081	337.6	2.92E-21	0.074	337.8	8.10E-21	0.068	338.0	1.82E-20	0.062
338.2	3.10E-20	0.056	338.4	3.24E-20	0.050	338.6	4.79E-20	0.043	338.8	5.25E-20	0.037	339.0	5.85E-20	0.031
339.2	4.33E-20	0.025	339.4	4.20E-20	0.019	339.6	3.99E-20	0.012	339.8	3.11E-20	0.006	340.0	2.72E-20	0.000
Photolysis File = HCHONEWM														
280.0	2.49E-20	0.350	280.5	1.42E-20	0.346	281.0	1.51E-20	0.341	281.5	1.32E-20	0.336	282.0	9.73E-21	0.332
282.5	6.76E-21	0.327	283.0	5.82E-21	0.323	283.5	9.10E-21	0.319	284.0	3.71E-20	0.314	284.5	4.81E-20	0.309
285.0	3.95E-20	0.305	285.5	2.87E-20	0.301	286.0	2.24E-20	0.296	286.5	1.74E-20	0.291	287.0	1.13E-20	0.287
287.5	1.10E-20	0.282	288.0	2.62E-20	0.278	288.5	4.00E-20	0.273	289.0	3.55E-20	0.269	289.5	2.12E-20	0.264
290.0	1.07E-20	0.260	290.5	1.35E-20	0.258	291.0	1.99E-20	0.256	291.5	1.56E-20	0.254	292.0	8.65E-21	0.252
292.5	5.90E-21	0.250	293.0	1.11E-20	0.248	293.5	6.26E-20	0.246	294.0	7.40E-20	0.244	294.5	5.36E-20	0.242
295.0	4.17E-20	0.240	295.5	3.51E-20	0.238	296.0	2.70E-20	0.236	296.5	1.75E-20	0.234	297.0	1.16E-20	0.232
297.5	1.51E-20	0.230	298.0	3.69E-20	0.228	298.5	4.40E-20	0.226	299.0	3.44E-20	0.224	299.5	2.02E-20	0.222
300.0	1.06E-20	0.220	300.4	7.01E-21	0.220	300.6	8.63E-21	0.221	300.8	1.47E-20	0.221	301.0	2.01E-20	0.221
301.2	2.17E-20	0.221	301.4	1.96E-20	0.221	301.6	1.54E-20	0.222	301.8	1.26E-20	0.222	302.0	1.03E-20	0.222
302.2	8.53E-21	0.222	302.4	7.13E-21	0.222	302.6	6.61E-21	0.223	302.8	1.44E-20	0.223	303.0	3.18E-20	0.223
303.2	3.81E-20	0.223	303.4	5.57E-20	0.223	303.6	6.91E-20	0.224	303.8	6.58E-20	0.224	304.0	6.96E-20	0.224
304.2	5.79E-20	0.224	304.4	5.24E-20	0.224	304.6	4.30E-20	0.225	304.8	3.28E-20	0.225	305.0	3.60E-20	0.225
305.2	5.12E-20	0.225	305.4	4.77E-20	0.225	305.6	4.43E-20	0.226	305.8	4.60E-20	0.226	306.0	4.01E-20	0.226
306.2	3.28E-20	0.226	306.4	2.66E-20	0.226	306.6	2.42E-20	0.227	306.8	1.95E-20	0.227	307.0	1.58E-20	0.227
307.2	1.37E-20	0.227	307.4	1.19E-20	0.227	307.6	1.01E-20	0.228	307.8	9.01E-21	0.228	308.0	8.84E-21	0.228
308.2	2.08E-20	0.228	308.4	2.39E-20	0.228	308.6	3.08E-20	0.229	308.8	3.39E-20	0.229	309.0	3.18E-20	0.229
309.2	3.06E-20	0.229	309.4	2.84E-20	0.229	309.6	2.46E-20	0.230	309.8	1.95E-20	0.230	310.0	1.57E-20	0.230
310.2	1.26E-20	0.233	310.4	9.26E-21	0.236	310.6	7.71E-21	0.239	310.8	6.05E-21	0.242	311.0	5.13E-21	0.245
311.2	4.82E-21	0.248	311.4	4.54E-21	0.251	311.6	6.81E-21	0.254	311.8	1.04E-20	0.257	312.0	1.43E-20	0.260
312.2	1.47E-20	0.263	312.4	1.35E-20	0.266	312.6	1.13E-20	0.269	312.8	9.86E-21	0.272	313.0	7.82E-21	0.275
313.2	6.48E-21	0.278	313.4	1.07E-20	0.281	313.6	2.39E-20	0.284	313.8	3.80E-20	0.287	314.0	5.76E-20	0.290
314.2	6.14E-20	0.293	314.4	7.45E-20	0.296	314.6	5.78E-20	0.299	314.8	5.59E-20	0.302	315.0	4.91E-20	0.305
315.2	4.37E-20	0.308	315.4	3.92E-20	0.311	315.6	2.89E-20	0.314	315.8	2.82E-20	0.317	316.0	2.10E-20	0.320
316.2	1.66E-20	0.323	316.4	2.05E-20	0.326	316.6	4.38E-20	0.329	316.8	5.86E-20	0.332	317.0	6.28E-20	0.335
317.2	5.07E-20	0.338	317.4	4.33E-20	0.341	317.6	4.17E-20	0.344	317.8	3.11E-20	0.347	318.0	2.64E-20	0.350
318.2	2.24E-20	0.353	318.4	1.70E-20	0.356	318.6	1.24E-20	0.359	318.8	1.11E-20	0.362	319.0	7.70E-21	0.365

Table A-3. (continued)

WL (nm)	Abs (cm^2)	QY	WL (nm)	Abs (cm^2)	QY	WL (nm)	Abs (cm^2)	QY	WL (nm)	Abs (cm^2)	QY	WL (nm)	Abs (cm^2)	QY
319.2	6.36E-21	0.368	319.4	5.36E-21	0.371	319.6	4.79E-21	0.374	319.8	6.48E-21	0.377	320.0	1.48E-20	0.380
320.2	1.47E-20	0.386	320.4	1.36E-20	0.392	320.6	1.69E-20	0.399	320.8	1.32E-20	0.405	321.0	1.49E-20	0.411
321.2	1.17E-20	0.417	321.4	1.15E-20	0.423	321.6	9.64E-21	0.430	321.8	7.26E-21	0.436	322.0	5.94E-21	0.442
322.2	4.13E-21	0.448	322.4	3.36E-21	0.454	322.6	2.39E-21	0.461	322.8	2.01E-21	0.467	323.0	1.76E-21	0.473
323.2	2.82E-21	0.479	323.4	4.65E-21	0.485	323.6	7.00E-21	0.492	323.8	7.80E-21	0.498	324.0	7.87E-21	0.504
324.2	6.59E-21	0.510	324.4	5.60E-21	0.516	324.6	4.66E-21	0.523	324.8	4.21E-21	0.529	325.0	7.77E-21	0.535
325.2	2.15E-20	0.541	325.4	3.75E-20	0.547	325.6	4.10E-20	0.554	325.8	6.47E-20	0.560	326.0	7.59E-20	0.566
326.2	6.51E-20	0.572	326.4	5.53E-20	0.578	326.6	5.76E-20	0.585	326.8	4.43E-20	0.591	327.0	3.44E-20	0.597
327.2	3.22E-20	0.603	327.4	2.13E-20	0.609	327.6	1.91E-20	0.616	327.8	1.42E-20	0.622	328.0	9.15E-21	0.628
328.2	6.79E-21	0.634	328.4	4.99E-21	0.640	328.6	4.77E-21	0.647	328.8	1.75E-20	0.653	329.0	3.27E-20	0.659
329.2	3.99E-20	0.665	329.4	5.13E-20	0.671	329.6	4.00E-20	0.678	329.8	3.61E-20	0.684	330.0	3.38E-20	0.690
330.2	3.08E-20	0.694	330.4	2.16E-20	0.699	330.6	2.09E-20	0.703	330.8	1.41E-20	0.708	331.0	9.95E-21	0.712
331.2	7.76E-21	0.717	331.4	6.16E-21	0.721	331.6	4.06E-21	0.726	331.8	3.03E-21	0.730	332.0	2.41E-21	0.735
332.2	1.74E-21	0.739	332.4	1.33E-21	0.744	332.6	2.70E-21	0.748	332.8	1.65E-21	0.753	333.0	1.17E-21	0.757
333.2	9.84E-22	0.762	333.4	8.52E-22	0.766	333.6	6.32E-22	0.771	333.8	5.21E-22	0.775	334.0	1.46E-21	0.780
334.2	1.80E-21	0.784	334.4	1.43E-21	0.789	334.6	1.03E-21	0.793	334.8	7.19E-22	0.798	335.0	4.84E-22	0.802
335.2	2.73E-22	0.798	335.4	1.34E-22	0.794	335.6	0.00E+00	0.790	335.8	1.25E-22	0.786	336.0	4.47E-22	0.782
336.2	1.23E-21	0.778	336.4	2.02E-21	0.773	336.6	3.00E-21	0.769	336.8	2.40E-21	0.764	337.0	3.07E-21	0.759
337.2	2.29E-21	0.754	337.4	2.46E-21	0.749	337.6	2.92E-21	0.745	337.8	8.10E-21	0.740	338.0	1.82E-20	0.734
338.2	3.10E-20	0.729	338.4	3.24E-20	0.724	338.6	4.79E-20	0.719	338.8	5.25E-20	0.714	339.0	5.85E-20	0.709
339.2	4.33E-20	0.703	339.4	4.20E-20	0.698	339.6	3.99E-20	0.693	339.8	3.11E-20	0.687	340.0	2.72E-20	0.682
340.2	1.99E-20	0.676	340.4	1.76E-20	0.671	340.6	1.39E-20	0.666	340.8	1.01E-20	0.660	341.0	6.57E-21	0.655
341.2	4.83E-21	0.649	341.4	3.47E-21	0.643	341.6	2.23E-21	0.638	341.8	1.55E-21	0.632	342.0	3.70E-21	0.627
342.2	4.64E-21	0.621	342.4	1.08E-20	0.616	342.6	1.14E-20	0.610	342.8	1.79E-20	0.604	343.0	2.33E-20	0.599
343.2	1.72E-20	0.593	343.4	1.55E-20	0.588	343.6	1.46E-20	0.582	343.8	1.38E-20	0.576	344.0	1.00E-20	0.571
344.2	8.26E-21	0.565	344.4	6.32E-21	0.559	344.6	4.28E-21	0.554	344.8	3.22E-21	0.548	345.0	2.54E-21	0.542
345.2	1.60E-21	0.537	345.4	1.15E-21	0.531	345.6	8.90E-22	0.525	345.8	6.50E-22	0.520	346.0	5.09E-22	0.514
346.2	5.15E-22	0.508	346.4	3.45E-22	0.503	346.6	3.18E-22	0.497	346.8	3.56E-22	0.491	347.0	3.24E-22	0.485
347.2	3.34E-22	0.480	347.4	2.88E-22	0.474	347.6	2.84E-22	0.468	347.8	9.37E-22	0.463	348.0	9.70E-22	0.457
348.2	7.60E-22	0.451	348.4	6.24E-22	0.446	348.6	4.99E-22	0.440	348.8	4.08E-22	0.434	349.0	3.39E-22	0.428
349.2	1.64E-22	0.423	349.4	1.49E-22	0.417	349.6	8.30E-23	0.411	349.8	2.52E-23	0.406	350.0	2.57E-23	0.400
350.2	0.00E+00	0.394	350.4	5.16E-23	0.389	350.6	0.00E+00	0.383	350.8	2.16E-23	0.377	351.0	7.07E-23	0.371
351.2	3.45E-23	0.366	351.4	1.97E-22	0.360	351.6	4.80E-22	0.354	351.8	3.13E-21	0.349	352.0	6.41E-21	0.343
352.2	8.38E-21	0.337	352.4	1.55E-20	0.331	352.6	1.86E-20	0.326	352.8	1.94E-20	0.320	353.0	2.78E-20	0.314
353.2	1.96E-20	0.309	353.4	1.67E-20	0.303	353.6	1.75E-20	0.297	353.8	1.63E-20	0.291	354.0	1.36E-20	0.286
354.2	1.07E-20	0.280	354.4	9.82E-21	0.274	354.6	8.66E-21	0.269	354.8	6.44E-21	0.263	355.0	4.84E-21	0.257
355.2	3.49E-21	0.251	355.4	2.41E-21	0.246	355.6	1.74E-21	0.240	355.8	1.11E-21	0.234	356.0	7.37E-22	0.229
356.2	4.17E-22	0.223	356.4	1.95E-22	0.217	356.6	1.50E-22	0.211	356.8	8.14E-23	0.206	357.0	0.00E+00	0.200
Photolysis File = CCHOR														
260.0	2.00E-20	0.310	270.0	3.40E-20	0.390	280.0	4.50E-20	0.580	290.0	4.90E-20	0.530	295.0	4.50E-20	0.480
300.0	4.30E-20	0.430	305.0	3.40E-20	0.370	315.0	2.10E-20	0.170	320.0	1.80E-20	0.100	325.0	1.10E-20	0.040
330.0	6.90E-21	0.000												
Photolysis File = RCHO														
280.0	5.26E-20	0.960	290.0	5.77E-20	0.910	300.0	5.05E-20	0.860	310.0	3.68E-20	0.600	320.0	1.66E-20	0.360
330.0	6.49E-21	0.200	340.0	1.44E-21	0.080	345.0	0.00E+00	0.020						
Photolysis File = ACET-93C														
250.0	2.37E-20	0.760	260.0	3.66E-20	0.800	270.0	4.63E-20	0.640	280.0	5.05E-20	0.550	290.0	4.21E-20	0.300
300.0	2.78E-20	0.150	310.0	1.44E-20	0.050	320.0	4.80E-21	0.026	330.0	8.00E-22	0.017	340.0	1.00E-22	0.000
350.0	3.00E-23	0.000	360.0	0.00E+00	0.000									
Photolysis File = KETONE														
210.0	1.10E-21	1.000	220.0	1.20E-21	1.000	230.0	4.60E-21	1.000	240.0	1.30E-20	1.000	250.0	2.68E-20	1.000
260.0	4.21E-20	1.000	270.0	5.54E-20	1.000	280.0	5.92E-20	1.000	290.0	5.16E-20	1.000	300.0	3.44E-20	1.000
310.0	1.53E-20	1.000	320.0	4.60E-21	1.000	330.0	1.10E-21	1.000	340.0	0.00E+00	1.000			
Photolysis File = GLYOXAL1														
230.0	2.87E-21	1.000	235.0	2.87E-21	1.000	240.0	4.30E-21	1.000	245.0	5.73E-21	1.000	250.0	8.60E-21	1.000
255.0	1.15E-20	1.000	260.0	1.43E-20	1.000	265.0	1.86E-20	1.000	270.0	2.29E-20	1.000	275.0	2.58E-20	1.000
280.0	2.87E-20	1.000	285.0	3.30E-20	1.000	290.0	3.15E-20	1.000	295.0	3.30E-20	1.000	300.0	3.58E-20	1.000
305.0	2.72E-20	1.000	310.0	2.72E-20	1.000	312.5	2.87E-20	1.000	315.0	2.29E-20	1.000	320.0	1.43E-20	1.000
325.0	1.15E-20	1.000	327.5	1.43E-20	1.000	330.0	1.15E-20	1.000	335.0	2.87E-21	1.000	340.0	0.00E+00	1.000
Photolysis File = GLYOXAL2														
355.0	0.00E+00	1.000	360.0	2.29E-21	1.000	365.0	2.87E-21	1.000	370.0	8.03E-21	1.000	375.0	1.00E-20	1.000
380.0	1.72E-20	1.000	382.0	1.58E-20	1.000	384.0	1.49E-20	1.000	386.0	1.49E-20	1.000	388.0	2.87E-20	1.000
390.0	3.15E-20	1.000	391.0	3.24E-20	1.000	392.0	3.04E-20	1.000	393.0	2.23E-20	1.000	394.0	2.63E-20	1.000
395.0	3.04E-20	1.000	396.0	2.63E-20	1.000	397.0	2.43E-20	1.000	398.0	3.24E-20	1.000	399.0	3.04E-20	1.000
400.0	2.84E-20	1.000	401.0	3.24E-20	1.000	402.0	4.46E-20	1.000	403.0	5.27E-20	1.000	404.0	4.26E-20	1.000
405.0	3.04E-20	1.000	406.0	3.04E-20	1.000	407.0	2.84E-20	1.000	408.0	2.43E-20	1.000	409.0	2.84E-20	1.000
410.0	6.08E-20	1.000	411.0	5.07E-20	1.000	411.5	6.08E-20	1.000	412.0	4.86E-20	1.000	413.0	8.31E-20	1.000
413.5	6.48E-20	1.000	414.0	7.50E-20	1.000	414.5	8.11E-20	1.000	415.0	8.11E-20	1.000	415.5	6.89E-20	1.000
416.0	4.26E-20	1.000	417.0	4.86E-20	1.000	418.0	5.88E-20	1.000	419.0	6.69E-20	1.000	420.0	3.85E-20	1.000
421.0	5.67E-20	1.000	421.5	4.46E-20	1.000	422.0	5.27E-20	1.000	422.5	1.05E-19	1.000	423.0	8.51E-20	1.000
424.0	6.08E-20	1.000	425.0	7.29E-20	1.000	426.0	1.18E-19	1.000	426.5	1.30E-19	1.000	427.0	1.07E-19	1.000
428.0	1.66E-19	1.000	429.0	4.05E-20	1.000	430.0	5.07E-20	1.000	431.0	4.86E-20	1.000	432.0	4.05E-20	1.000
433.0	3.65E-20	1.000	434.0	4.05E-20	1.000	434.5	6.08E-20	1.000	435.0	5.07E-20	1.000	436.0	8.11E-20	1.000
436.5	1.13E-19	1.000	437.0	5.27E-20	1.000	438.0	1.01E-19	1.000	438.5	1.38E-19	1.000	439.0	7.70E-20	1.000
440.0	2.47E-19	1.000	441.0	8.11E-20	1.000	442.0	6.08E-20	1.000	443.0	7.50E-20	1.000	444.0	9.32E-20	1.000
445.0	1.13E-19	1.000	446.0	5.27E-20	1.000	447.0	2.43E-20	1.000	448.0	2.84E-20	1.000	449.0	3.85E-20	1.000
450.0	6.08E-20	1.000	451.0	1.09E-19	1.000	451.5	9.32E-20	1.000	452.0	1.22E-19	1.000	453.0	2.39E-19	1.000
454.0	1.70E-19	1.000	455.0	3.40E-19	1.000	455.5	4.05E-19	1.000	456.0	1.01E-19	1.000	457.0	1.62E-20	1.000

Table A-3. (continued)

WL (nm)	Abs (cm^2)	QY	WL (nm)	Abs (cm^2)	QY	WL (nm)	Abs (cm^2)	QY	WL (nm)	Abs (cm^2)	QY	WL (nm)	Abs (cm^2)	QY
458.0	1.22E-20	1.000	458.5	1.42E-20	1.000	459.0	4.05E-21	1.000	460.0	4.05E-21	1.000	460.5	6.08E-21	1.000
461.0	2.03E-21	1.000	462.0	0.00E+00	1.000									
Photolysis File = MEGLYOX1														
220.0	2.10E-21	1.000	225.0	2.10E-21	1.000	230.0	4.21E-21	1.000	235.0	7.57E-21	1.000	240.0	9.25E-21	1.000
245.0	8.41E-21	1.000	250.0	9.25E-21	1.000	255.0	9.25E-21	1.000	260.0	9.67E-21	1.000	265.0	1.05E-20	1.000
270.0	1.26E-20	1.000	275.0	1.43E-20	1.000	280.0	1.51E-20	1.000	285.0	1.43E-20	1.000	290.0	1.47E-20	1.000
295.0	1.18E-20	1.000	300.0	1.14E-20	1.000	305.0	9.25E-21	1.000	310.0	6.31E-21	1.000	315.0	5.47E-21	1.000
320.0	3.36E-21	1.000	325.0	1.68E-21	1.000	330.0	8.41E-22	1.000	335.0	0.00E+00	1.000			
Photolysis File = MEGLYOX2														
350.0	0.00E+00	1.000	354.0	4.21E-22	1.000	358.0	1.26E-21	1.000	360.0	2.10E-21	1.000	362.0	2.10E-21	1.000
364.0	2.94E-21	1.000	366.0	3.36E-21	1.000	368.0	4.21E-21	1.000	370.0	5.47E-21	1.000	372.0	5.89E-21	1.000
374.0	7.57E-21	1.000	376.0	7.99E-21	1.000	378.0	8.83E-21	1.000	380.0	1.01E-20	1.000	382.0	1.09E-20	1.000
384.0	1.35E-20	1.000	386.0	1.51E-20	1.000	388.0	1.72E-20	1.000	390.0	2.06E-20	1.000	392.0	2.10E-20	1.000
394.0	2.31E-20	1.000	396.0	2.48E-20	1.000	398.0	2.61E-20	1.000	400.0	2.78E-20	1.000	402.0	2.99E-20	1.000
404.0	3.20E-20	1.000	406.0	3.79E-20	1.000	408.0	3.95E-20	1.000	410.0	4.33E-20	1.000	412.0	4.71E-20	1.000
414.0	4.79E-20	1.000	416.0	4.88E-20	1.000	418.0	5.05E-20	1.000	420.0	5.21E-20	1.000	422.0	5.30E-20	1.000
424.0	5.17E-20	1.000	426.0	5.30E-20	1.000	428.0	5.21E-20	1.000	430.0	5.55E-20	1.000	432.0	5.13E-20	1.000
434.0	5.68E-20	1.000	436.0	6.22E-20	1.000	438.0	6.06E-20	1.000	440.0	5.47E-20	1.000	441.0	6.14E-20	1.000
442.0	5.47E-20	1.000	443.0	5.55E-20	1.000	443.5	6.81E-20	1.000	444.0	5.97E-20	1.000	445.0	5.13E-20	1.000
446.0	4.88E-20	1.000	447.0	5.72E-20	1.000	448.0	5.47E-20	1.000	449.0	6.56E-20	1.000	450.0	5.05E-20	1.000
451.0	3.03E-20	1.000	452.0	4.29E-20	1.000	453.0	2.78E-20	1.000	454.0	2.27E-20	1.000	456.0	1.77E-20	1.000
458.0	8.41E-21	1.000	460.0	4.21E-21	1.000	464.0	1.68E-21	1.000	468.0	0.00E+00	1.000			
Photolysis File = BZCHO														
299.0	1.78E-19	1.000	304.0	7.40E-20	1.000	306.0	6.91E-20	1.000	309.0	6.41E-20	1.000	313.0	6.91E-20	1.000
314.0	6.91E-20	1.000	318.0	6.41E-20	1.000	325.0	8.39E-20	1.000	332.0	7.65E-20	1.000	338.0	8.88E-20	1.000
342.0	8.88E-20	1.000	346.0	7.89E-20	1.000	349.0	7.89E-20	1.000	354.0	9.13E-20	1.000	355.0	8.14E-20	1.000
364.0	5.67E-20	1.000	368.0	6.66E-20	1.000	369.0	8.39E-20	1.000	370.0	8.39E-20	1.000	372.0	3.45E-20	1.000
374.0	3.21E-20	1.000	376.0	2.47E-20	1.000	377.0	2.47E-20	1.000	380.0	3.58E-20	1.000	382.0	9.90E-21	1.000
386.0	0.00E+00	1.000												
Photolysis File = ACROLEIN														
250.0	1.80E-21	1.000	252.0	2.05E-21	1.000	253.0	2.20E-21	1.000	254.0	2.32E-21	1.000	255.0	2.45E-21	1.000
256.0	2.56E-21	1.000	257.0	2.65E-21	1.000	258.0	2.74E-21	1.000	259.0	2.83E-21	1.000	260.0	2.98E-21	1.000
261.0	3.24E-21	1.000	262.0	3.47E-21	1.000	263.0	3.58E-21	1.000	264.0	3.93E-21	1.000	265.0	4.67E-21	1.000
266.0	5.10E-21	1.000	267.0	5.38E-21	1.000	268.0	5.73E-21	1.000	269.0	6.13E-21	1.000	270.0	6.64E-21	1.000
271.0	7.20E-21	1.000	272.0	7.77E-21	1.000	273.0	8.37E-21	1.000	274.0	8.94E-21	1.000	275.0	9.55E-21	1.000
276.0	1.04E-20	1.000	277.0	1.12E-20	1.000	278.0	1.19E-20	1.000	279.0	1.27E-20	1.000	280.0	1.27E-20	1.000
281.0	1.26E-20	1.000	282.0	1.26E-20	1.000	283.0	1.28E-20	1.000	284.0	1.33E-20	1.000	285.0	1.38E-20	1.000
286.0	1.44E-20	1.000	287.0	1.50E-20	1.000	288.0	1.57E-20	1.000	289.0	1.63E-20	1.000	290.0	1.71E-20	1.000
291.0	1.78E-20	1.000	292.0	1.86E-20	1.000	293.0	1.95E-20	1.000	294.0	2.05E-20	1.000	295.0	2.15E-20	1.000
296.0	2.26E-20	1.000	297.0	2.37E-20	1.000	298.0	2.48E-20	1.000	299.0	2.60E-20	1.000	300.0	2.73E-20	1.000
301.0	2.85E-20	1.000	302.0	2.99E-20	1.000	303.0	3.13E-20	1.000	304.0	3.27E-20	1.000	305.0	3.39E-20	1.000
306.0	3.51E-20	1.000	307.0	3.63E-20	1.000	308.0	3.77E-20	1.000	309.0	3.91E-20	1.000	310.0	4.07E-20	1.000
311.0	4.25E-20	1.000	312.0	4.39E-20	1.000	313.0	4.44E-20	1.000	314.0	4.50E-20	1.000	315.0	4.59E-20	1.000
316.0	4.75E-20	1.000	317.0	4.90E-20	1.000	318.0	5.05E-20	1.000	319.0	5.19E-20	1.000	320.0	5.31E-20	1.000
321.0	5.43E-20	1.000	322.0	5.52E-20	1.000	323.0	5.60E-20	1.000	324.0	5.67E-20	1.000	325.0	5.67E-20	1.000
326.0	5.62E-20	1.000	327.0	5.63E-20	1.000	328.0	5.71E-20	1.000	329.0	5.76E-20	1.000	330.0	5.80E-20	1.000
331.0	5.95E-20	1.000	332.0	6.23E-20	1.000	333.0	6.39E-20	1.000	334.0	6.38E-20	1.000	335.0	6.24E-20	1.000
336.0	6.01E-20	1.000	337.0	5.79E-20	1.000	338.0	5.63E-20	1.000	339.0	5.56E-20	1.000	340.0	5.52E-20	1.000
341.0	5.54E-20	1.000	342.0	5.53E-20	1.000	343.0	5.47E-20	1.000	344.0	5.41E-20	1.000	345.0	5.40E-20	1.000
346.0	5.48E-20	1.000	347.0	5.90E-20	1.000	348.0	6.08E-20	1.000	349.0	6.00E-20	1.000	350.0	5.53E-20	1.000
351.0	5.03E-20	1.000	352.0	4.50E-20	1.000	353.0	4.03E-20	1.000	354.0	3.75E-20	1.000	355.0	3.55E-20	1.000
356.0	3.45E-20	1.000	357.0	3.46E-20	1.000	358.0	3.49E-20	1.000	359.0	3.41E-20	1.000	360.0	3.23E-20	1.000
361.0	2.95E-20	1.000	362.0	2.81E-20	1.000	363.0	2.91E-20	1.000	364.0	3.25E-20	1.000	365.0	3.54E-20	1.000
366.0	3.30E-20	1.000	367.0	2.78E-20	1.000	368.0	2.15E-20	1.000	369.0	1.59E-20	1.000	370.0	1.19E-20	1.000
371.0	8.99E-21	1.000	372.0	7.22E-21	1.000	373.0	5.86E-21	1.000	374.0	4.69E-21	1.000	375.0	3.72E-21	1.000
376.0	3.57E-21	1.000	377.0	3.55E-21	1.000	378.0	2.83E-21	1.000	379.0	1.69E-21	1.000	380.0	8.29E-24	1.000
381.0	0.00E+00	1.000												

Table A-4. Values of chamber-dependent parameters used in the model simulations of the environmental chamber experiments for this study. [a]

Parm.	Value(s)	Discussion
Default Chamber Model		The following are the parameters for the default chamber effects model which was assumed to be unaffected by TDI exposure. They were used when simulating all experiments in this study.
k(1)	0.172 min^{-1} (first experiment) - through - 0.157 min^{-1} (last experiment)	Derived from trend of results of quartz tube NO_2 actinometry measurements carried out around the time of the experiments as discussed in the text.
k(O3W)	$1.5x10^{-4}$ min^{-1}	The results of the O_3 dark decay experiments in this chamber are reasonably consistent with the recommended default of Carter et al (1995c) for Teflon bag chambers in general.
k(N25I) k(N25S)	$2.8\ x10^{-3}$ min^{-1}, $1.5x10^{-6}$ - k_g ppm^{-1} min^{-1}	Based on the N_2O_5 decay rate measurements in a similar chamber reported by Tuazon et al. (1983). Although we previously estimated there rate constants were lower in the larger Teflon bag chambers (Carter and Lurmann, 1990, 1991), we now consider it more reasonable to use the same rate constants for all such chambers (Carter et al., 1995c).
k(NO2W) yHONO	$1.6x10^{-4}$ min^{-1} 0.2	Based on dark NO_2 decay and HONO formation measured in a similar chamber by Pitts et al. (1984). Assumed to be the same in all Teflon bag chambers (Carter et al, 1995c).
k(XSHC)	250 min^{-1}	Estimated by modeling pure air irradiations. Not an important parameter affecting model predictions except for pure air or NO_x-air runs.
No TDI Exposure		Used for all base case and characterization and control runs where the reactor was not previously exposed to TDI. Applies to runs in Side A before DTC446 and runs in Side B before DTC462.
RS/K1	$3.27x10^{6}$ $e^{-7297/T}$ ppm	Based on model simulations of n-butane - NO_x experiments as discussed by Carter et al (1995c,d). The temperature dependence is derived from simulating outdoor experiments as discussed by Carter et al. (1995c). Results of non-TDI exposed n-butane - NO_x and CO - NO_x runs consistent with this, except for apparently anomalous run DTC461B.
E-NO2/K1	0.03 ppb	Based on model simulations of pure air experiments. Results of pure air run DTC464B consistent with this.

Table A-4 (continued)

Parm.	Value(s)	Discussion
TDI Exposure — Side A		Used in runs in Side A after reactor was exposed to TDI in the TDI injection and analysis tests. Applies to runs in Side A after DTC446.
RS/K1	2.31×10^{-4} ppm	Average of radical source rate which fit data for n-butane - NO_x runs DTC448A, DTC463A, and DTC468A, and CO - NO_x run DTC457A.
E-NO2/K1	0.06 ppb	Based on pure air run DTC464A.
TDI Exposure — Side B		Used in runs in Side B after reactor was exposed to TDI in run DTC462B. Applies to runs in Side A after DTC462.
RS/K1	1.39×10^{-4} ppm	Average of radical source rate which fit data for n-butane - NO_x runs DTC463B and DTC468B.
E-NO2/K1	0.06 ppb	Pure air run DTC462B was consistent with the default NO_x offgasing rate.

[a] See Table A-2 for definitions of the parameters.